Debiased Orbital and Absolute Magnitude Distribution of the Near-Earth Objects

William F. Bottke, Jr.[1]

Alessandro Morbidelli[2]

Robert Jedicke[3]

Jean-Marc Petit[2]

Harold F. Levison[1]

Patrick Michel[2]

Travis S. Metcalfe[4]

[1]Southwest Research Institute, 1050 Walnut St, Suite 426, Boulder, CO 80302
[2]Obs. de la Côte d'Azur, B.P. 4229, 06034 Nice Cedex 4, France
[3]Lunar and Planetary Laboratory, University of Arizona, Tucson, AZ 85721
[4]Department of Astronomy, University of Texas, Austin, TX 78712

Prepared for *Icarus*

October 18, 2001

65 manuscript pages
5 tables
19 figures (6 in color)

Running Head:
NEO Orbital and Absolute Magnitude Distribution
Editorial Correspondence and Proofs:

William F. Bottke, Jr.
Department of Space Studies
Southwest Research Institute
1050 Walnut St, Suite 426
Boulder, CO 80302

Tel: (303) 546-6066
Fax: (303) 546-9687
E-mail: bottke@boulder.swri.edu

ABSTRACT

The orbital and absolute magnitude distribution of the Near-Earth Objects (NEOs) is difficult to compute, partly because only a modest fraction of the entire NEO population has been discovered so far, but also because the known NEOs are biased by complicated observational selection effects. To circumvent these problems, we created a model NEO population which was fit to known NEOs discovered or accidentally rediscovered by Spacewatch. Our method was to numerically integrate thousands of test particles from five source regions which we believe provide most NEOs to the inner solar system. Four of these source regions are in or adjacent to the main asteroid belt, while the fifth one is associated with the Transneptunian disk. The nearly-isotropic comets, which include the Halley-type comets and the long-period comets, were not included in our model. Test bodies from our source regions which passed into the NEO region (perihelia $q < 1.3$ AU and aphelia $Q \geq 0.983$ AU) were tracked until they were eliminated by striking the Sun, a planet, or were ejected out of the inner solar system. These integrations were used to create five residence time probability distributions in semimajor axis, eccentricity, and inclination space (one for each source). These distributions show where NEOs from a given source are statistically most likely to be located. Combining these five residence time probability distributions with an NEO absolute magnitude distribution computed from previous work and a probability function representing the observational biases associated with the Spacewatch NEO survey, we produced a NEO model population which could be fit to 138 NEOs discovered or accidentally rediscovered by Spacewatch. By testing a range of possible source combinations, a "best-fit" NEO model was computed which (i) provided the debiased orbital and absolute magnitude distributions for the NEO population and (ii) indicated the relative importance of each NEO source region.

Our best-fit model is consistent with 960 ± 120 NEOs having $H < 18$ and $a < 7.4$ AU. Approximately 44% (as of December 2000) have been found so far. The limits on this estimate are conditional, since our model does not include nearly-isotropic comets. Nearly-isotropic comets, however, are generally restricted to a Tisserand parameter (with respect to Jupiter) of $T < 2$, such that few are believed to have $a < 7.4$ AU. Our computed NEO orbital distribution, which is valid for bodies as faint as $H < 22$, indicates that the Amor, Apollo, and Aten populations contain 32$\pm$1%, 62$\pm$1%, and 6$\pm$1% of the NEO population, respectively. We estimate that the population of objects completely inside Earth's orbit (IEOs) arising from our source regions is 2% the size of the NEO population. This value does not include the putative Vulcanoid population located inside Mercury's orbit. Overall, our model predicts that $\sim$ 61% of the NEO population comes from the inner main belt ($a < 2.5$ AU), $\sim$ 24% comes from the central main belt ($2.5 < a < 2.8$ AU), $\sim$ 8% comes from the outer main belt ($a > 2.8$ AU), and $\sim$ 6% comes from the Jupiter-family comet region ($2 < T \lesssim 3$).

The steady-state population in each NEO source region, as well as the influx rates needed to replenish each region, were calculated as a by-product of our method. The population of extinct comets in the Jupiter-family comet region was also computed.

Keywords: Asteroids, Asteroids-Dynamics, Orbits

1. Introduction

One of the major successes of lunar and terrestrial planet geology has been the recognition that craters on the Moon and terrestrial planets are derived from impacts rather than volcanism (e.g., Wilhelms 1993). Accordingly, it is now widely accepted that the Earth-Moon system has been incessantly bombarded by asteroids and comets over solar system history. By convention, we refer to the population of objects capable of striking the Earth or passing close to the Earth as "near-Earth objects" (NEOs). The NEO population is comprised of both asteroids and active/extinct comets. NEOs have perihelion distances $q \leq 1.3$AU and aphelion distances $Q \geq 0.983$ AU (e.g., Rabinowitz *et al.* 1994). Sub-categories of the NEO population include the Apollos ($a \geq 1.0$ AU; $q \leq 1.0167$ AU) and Atens ($a < 1.0$ AU; $Q \geq 0.983$ AU), which are on Earth-crossing orbits, and the Amors (1.0167 AU $< q \leq 1.3$ AU), which are on nearly-Earth-crossing orbits (see Fig. 1). Over the last 3 Gyr, this population has included bodies ranging in size from dust-sized fragments to objects tens of km in diameter (Shoemaker 1983). (Note: A glossary of acronyms and variable names can be found in Table 1).

EDITOR: PLACE FIGURE 1 HERE.

EDITOR: PLACE TABLE 1 HERE.

The ultimate sources of the NEOs have speculated about for many years. In the 1970's, it was conjectured that many NEOs were extinct cometary nuclei, primarily because limited knowledge existed on how objects migrate from the main asteroid belt to the near–Earth space (Wetherill, 1976). The first indication that resonances can force main belt asteroids to cross the orbits of the planets came from J. G. Williams (see Wetherill 1979) and Wisdom (1983). Following these pioneering works, several studies confirmed, both analytically and numerically, the role that resonances have in increasing asteroid eccentricities to Mars–crossing or even Earth–crossing values. Two efficient transport routes for the origin of NEOs have been identified: the ν_6 secular resonance, which occurs when the mean precession rates of the longitudes of perihelia of the asteroid and of Saturn are equal to each other, and the 3:1 mean motion resonance with Jupiter (for a review of secular and mean motion resonances see Froeschlé and Morbidelli 1994 and Moons 1997, respectively).

Using these advances, Wetherill (1979, 1985, 1987, 1988) developed Monte Carlo models of the orbital evolution of NEOs coming from the ν_6 and 3:1 resonances. Wetherill hypothesized that NEOs were resupplied via a two-step process: (i) catastrophic collisions and/or cratering events in the main belt injected debris into main belt resonances, and (ii) resonant motion would move the fragments into the NEO region over ~ 1 Myr timescales. His Monte-Carlo code work was later refined and extended by Rabinowitz (1997a,b) [1] Since an analysis of lunar and terrestrial craters suggested the impact flux on the Earth-Moon system has been more-or-less constant for the last ~ 3 Gyr (e.g., Shoemaker and Grieve 1994), it was assumed that enough material reached the resonances via collisional injection to keep the NEO population in steady state over this time. [2]

In the 1990's, however, the availability of new numerical integration codes (Wisdom and Holman 1991; Levison and Duncan 1994) and of fast inexpensive workstations allowed the first direct simulations of the dynamical evolution of a statistically significant number of test particles initially placed in the transportation resonances (Farinella *et al.* 1994; Gladman *et al.* 1997). The results of these new simulations pointed out that Monte-Carlo codes do not adequately treat the inherently chaotic behavior of bodies in the inner solar system (Dones *et al.* 1999; Gladman *et al.* 2000). Accordingly, it was suggested that new modeling efforts would be required to accurately reconstruct the orbital distribution of NEOs.

In the meantime, Migliorini *et al.* (1998) stressed that the number and orbital distribution of the Mars–crossing asteroids that are not in the NEO region (i.e., bodies with $q > 1.3$ AU, intersecting the orbit of Mars during a secular oscillation cycle of their eccentricity) are inconsistent with a possible origin of these bodies through the ν_6 and 3:1 transport routes. Morbidelli and Nesvorný (1999) showed that the Mars–crossers are most likely produced by a variety of weak mean motion resonances with Jupiter or Mars and by three–body mean motion resonances with Jupiter and Saturn (see also Nesvorný and Morbidelli 1998). These resonances slowly increase the eccentricity of main belt asteroids residing in those resonances until their orbits cross that of Mars. Migliorini *et al.* (see also Michel *et al.* 2000b) showed that objects on solely Mars–crossing orbits can become NEOs over a timescale of several 10^7 yr. These works argue that the Mars crossers should be considered as a potentially important intermediate source of NEOs (i.e., halfway between the main belt and NEO population) in addition to the ν_6 and 3:1 resonances.

---

[1]Rabinowitz (1997a,b) predicted the existence of 875 NEOs larger than 1 km, in good agreement with current estimates.

[2]We point out that the view of a steady-state NEO population over the last 3 Gyr has recently been challenged by Culler *et al.* (2000), who dated the formation age of 155 lunar spherules found in Apollo 14 soil samples using the ^{40}Ar/^{39}Ar isochron technique. These spherules, 100-500 microns in size, are presumably droplets of lunar surface material that were melted and thrown several meters to hundreds of kilometers by an impact. If these spherules come from a variety of different craters, their formation ages should reflect the impact history of the Moon. The spherule ages analyzed by Culler *et al.* suggest that the lunar impactor flux has decreased by a factor of 2-3 over the last ~ 3.5 Gyr to a low about 500 to 600 Myr ago, then increased by a factor of 3.7 ± 1.2 over the last 400 Myr. If true, the NEO population is currently larger than it has been over previous epochs. The interpretation of lunar spherule ages by Culler *et al.* , however, is still considered controversial (e.g., Hörz 2000). Regardless, the repercussions of these results on our paper are minimal because NEO dynamical lifetimes are relatively short (i.e., ~ 10 Myr; Gladman *et al.* 1997) compared to the timescale of the Culler *et al.* events (i.e., several hundred Myr). Thus, the current NEO population is almost certainly in steady state, though it may be a different steady state than that which existed 0.5-3 Gyr ago.

Comets in the NEO population, on the other hand, are thought to be predominantly supplied by several comet reservoirs residing near or beyond the orbit of Neptune: the Kuiper belt (e.g., Levison and Duncan 1994), the scattered comet disk associated with the Kuiper belt (Duncan and Levison 1997) and the Oort cloud (Weissman 1996). The first two are often lumped together and called the Transneptunian region. Some NEOs with comet-like properties may also come from the Trojan population as well (Levison *et al.* 1997). The Tisserand parameter T, the pseudo-energy of the Jacobi integral that must be conserved in the restricted circular three-body problem, has been used in the past to classify different comet populations (e.g., Carusi *et al.* 1987). Writing T with respect to Jupiter, we get (Kresak 1979):

$$T = \frac{a_J}{a} + 2\sqrt{(1-e^2)\frac{a}{a_J}}\cos i, \tag{1}$$

where a_J is the semimajor axis of Jupiter. Fig. 1 shows the $T = 2$ and $T = 3$ boundaries for $i = 0°$. Adopting the nomenclature provided by Levison (1996), we refer to $T > 2$ bodies as ecliptic comets, since they tend to have small inclinations, and $T < 2$ bodies as nearly-isotropic comets, since they tend to have high inclinations. Numerical simulations suggest that ecliptic comets come from particular regions of the Transneptunian region which are dynamically unstable over the lifetime of the solar system (e.g., Levison and Duncan 1997; Duncan and Levison 1997). Ecliptic comets that reach Jupiter- crossing orbits ($2 < T < 3$) are called Jupiter-family comets (JFCs). These bodies frequently experience low-velocity encounters with Jupiter. Though most model-JFCs are readily thrown out of the inner solar system via a close encounter with Jupiter (i.e., over a timescale of ~ 0.1 Myr), a small component of this population achieves NEO status (Levison and Duncan 1997). We include Trojans as part of the ecliptic comet population, since they start on $2 < T < 3$ orbits. Numerical simulations by Levison *et al.* (1997) have shown that Trojans leaking out of stable orbital configurations near Jupiter's L_4 and L_5 Lagrange points attain orbits similar to known JFCs. Nearly-isotropic comets, comprised of the long-period comets and the Halley- type comets, come from the Oort cloud (Weissman *et al.* 1996) and possibly the Transneptunian region (Levison and Duncan 1997; Duncan and Levison 1997). Numerical work has shown that nearly-isotropic comets can be thrown into the inner solar system by a combination of stellar and galactic perturbations (Duncan *et al.* 1987). The orbital components of test bodies from these simulations are often similar to observed Halley-family comets (Levison *et al.* 2001). Again, some of these objects attain NEO status during their orbital evolution.

Discriminating between asteroids and extinct comets in the NEO population is difficult, especially since both probably contribute to a spectrum of objects running the gamut from dusty comets to icy asteroids. Previous attempts to dynamically classify NEOs have concentrated on the use of the Tisserand parameter T. Objects with $2 < T < 3$ can pass within Jupiter's Hill sphere, such that many stay under the perturbing control of Jupiter until they are scattered out of the inner solar system. For this reason, NEOs on $2 < T < 3$ orbits are frequently assumed to be comets, since all active comets, with a few notable exceptions (e.g., 2P/Encke), fit this criterion. Accordingly, if a NEO in this region does not show any signs of cometary activity, it may be a dormant or possibly extinct comet (e.g., Shoemaker *et al.* 1994). It is thought that active comets often evolve into dormant, asteroidal-appearing objects, with their icy surfaces covered by a lag deposit of non-volatile dust grains, organics, and/or radiation processed material which prevents volatiles from sputtering away (see reviews by Weissman *et al.* 1989 and Weissman 1996). This hypothesis is supported by the Giotto spacecraft observations of the nucleus comet 1P/Halley, which showed that only 20%-30% of its surface was active during the flyby while the rest of Halley's surface was dark and apparently inactive (Keller *et al.* 1987). Indeed, some asteroidal-appearing objects have been found on $T < 2$ orbits (e.g., 1996 PW, with $T \sim 1.7$; Weissman and Levison 1997). From a dynamical standpoint, however, the issue is less clear-cut. Numerical simulations have shown that test bodies in chaotic resonances intersecting the main belt (e.g., the 3:1 mean motion resonance with Jupiter) often get their eccentricities and inclinations pumped up to $T < 3$ or even $T < 2$ values (Farinella *et al.* 1994; Gladman *et al.* 1997). Thus, it is plausible that some asteroidal-appearing objects on $T < 2$ orbits could, in fact, be asteroids rather than extinct comets.

Conversely, NEOs with $T > 3$ are often assumed to by asteroids, partly because the most prominent source of small bodies in this region is the main belt, but also because observations suggest that many $T > 3$ NEOs have spectral features consistent with those of main belt asteroids (e.g., S-type asteroids, C-type asteroids, prominent main belt asteroids like (4) Vesta; McFadden *et al.* 1989; Cruikshank *et al.* 1991; Binzel *et al.* 1996; Rabinowitz *et al.* 1998). There are many exceptions to this rule, though. The most striking example is active comet 2P/Encke, whose $T = 3.03$ orbit ($a = 2.2$ AU, $e = 0.85$, $i = 11.8°$) does not fit this dynamical criteria (Levison and Duncan 1994; Valsecchi 1999). Other $T > 3$ objects have been seen with sporadic comet-like tails (e.g., (4015) Wilson-Harrington; Bowell *et al.* 1992), possible CN-band emission (e.g., (2201) Oljato; McFadden *et al.* 1993; Chamberlin *et al.* 1996), and/or associated meteor streams (e.g., (3200) Phaethon; Gustafson 1989). These so-called "transitional objects" may be nearly-dormant comets, volatile-rich asteroids, or some combination of both categories.

Given this muddled situation, we want to be very clear about how we define the objects discussed in this paper. Thus, from this point on, the asteroidal component of the NEO population will be referred to as near-Earth asteroids (NEAs) and the cometary component will be referred to as near-Earth comets (NECs). To avoid the confusion that sometimes develops when NEOs are classified based on their appearance, we will discriminate NEAs from NECs according to each object's starting location. Objects originating in small body reservoirs located inside Jupiter's semimajor axis ($a < a_J$) will be considered NEAs, while those coming form small body reservoirs located near or outside Jupiter's semimajor axis ($a \gtrsim a_J$) will be considered NECs. Thus, potential NEA reservoirs include the main belt and Hungaria asteroid populations, while potential NEC reservoirs include the Trojans, the Transneptunian region, and the Oort cloud. This scheme does not necessarily help us classify known NEOs, whose source region is often unknown, but it does avoid the ambiguous nature of traditional "asteroid" and "comet" definitions.

Since NEO taxonomy based on the Tisserand parameter has been blurred by observational and numerical work, it would be useful to come up with an alternative way of discriminating between NEAs and NECs. The method we use in this paper is to construct a steady-state model of the orbital and absolute magnitude distributions of the NEO population. By tracking the dynamical evolution of comets and asteroids from their source populations to the NEO region, we can characterize the dominant orbital pathways taken by those objects. Ideally, an NEO's orbital (a, e, i) parameters can then be used to compute the relative probability that it came from a given source (and whether it should be classified as an NEA or an NEC).

This method does have some limitations. For example, there are regions where NEA and NEC pathways overlap, making it difficult to distinguish asteroids from comets, let alone the region they came from. In addition, the NEA and NEC populations may be fed by a variety of distinctive regions inside the main belt and comet reservoirs, each with their own size distribution. Hence, while dynamical identification of NEOs may be useful, "transitional objects' like those described above will probably require in situ observations or sample return mission to establish their true source.

The procedure used to create our NEO model is similar to that described by Bottke *et al.* (2000a), whose group modeled the orbital and absolute magnitude distributions of the NEA population alone. In that model, variables included the NEO size distribution and the relative importance of 3 NEA source regions (and their dominant pathways) to each other. We point out that the model fit obtained by Bottke *et al.* (2000a) was constrained to NEOs coming from the main belt with $a < 2.8$ AU. NEO orbits with $a > 2.8$ AU were not adequately fit by these three sources. For this reason, we investigate several additional NEO sources in this paper. The shape of the absolute magnitude distribution derived in Bottke *et al.* (2000a), however, can still be considered valid, such that we no longer treat it as a variable in our NEO model. The justification for this assumption is given in Sec. 3.2.

The various components of our model are described in the following sections. In Sec. 2, we tracked the dynamical evolution of test bodies coming out of several so-called intermediate sources (IS) of NEOs, a term which we will define below. In Sec. 3, we created a model steady-state NEO orbit and absolute magnitude distribution, with the contribution of each of our chosen IS regions to the overall orbital distribution represented by weighting coefficients. The NEO absolute magnitude distribution is taken from previous work, and is assumed to be orbit- and source-independent. At this point, in order to compute the free parameters, we would like to fit our model NEO distribution to the orbits and absolute magnitude values of NEOs discovered or accidentally re-discovered by the Spacewatch survey program. We can do this by assuming that the most important components of the NEO population have been sampled by observations from Spacewatch, and that our chosen IS regions can be identified in our attempt to fit these observations with our NEO model. Before any fit can be made, however, we must first account for the observational biases associated with the Spacewatch survey as well as important issues such as degeneracy between the source regions (i.e., a condition where test bodies from two different source regions follow very similar orbital paths). Our methods for overcoming these obstacles is discussed in Sec. 4. In Sec. 5, we take our bias-modified NEO model distribution and fit it to the NEO data. By calculating the "goodness of fit" between model and data, we will attempt to quantify whether our method produces reasonable results. The best-fit parameters extracted from this technique are then used to calculate the debiased NEO population (Sec. 6). In Sec. 7, several by-products of our NEO model are examined, including the estimated flux needed from each IS region to keep the NEO population in steady state, and the steady state population of each of our source regions. In Sec. 8, we examine the comet populations which supply NEOs to $T < 2$ orbits. Using our NEO model, we infer the population size of the Transneptunian regions, the ecliptic comet population, and the extinct comet population in the NEO region. We also examine which NEOs might actually be extinct comets. Finally, in Sec. 9, we summarize our principal results.

2. Intermediate Source Regions of the NEO Population

2.1. Method

In order to determine the orbital distribution of the NEOs and dynamically discriminate between NEAs and NECs, we must first identify the dominant regions which provide these objects. The ultimate sources of the NEO population were described above: the main belt, the Hungaria asteroids, the Trojan population, the Transneptunian region, and the Oort cloud. Within these populations, resonances and/or planetary close encounters are often powerful enough to push objects onto dynamical pathways which eventually take them to NEO orbits. By identifying these special zones, what we call "intermediate sources" (IS) of NEOs, we can narrow our investigation of the ultimate sources to a more focused range of (a, e, i) space. Note that the term IS is somewhat nebulous, since it can describe a single resonance replenished over time by a small body reservoir or a large (a, e, i) zone which acts as a "clearinghouse" for numerous small bodies. In either case, the IS region in question needs to produce NEOs with identifiable orbital characteristics.

To create our model of the steady state orbital distribution of NEOs, we need to identify the important IS regions and combine their contributions into a single function. Each potential source must be weighted with respect to one another according to the number of steady-state NEOs they produce. At the same time, we also want to minimize the number of free parameters in our model, particularly since NEO data from Spacewatch is limited. For this reason, we would like to separate primary IS regions, which provide the majority of NEOs, from secondary IS regions, which provide relatively few NEOs. One way to do this is to evaluate each IS according to three factors: (1) **Strength**, the IS's efficiency at moving material onto NEO orbits; (2) **Material Availability**, the amount of asteroidal or cometary material located near (or in) the IS, and (3) **Persistence**, the mean lifetime spent by the objects once they enter the NEO region. When these factors are quantified and, in essence, multiplied together, primary ISs should dominate secondary ISs.

As part of our modeling procedure, we numerically integrated thousands of test bodies in many potential IS region using the N-body code SWIFT-RMVS3 (e.g., Levison and Duncan 1994), which is in turn based on a symplectic algorithm published by Wisdom and Holman (1991). We also utilized or augmented our runs with numerical integration data computed from: (i) the collaborative project GAPTEC described in Gladman *et al.* (1997), (ii) the main belt and Mars-crossing asteroid integrations described in Migliorini *et al.* (1998) and Michel *et al.* (2000b), and (iii) the ecliptic comet integrations described in Duncan *et al.* (1995) and Levison and Duncan (1997). For the asteroidal IS regions, our integrations, and those from (i) and (ii), include the gravitational perturbations from Venus-Neptune. For the cometary IS regions, we use the integration results provided by (iii) alone, where only the planets Jupiter-Neptune were included. The terrestrial planets were excluded from (iii) to increase computation speed. The limitations of this approach will be described in Sec. 2.6.

Test bodies started in the asteroidal ISs were followed for at least 100 Myr of integration time. Those found to penetrate the NEO region were tracked until they collided with the Sun, were thrown beyond 10 AU from the Sun (usually by a close encounter with Jupiter) or they collided with a planet. We classify the first two loss mechanisms as "major sinks" for the population, while the last is only a "minor sink". Cometary test bodies were followed for 4 billion years, with most exiting the system via the major sinks (Levison and Duncan 1997; Duncan and Levison 1997). The ejection distance limit for the cometary runs was 1000 AU from the Sun.

To understand the orbital paths followed by test bodies from our IS regions, we tracked their evolutionary paths across a network of (a, e, i) cells placed throughout the solar system. None of the initial orbits of the test bodies were placed inside the NEO region. Regularly placed cells in the range of $a < 4.2$ AU, $e < 1.0$, and $i < 90°$ were used, with the bins being (0.05 AU $\times 0.02 \times 5°$) in volume. We refer to this region as the *extended target region (ETR)*, for reasons we describe later in the paper. The steady-state orbital distribution of NEOs coming from each IS was determined by computing the cumulative time spent by particles in each cell and then normalizing those values by the total time spent in all cells. The resultant residence time probability distribution, which we define as $R_{\rm IS}(a, e, i)$, shows where asteroids and comets from each IS spend their time (Morbidelli and Gladman 1998).

The following subsections describe our efforts to characterize the primary IS regions for our NEO model. We start with the three primary IS regions identified by Bottke *et al.* (2000a): (1) asteroids in the 3:1 mean-motion resonance with Jupiter, (2) asteroids in the ν_6 secular resonance, and (3) asteroids on Mars-crossing orbits adjacent to the main belt which have not yet achieved $q < 1.3$ AU orbits. Numerical simulations show that test bodies started in those regions are subject to resonant perturbations and/or planetary encounters, enough so that most are eventually pushed into the $q < 1.3$ AU region over time. All three of these IS regions are believed to produce copious numbers of NEAs, many with orbits consistent with the observed population (e.g., Bottke *et al.* 2000a). After this, we examine other potential sources of NEAs (e.g., the outer main belt and asteroid populations near/in the main belt, like the Hungarias and Phocaeas) and NECs (e.g., Transneptunian region, the Trojans, and the Oort cloud). In our judgement, several of these regions can be considered primary IS regions of NEOs as well, though not all can be included (e.g., Oort cloud) at this time.

2.2. The 3:1 Resonance

The 3:1 mean-motion resonance with Jupiter, intersecting the main belt at ~ 2.5 AU, has long been known as a wellspring of NEAs and meteorites (Wisdom 1983; Wetherill 1985; Wetherill 1987; Wetherill 1988). To calculate $R_{3:1}(a,e,i)$, we started 2354 test bodies within the boundaries of the 3:1 (Morbidelli and Moons 1995). All of our bodies were given initial $e < 0.35$ and $i < 15°$, similar to the integration conditions described in Gladman *et al.* (1997) and Morbidelli and Gladman (1998). Test results suggest that starting conditions in the 3:1 resonance have little influence on the evolutionary paths followed by various particles. A representation of $R_{3:1}(a,e,i)$ is shown in Fig. 2.

EDITOR: PLACE FIGURE 2 HERE.

The 3:1 resonance is powerful enough to pump up the eccentricities of test bodies to Mars- and Earth-crossing orbits in less than 1 Myr. In most cases, particles removed from the 3:1 resonance via a close encounter with a planet are readily pushed into the major sinks; we find that the mean time spent by these objects in the NEO region is 2.2 Myr, in basic agreement with Gladman *et al.* (1997). 38% of the flux from the 3:1 resonance attains $a < 2$ AU, a region where the major sinks play a lesser role (i.e., fewer powerful resonances) and the minor sinks grow in importance. The rest enter the major sinks. Most of the long-lived NEAs in our simulations reside on $a < 2$ AU orbits.

2.3. The ν_6 resonance

The ν_6 secular resonance defines the boundary of the inner main belt, and is fed by the material adjacent to this boundary. To calculate $R_{\nu_6}(a,e,i)$, we followed 3519 test bodies started in the "strong" part of the ν_6 secular resonance, where periodic oscillations in e are capable of moving test bodies onto NEA orbits in ~ 1 Myr (Morbidelli *et al.* 1994). Test bodies in these locations are on the "fast-track" to becoming NEAs. The boundary between the fast- and slow-track (i.e., test bodies take >> 1 Myr to reach the NEA orbits) was identified numerically by Morbidelli and Gladman (1998), who computed how long test bodies in various locations near and/or inside the ν_6 resonance took to reach Earth-crossing orbits. Using these results, we selected the following starting conditions: ($a \sim 2.06$ AU, $i = 2.5°$), ($a \sim 2.08$ AU, $i = 5°$), ($a \sim 2.115$ AU, $i = 7.5°$), ($a \sim 2.16$ AU, $i = 10°$), ($a \sim 2.24$ AU, $i = 12.5°$), and ($a \sim 2.315$ AU, $i = 15°$). For all cases, $e = 0.1$. A representation of $R_{\nu_6}(a,e,i)$ is shown in Fig. 3. More information on the initial conditions can be found in Morbidelli and Gladman (1998).

EDITOR: PLACE FIGURE 3 HERE.

The average time spent by these objects in the NEA region was 6.5 My. 70% of the steady-state population coming from the ν_6 resonance attained $a < 2$ AU, nearly twice the fraction of the 3:1 NEAs. Based on this result and the fact that the ν_6 resonance is located near many inner main belt asteroids, we consider this IS to be another primary source of NEAs for the inner solar system.

2.4. The Mars-crossing asteroid population

2.4.1. The intermediate source Mars-crossers

The third IS used in our model is the subset of the Mars-crossing asteroid population which borders the main belt. We refer to this population as the Intermediate source Mars-Crossers (IMC), with orbital parameters $q > 1.3$ AU, 2.06 AU $\leq a \leq$ 2.48 AU or 2.52 AU $\leq a <$ 2.8 AU, i below the location of the ν_6 resonance ($i \sim 15°$ or less; Morbidelli and Gladman 1998), and a combination of (a, e, i) values such that they cross the orbit of Mars during a secular oscillation cycle of their eccentricity (Migliorini *et al.* 1998). Hence, the IMCs are bracketed by the main belt, the NEA population, the ν_6 resonance, and 2.0 AU $< a <$ 2.8 AU, while they are split into two disconnected sub-populations by the 3:1 resonance gap. These sub-populations will be referred to as the "inner" ($a <$ 2.5 AU) and "outer" ($a >$ 2.5 AU) IMC regions.

We choose this specific part of the Mars-crossing asteroid population as a primary IS because (i) the IMC population is much more numerous than any other portion of the Mars-crossing asteroid population, (ii) many asteroids in the IMC region evolve into relatively long-lived NEAs, and (iii) the IMCs can be directly replenished by an extensive network of resonances residing in the main belt (Migliorini *et al.* 1998; Michel *et al.* 2000b; Gladman *et al.* 2000). Concerning the last point, IMC asteroids escape the main belt via mean motion resonances with Mars, three-body mean motion resonances (e.g., Jupiter-Saturn-asteroid) and slow-track paths associated with the ν_6 resonance (Morbidelli and Nesvorny 1999). Note that bodies residing near (but not "in") the strong part of the ν_6 resonance often have libration amplitudes large enough to reach Mars-crossing orbits (Wetherill and Williams 1979). A smaller portion of the IMC population is provided by asteroids removed from the 3:1 and ν_6 IS regions (discussed above) by close encounters with Mars.

The IMC population increases and decreases over time as secular perturbations modify Mars's eccentricity. For example, when Mars's eccentricity is near its maximum ($e \sim 0.12$; Laskar 1988; Ward 1992), main belt asteroids with $q <$ 1.78 AU can be considered Mars-crossing objects. On the other hand, when Mars's eccentricity is near its minimum ($e \sim 0.01$), only asteroids with $q <$ 1.6 AU can potentially strike Mars. The period of this oscillation is roughly $\sim$ 2 Myr (Laskar 1988; Ward 1992). Hence, to understand the evolution of the actual IMC population, we first used the criteria established by Migliorini *et al.* (1998) to identify those bodies (see also Michel *et al.* 2000b). Taking the known population of objects with perihelia 1.3 AU $< q <$ 1.78 AU, 2.00 AU $< a <$ 2.8 AU, and $i < 15°$ (orbital parameters supplied by the public-domain asteroid orbit database "astorb.dat" provided by E. Bowell at http://asteroid.lowell.edu), we checked to see which bodies intersected (in terms of nodal distance) the most eccentric orbit of Mars within 0.3 Myr. These objects were considered Mars- crossers. The 0.3 Myr timescale is arbitrary, but it accounts for some oscillation in the eccentricity of both the asteroids and Mars. Objects found within the strong part of the ν_6 resonance, the 3:1 resonance, or with $q <$ 1.3 AU orbits were removed (boundaries defined in Morbidelli and Gladman 1998). The 1011 Mars-crossers emerging from this test were then integrated for 100 Myr. Our results show that 500 of these objects entered $q <$ 1.3 AU orbits over this time. Those particular bodies were then tracked until they entered one of the sinks. The evolution of these bodies was used to produce a preliminary version of $R_{\rm IMC}(a, e, i)$.

Next, to increase our statistics, we simply integrated the 2977 known asteroids having perihelia 1.3 $< q <$ 1.8 AU, 2.00 AU $< a <$ 2.8 AU, and $i < 15°$ for 100 Myr. 95% of these objects had $H < 18$. Once again, all objects initially located inside the strong part of the ν_6 or 3:1 resonances were removed. These bodies were integrated using a different starting epoch and different computers, so the outcome results for individual objects were different than those in the first set of integrations. For this set of runs, the longer integration window gave us better coverage of the eccentricity oscillation of both the asteroids and Mars. It also allows us to include asteroids which diffused out of the main belt via Mars- or three-body resonances; many of these objects were not originally Mars-crossers in the sense defined above. Not surprisingly, our results showed that more objects (755) entered the NEA region over the integration time. These objects were also followed until they entered a sink. The shape of $R_{\rm IMC}(a, e, i)$ produced from these runs was similar to previous results. We conclude that the chaotic paths followed by IMCs into the NEO region can be reasonably well characterized if the starting set of test objects is sufficiently large. Both sets were used to produce our final version of $R_{\rm IMC}(a, e, i)$. (Fig. 4)

EDITOR: PLACE FIGURE 4 HERE.

A problem with using known asteroids to map out IMC orbital paths is that these objects are biased by observational selection effects. For example, asteroids in the inner IMC region are more readily discovered than those in the outer IMC region, partly because they have brighter albedos, but also because their orbits make them better targets for asteroids surveys. To compensate for these effects, we weighted the orbital paths of all IMCs with a numerical factor corresponding to the weighted average observational biases associated with their starting orbits (e.g., Jedicke 1996; Jedicke and Metcalfe 1998). These bias factors were based on absolute magnitude H rather than diameter D in order to eliminate complications caused by asteroid albedo variations. An examination of our 2977 objects indicated that the shape of the H distribution for the inner and outer IMC regions was quite similar, enough to make us believe that a more complicated debiasing procedure was unwarranted.

Dividing the IMC and near-IMC regions ($q < 1.8$ AU) into three semimajor axis zones (i.e., Zone a_1: 2.1 AU $\leq a <$ 2.3 AU; Zone a_2: 2.3 AU $\leq a <$ 2.5 AU; Zone a_3: 2.5 AU $\leq a \leq$ 2.8 AU) and three inclination zones (i.e., Zone i_1: $i < 5°$ AU; Zone i_2: $5° \leq i < 10°$; Zone i_3: $10° \leq i < 15°$, we determined the observational biases in each zone with respect to various H values (H = 13-18) using the results of Jedicke and Metcalfe (1998). We found that the ratios of the biases in Zones a_2 and a_3 over Zone a_1 were $\sim$ 1.3 and $\sim$ 1.8, respectively, while the ratios of the biases in Zones i_2 and i_3 over Zone i_1 were $\sim$ 2.7 and $\sim$ 4.4, respectively. Varying H did not appreciably change these values. Thus, we used these ratios to weight the orbital paths of under-represented IMCs in each zone when $R_{\mathrm{IMC}}(a, e, i)$ was calculated.

Using these factors to develop a weighted mean, we found that the average time spent by an IMC object in the NEO region before entering a sink was 3.85 My. In this case, 53% of the steady-state NEA population from the IMC region had $a < 2$ AU.

2.4.2. Other potential contributors to the NEA population

There are additional ISs adjacent to the Mars-crossing region which are capable of producing NEAs. Here we list them, in order of increasing distance from the Sun, using the nomenclature described in Michel *et al.* (2000b). Fig. 5 shows their approximate location in (a, i) space:

- The evolved Mars-crossing population (EV), having $a < 1.77$ AU or $1.77 < a < 2.06$ AU and $i < 15°$.
- The Hungarias (HU), having $1.77 < a < 2.06$ AU and $i > 15°$.
- The Phocaeas (PH), with $2.1 < a < 2.5$ AU and i which places them above the ν_6 resonance.
- The MB2 population, with $a > 2.5$ AU and i which places them above the ν_6 resonance.

EDITOR: PLACE FIGURE 5 HERE.

To determine whether any of these potential IS regions provide a substantial number of Mars- crossers, Michel *et al.* (2000b) did the following: (i) they integrated the known asteroids in each IS to determine their efficiency at producing long-lived NEAs and (ii) they estimated the number of asteroids in each IS region in order to determine the flux of new NEAs produced. To compensate for incompleteness and observational biases when determining the size of each IS population, the number of $D > 5$ km bodies between $2.0 < a < 2.5$ was multiplied by 1.5 while those between $2.5 < a < 2.8$ were multiplied by 3.0. Using values derived from their Table 2, one can estimate the relative contribution of Earth-crossers from each IS region by multiplying N_{esc}, the number of particles escaping from each source per Myr, by the total residence time spent in the Earth-crossing region. We find that the relative contribution of inner-IMC ($a < 2.5$ AU) and outer-IMC ($a > 2.5$ AU) is 7.7 and 6.8, respectively, while that of the HU, PH, and MB2 regions is 0.4, 1.3, and 0.2, respectively. These results suggest that the IMC region can be considered a primary source of NEAs, while the high inclination IS regions are smaller contributors to the NEA population.

An independent check on this conclusion can be obtained from the results of Jedicke and Metcalfe (1998). Recall that material availability is an important component to consider when discriminating between primary and secondary sources of NEAs. Since the HU, IMC, PH, and MB2 regions are all resupplied by resonances intersecting the main belt, the population of the main belt adjacent to these regions may tell us something about the strengths of each IS. Jedicke and Metcalfe (1998), using observations of nearly 60,000 asteroids by Spacewatch down to a limiting magnitude of $V \sim 21$, estimated the debiased orbital and absolute magnitude distribution of the main belt. They report that only $\sim 5\%$ and $\sim 20\%$ of all main belt asteroids with $2.0 < a < 2.6$ AU and $2.6 < a < 3.0$ AU, respectively, have $i > 15°$ orbits. This result implies that the population feeding the IMCs is potentially 5-20 times larger than the population feeding the PH and MB2 regions. The size of the source population replenishing the HUs is not precisely known, but it is unlikely to be significantly larger than the population of high-inclination objects residing in the main belt.

Finally, the EV population, unlike the IMC, PH, MB2, or HU populations, is not adjacent to any "stable" asteroid reservoir. Numerical results suggest that most EV asteroids come from the NEO region or the HU population (Migliorini *et al.* 1998; Michel *et al.* 2000b; Bottke *et al.* 2000a). Since these objects are already accounted for in our procedure (i.e., in a steady state, the flux into the EV region must equal the flux out), the EV region is rejected as a possible IS.

2.5. The outer main belt population

There is another potential source of NEAs which we have not yet described. It is possible that the outer main belt (OB), with $a \geq 2.8$ AU, provides large numbers of asteroids to powerful resonances like the 5:2, 7:3, 9:4, and 2:1 mean-motion resonances with Jupiter and to numerous three-body resonances. If true, we would expect that many OB asteroids currently reside on unstable orbits, such that they will eventually evolve into the NEO region. To test this idea, we integrated nearly 2000 observed main belt asteroids with $2.8 < a < 3.5$ AU and $i < 15°$ for 100 Myr, using the orbital parameters provided by the database of Ted Bowell (http://asteroid.lowell.edu). The asteroids were divided into five sets labeled OB1-OB5. These bodies were followed for at least 100 Myr of integration time; those that entered the NEO region were tracked until they entered a sink. The orbital parameters for each set and the mean time spent by the asteroids in the NEO region before entering a sink can be found in Table 2. Fig. 1 shows the location of OB1-OB5 in (a, e) space.

EDITOR: PLACE TABLE 2 HERE.

Using these integrations, we created a residence time plot using the objects which entered the NEO region (Fig. 6). We found that most of the OB objects that entered the NEO region were readily pushed onto Jupiter-crossing orbits and were subsequently ejected from the inner solar system. The mean time spent in the NEO region by the OB1-OB5 particles was 0.14 Myr, about 16 times shorter than the comparable value for the 3:1 resonance and much smaller than the other primary IS regions described so far. Only 6% of the asteroids evolving from the OB region achieve $a < 2.0$ orbits, a small fraction compared to other IS sources. Hence, since the *persistence* factor is small, the only way that OBs can be considered a primary source of NEAs is if *strength* or *material availability* is large relative to the other primary IS regions.

EDITOR: PLACE FIGURE 6 HERE.

To evaluate the *strength* factor, we turn to the numerical integration results tabulated in Table 2. In regions OB1, OB3, and OB5, 16%, 35%, and 26% of the integrated objects escaped the main belt in 100 Myr, respectively. These values are comparable to the number of objects escaping the IMC region over the same interval of time. Hence, we cannot rule out the OB region on this basis.

To evaluate material availability in the outer main belt, we used two methods. For our first attempt, we examined 682 asteroids in the main belt with diameter $D > 50$ km (e.g., Bottke *et al.* 1994). This population is considered observationally complete, such that it can be used to crudely estimate the flux of material reaching various main belt escape hatches. The ratio of $D > 50$ km bodies in the outer main belt ($a > 2.8$ AU) to those in the inner main belt is 1.6. (Note: comparable results can be obtained by examining the debiased orbital and absolute magnitude asteroid population calculated from Spacewatch results; Jedicke and Metcalfe 1998). For our second attempt, we computed the observed number of $H < 15$ objects in the diffusive OB1, OB3, and OB5 regions (883) and compared this value to the observed number of $H < 15$ objects in the IMC region (326). Objects with $H < 15$ in the main belt are currently incomplete, but they nevertheless provide a useful benchmark for estimating how the small body populations change from region to region (e.g., Jedicke and Metcalfe 1998). We find that our selected OB regions have nearly 3 times as many $H < 15$ objects as the IMC region, such that the asteroidal flux out of the OB region may partially compensate for its poor location (i.e., the proximity of Jupiter to the OB region guarantees most NEOs will not survive for long). Accordingly, we designate the OB region as a primary IS.

2.6. The ecliptic comet population

The ecliptic comet (ECOM) population, defined by Levison (1996) as having $T > 2$, contains the Encke-type comets, only 1 which is known, the Jupiter-family comets (JFCs), the Centaurs, and part of the scattered comet disk beyond Neptune. The "JFC region" is defined as the population of objects having $2 < T < 3$. The observed population of active JFCs inside and outside the NEO region currently stands at ~ 150 objects. Many JFCs are believed to have evolved from the Transneptunian region (Duncan *et al.* 1988; Levison and Duncan 1997; Duncan and Levison 1997), though some may also come from the Trojan populations (e.g., Rabe 1971; Levison *et al.* 1997). Numerical integrations results suggest that both escaped Trojans and ECOMs reaching the JFC region follow very similar dynamical paths (Levison *et al.* 1997). The estimated escape flux of Trojans is small enough, however, that Trojans may only make up $\lesssim 10\%$ of the total JFC population. For this reason, we treat the Trojan population as a secondary IS and assume its contribution can be folded into JFC component derived from the ECOM integrations.

To understand how these objects evolve inward from the Transneptunian region, Duncan *et al.* (1995) integrated 1300 test bodies started on low-eccentricity (0.01-0.3), low-inclination (1°) orbits for up to 4 Gyr. Objects reaching Neptune-encountering orbits after 1 Gyr of integration time were considered representative of objects currently leaving the Transneptunian region. Levison and Duncan (1997) then chose 20 of these test bodies, all with initial $e = 0.05$ and $i < 16°$ for their first encounter with Neptune, as their initial conditions for a new set of Kuiper belt integrations. These bodies were then cloned 99 or 149 times, depending on the speed of the computer on which the run was performed. Together, a total of 2200 clones were integrated. We assume that these orbits constitute the IS region of the JFCs. The orbits of these bodies were tracked until they entered a major sink or until time elapsed. Particles reaching $a < 2.5$ AU orbits were cloned 9 times to increase statistics in this zone. Numerical results suggest the median dynamical lifetime of ECOM objects before entering a sink is 45 Myr, though the majority spend much of their time on $a > 32$ AU orbits. Roughly 30% of the objects reach $q < 2.5$ AU at some point in their evolution, with 99.7% of these objects being JFCs when they first become "visible" (i.e., when they enter $q < 2.5$ AU orbits for the first time).

We find the vast majority of NEOs from the ECOM source have $2 < T < 3$ orbits, consistent with the parameters of the JFC population. Hence, we label the ECOM contribution to the NEO population as $R_{\rm JFC}(a, e, i)$ (Fig. 7). Some of our integrated test bodies in the NEO region, however, have pushed beyond the nominal perimeter of the JFC region. Thus, we do not confine our model to strict values of T, but instead use integration information for all ECOM bodies with $q < 1.3$ AU.

EDITOR: PLACE FIGURE 7 HERE.

The upper limit of our model was set to $a = 7.4$ AU, since NEOs with $a > 7.4$ AU obtain Tisserand values with respect to Jupiter of $T < 2$. We suspect that the contribution of nearly-isotropic population comets, which are not included in our model (see the discussion in the next section) dominates the $T < 2$ region.

In order to determine whether the JFC population constitutes a primary IS, we need to evaluate its *material availability*. This is difficult, since (a) the ratio of inactive-to-all JFCs is not clearly known, and (b) determining the nucleus diameter of an active comet from the comet's total magnitude is problematic (Zahnle *et al.* 1998). Nevertheless, efforts have been made by many groups, with most recent efforts by Levison and Duncan (1997) and Levison *et al.* (2000). Levison *et al.* (2000) estimated that the steady-state ECOM population with $D > 1$ km is $\sim 6.5 \times 10^7$. Numerical integration results suggest the fraction of ECOMs which enter the JFC region and have $q < 1.3$ AU is 1×10^{-5}. Multiplied together, these values suggest that the steady-state number of km-sized objects in the JFC region is ~ 650. We believe this value is large enough that Spacewatch should have discovered at least a few of them so far. In fact, Spacewatch has discovered 5 NEOs and accidentally re-discovered 1 NEO in the JFC region (Fig. 1). These objects lie near the peak of $R_{\rm JFC}(a, e, i)$ (Fig. 7). This fact, combined with the short persistence of objects in the JFC region (~ 0.1 Myr; Levison and Duncan 1994), suggests that a large source of material like the ECOM population may produce these Spacewatch objects. Accordingly, we believe the JFCs should be considered a primary IS.

It is generally believed that JFCs supply some of these objects found on Encke-type orbits ($T > 3$ and $a < a_J$), with the rest provided by the asteroid belt. A problem in using Levison and Duncan's comet integrations for our NEO model is that no test objects are as strongly decoupled from Jupiter as 2P/Encke (though some do reach $T > 3$ orbits). Based on this result, Levison and Duncan (1997) concluded that their integrations must be missing some important physical process. Possibilities include the gravitational perturbations of the terrestrial planets and/or non-gravitational forces produced by an active comet. The question of a missing mechanism is important because 2P/Encke may be the only active member of a significant population of extinct comets on $T > 3$ orbits. Such a population could provide a natural explanation for at least some of the transitional objects described in Sec. 1.

Though we have not attempted to update the Levison and Duncan (1997) integrations for this paper, we can draw some insights from our OB integrations, which did include the terrestrial planets (but not non-gravitational forces). As a test, we computed the residence time function $R_{\rm OB}(a, e, i)$ only after OB asteroids had achieved $T < 3$ orbits and Jupiter-crossing orbits ($Q > 4.61$ AU). We found that 343 of the 363 OB test bodies that met this dynamical criterion also attained $T < 3$ orbits, presumably via the combined efforts of chaotic resonances and close encounters with the terrestrial planets. The residence time function produced from these objects was similar to that plotted in Fig. 6. After reaching $T < 3$ orbits, many of these particles evolved temporarily back into the $T > 3$ region. From our residence time function, we found that 51% of the steady state population should be on $T > 3$ orbits (i.e., 14% with $a > 3.0$ AU, 33% with $2.5 < a < 3.0$ AU, and 4% with $a < 2.5$ AU). A few test bodies even reached the same (a, e, i) bin as 2P/Encke, which resides at ($a = 2.2$ AU, $e = 0.85$, $i = 11.8°$). In contrast, only 3% of the steady state population from $R_{\rm JFC}(a, e, i)$ achieved $T > 3$ orbits, with none reaching $T > 3$; $a < 2.5$ AU.

Using values from our OB integrations, we can use a back-of-the-envelope calculation to estimate the expected number of active NECs with $a < 2.5$ AU. Levison *et al.* (2000) claims there are 650 bodies larger than 1 km in the JFC population. Multiplying this value by 4%, the fraction on NEO orbits with $a < 2.5$ AU, we estimate there are ~ 30 km-sized NECs with $a < 2.5$ AU. On the other hand, Bottke *et al.* (2000a) suggested there may be ~ 800 km-sized NEAs with $a < 2.5$ AU. By this reckoning, the Encke-type NECs with $a < 2.5$ AU are not a significant component of the overall NEO population. The spectroscopic similarity of many observed NEOs to objects in the inner main belt provides additional support for this claim (e.g., Shoemaker *et al.* 1990). On the other hand, our results also predict there may be ~ 200 km- sized Encke-type objects with $2.5 < a < 3.0$ AU, many more than the ~ 100 predicted by Bottke *et al.* (2000a). More complete integrations and more precise estimates of the JFC population will be needed to clarify this issue. We also caution that our OB predictions should not be taken too far, since there may be significant differences between $T < 3$ test objects started in the main belt, many which evolve out onto $T > 3$ orbits via mean motion resonances with Jupiter, and test objects evolving from comet reservoirs in the Transneptunian region.

Based on these results, we make a few predictions. (i) Non-gravitational forces may not be needed to move active and extinct comets onto Encke-type orbits, though further testing is needed, and (ii) tests suggest that objects evolving from the JFC region onto $T > 3$ orbits are unlikely to overwhelm the population of asteroids with $a < 2.5$ AU. For these reasons, as well as those described above, we believe it is a reasonable approximation to assume that Levison and Duncan's integration results adequately describe the dynamics of objects evolving from the ECOM population. Until a more complete cometary dynamical model is ready, this is the best we can do with the available data.

2.7. The nearly-isotropic population comets

The nearly-isotropic population comets (NICs) are thought to come from the Oort cloud, which is located at a distance of $a > 3000$ AU (Weissman 1996). There are two main types of NICs: (i) Long period comets (LPCs), with periods longer than 200 years and $T < 2$, and (ii) Halley- type comets (HTCs), with periods less than 200 years and $T < 2$ (Levison 1996). Both reside outside the JFC region. The observed population of LPCs has nearly-isotropic inclinations, while HTCs show a preference for prograde orbits (Levison *et al.* 2001). By definition, LPCs must have $a > 35$ AU, but about one-third of the observed LPCs have $a \sim 20,000$ AU (Weissman 1996). Most of the observed HTCs, which have traditionally been considered the short-period tail of the LPCs, have $a \sim$ 10-30 AU (Weissman 1996). In either case, for NICs to reach $q < 1.3$ AU orbits, they need $e \sim 1$. Fig. 1 shows the NIC region for $T < 2$; $i = 0°$. We caution that this figure is a bit misleading, since NICs are unlikely have $i \sim 0°$ orbits, and the $T < 2$ range moves to $a \gtrsim 2.6$ AU as i approaches 90°. Unfortunately, the parameters that do a good job at characterizing various asteroid populations on plots, namely a, e, and i, are not as useful for plotting comet populations. The size of the NIC population is not well known. To explain the orbital distribution of the observed population, several groups have postulated that returning NICs "fade" away with time, possibly from the depletion of their volatiles or by splitting events which cause them to break into smaller (and harder-to-see and/or short-lived) components (Weissman 1996; Wiegert and Tremaine 1999; Levison *et al.* 2001). Since the number of faded comets to new comets has yet to be determined, calculating the population of NICs on NEO orbits is problematic. Despite this, best-guess estimates suggest that impacts from NICs may be responsible for 10-30% of the craters on Earth (Shoemaker 1983; Weissman 1990; Zahnle *et al.* 1998). If true, NICs must be considered a primary source of NEOs.

At this time, $R_{\rm NIC}(a, e, i)$ is unknown. Moreover, Spacewatch has yet to discover a NIC with a $q < 1.3$ AU orbit. This scarcity of discoveries is not surprising when one considers that NICs spend most of their time far from Earth. Since we lack the statistical information necessary to calibrate the NIC population, we leave this potential primary IS to future work. Thus, as stated in the previous section, our NEO model neglects a possible contributor to $T < 2$ orbits. The lack of NIC detections in the inner solar system and the distribution of the known HTCs, however, suggests that the NIC population with $a < 7.4$ AU may be small. We leave this issue to future work.

3. Modeling the NEO Population

3.1. The orbital distribution of NEOs

In Sec. 2, we identified five primary IS regions (i.e., ν_6 resonance, IMC region, 3:1 resonance, OB region, and JFC region) capable of producing NEOs in the inner solar system. Each IS produces NEOs with a distinctive relative orbital distribution ($R_{\rm IS}(a, e, i)$). Neglecting the contribution of secondary IS sources, the relative orbital distribution of the entire NEO population will be a linear combination of the sub-populations coming from each primary IS. Thus, we define:

$$R_{\rm NEO} = \alpha_{\nu_6} R_{\nu_6} + \alpha_{\rm IMC} R_{\rm IMC} + \alpha_{3:1} R_{3:1} + \alpha_{\rm OB} R_{\rm OB} + \alpha_{\rm JFC} R_{\rm JFC}. \tag{2}$$

where the coefficients $\alpha_{\rm IS}$ are free positive parameters, with total sum equal to 1.0. If the $R_{\rm IS}(a, e, i)$ functions are statistically distinct, we can determine the coefficients $\alpha_{\rm IS}$ by fitting an observed distribution of NEOs with $R_{\rm NEO}(a, e, i)$. To perform this procedure, we require an estimate of the relative absolute magnitude distribution of the NEOs and of the biases associated with NEO discoveries.

3.2. The absolute magnitude distribution of the NEOs

The absolute magnitude distribution of the NEOs ($N_{\rm NEO}(H)$; cumulative form) has been estimated by several groups over the last decade: Rabinowitz (1993), Rabinowitz *et al.* (1994); Rabinowitz *et al.* (2000), and Bottke *et al.* (2000a). In the papers led by Rabinowitz, observational data from Spacewatch and NEAT were used to calibrate computer codes capable of simulating a NEO survey looking for realistically-distributed objects. The paper led by Bottke used observational selection effects associated with the Spacewatch NEO survey which were derived analytically and solved numerically (Jedicke 1996), with the results applied to NEO data. The resultant function in both cases was a debiased version of $N_{\rm NEO}(H)$.

The latest two versions of the cumulative distribution $N_{\rm NEO}(H)$ derived by Rabinowitz *et al.* (2000) and Bottke *et al.* (2000a) have the same functional form for 13-15$< H < 22$ objects:

$$N_{\rm NEA}(H) = C_{\rm NEA} \times 10^{\gamma(H-H_0)} \tag{3}$$

with $\gamma = 0.35 \pm 0.02$, $C_{\rm NEA}$ being a normalization constant of material coming from the asteroid sources, and H_0 being the lower limit of the H range. Since the biases computed by Jedicke (1996) are only applicable to $H < 22$ objects, we do not examine the $H > 22$ population at this time. As discussed in the papers by Rabinowitz, small objects are usually found through a direct examination of the image by the observer and therefore must suffer from a different bias than automated NEO detections. In this paper, we have constrained our model to the H range where the automated detections are common.

Bottke *et al.* (2000a) defined $C_{\rm NEA}$ using the total number of $13 < H < 15$ objects in the NEO population with $a < 3.0$ AU. Determining a precise value for $C_{\rm NEA}$ is difficult because the population of $13 < H < 15$ objects is currently incomplete. As of December 2000, the known population of $H < 15$ objects with $a < 2.8$ AU stood at 53. To get the total number of NEOs with $H < 15$, we need to estimate the completeness of this population. One way to estimate this value is to use observational data. For example, between March 1996 and August 1998, the NEAT program found 12 $H < 16$ objects, 10 of which were already known (Rabinowitz *et al.* 2000). 10 of 12 yields a completeness value of $\sim 80\%$. We assume this value is applicable to the $H < 15$ objects as well. Hence, $53/0.80 \approx 66$ NEOs with $H < 15$. An alternative way to get this value is to divide the number of already-discovered NEOs by the ratio of the number of new discoveries to total detections (i.e., new discoveries plus re-detections) in the year 1999 (Harris 2000). Doing this yields a completeness factor near 73%, such that there may be 73 ± 7 NEOs with $H < 15$. It is not clear which method yields the most accurate result. For this reason, Bottke *et al.* (2000a) split the difference and assumed there were 70 $H < 15$ NEOs. Since we know of 4 $H < 13$ NEOs, the number of $13 < H < 15$ objects was set to 66. This value yields $C_{\rm NEA} = 13.26$. Hence, Bottke *et al.* (2000a) found that:

$$N_{\rm NEA}(H) = 15.42 \times 10^{0.35(H-13)} dH. \tag{4}$$

This function was originally obtained by Bottke *et al.* (2000a) to apply solely to bodies on $a < 3.0$ AU orbits. In this paper, however, we must also consider comets from the JFC region, many with $a > 3.0$ orbits. To extend the reach of this equation into the JFC region, we multiply $C_{\rm NEA}$ by the ratio of the total residence time of the NEO region with $a < 3.0$ AU over the total residence time of the entire NEO region, yielding:

$$C_{\rm NEO} = C_{\rm NEA} \times \frac{\sum_{a,e,i} R_{\rm NEO}(a,e,i)}{\sum_{a<3{\rm AU},e,i} R_{\rm NEO}(a,e,i)}. \tag{5}$$

$C_{\rm NEO}$ will be determined once the $\alpha_{\rm IS}$ coefficients are computed. The result will be used to find $N_{\rm NEO}(H)$:

$$N_{\rm NEO}(H) = C_{\rm NEO} \times 10^{0.35(H-H_0)} dH \tag{6}$$

To convert H into a characteristic NEO diameter, we need to understand the albedo distribution of the NEO population. The ratio of bright-to-dark objects in the NEO population, however, is unknown. The latest work on this topic that we can find was completed over ten years ago (Luu and Jewitt 1989; Shoemaker *et al.* 1990). We find it useful (though not necessarily accurate) to use the approximation suggested by Rabinowitz *et al.* (1994) and assume the NEO population has a 50-50% mix of bright/dark objects. Applying the bolometric geometric albedos for S-type (i.e., a representative bright body) and C-type (i.e., a representative dark body) asteroids described in Tholen and Barucci (1989), our conversion formula between H and diameter D works out to be (Bowell *et al.* 1989):

$$D({\rm km}) = 4365 \times 10^{-H/5}. \tag{7}$$

To change $N_{\rm NEO}(H)$ into a cumulative size distribution without worrying about the albedo distribution, however, all we need to know is $D \propto 10^{-H/5}$ (e.g., Jedicke and Metcalfe 1998). Thus, $N(>D) \propto D^{-1.75\pm0.1}$ for objects between 200 m and 4 km in diameter. The value of this slope index is shallower than the slope index of a population in simple collisional equilibrium (i.e., 2.5; Dohnanyi 1969) or one dominated by fresh collisional debris (i.e., > 2.5; Tanga *et al.* 1999). This value, however, does agree with the size distributions of youthful cratered surfaces on Venus, Earth, Mars, and the Moon. On Earth, the cumulative size distribution of craters larger than 20-30 km has a power-law slope of 1.8 (Grieve and Shoemaker 1994). On the Moon, craters on the maria with $3 < D_{\rm crater} < 100$ km in diameter have a power-law slope of 1.7, though some of the larger craters have been enlarged by collapse. A correction for crater collapse increases the slope to 1.84 (Shoemaker 1983). On Mars, craters on the young plains units with $10 < D_{\rm crater} < 50$ km have a power-law slope of 2.0 (Strom *et al.* 1992), while on Venus, craters with $D_{\rm crater} > 35$ km have a power-law slope of ~ 2.0 (Schaber *et al.* 1992).

A caveat about our procedure should be mentioned here. Eq. (6) assumes that the slope index of the NEO size distribution is the same for all primary IS regions. This approximation is justified if NEAs, supplied to resonances by the Yarkovsky effect from a collisionally-evolved main belt population, get trapped in the IS regions in size-independent proportions. If our asteroid $\alpha_{\rm IS}$ values change with asteroid size, however, our model will need to become correspondingly more sophisticated. Sec. 7.1 discusses this issue in more detail. In addition, our method of using a single H distribution function becomes questionable when it is applied to the NEC population. Since NECs are supplied by a different ultimate source (i.e., the Transneptunian region and Oort cloud), they may have an H distribution with a very different shape than the NEAs.

At this time, we lack the observational data needed to determine whether the H of various IS regions in the main belt and/or the NEC H distributions differ significantly. In terms of the asteroid vs. comet population, though, the existing evidence from cratered surfaces, suggests that the two populations may be similar. For example, asteroids, which are believed to dominate the impactor flux on the terrestrial planets, produced crater size distributions with $N(> D_{\rm crater}) \propto D_{\rm crater}^{-1.8}$ to $D_{\rm crater}^{-2.0}$. Comets, which dominate the impactor flux on the Galilean satellites, produced crater size distributions with $N(> D_{\rm crater}) \propto D_{\rm crater}^{-2.2}$ (Passey and Shoemaker 1982; Shoemaker and Wolfe 1982). Converting these crater distributions back into impactor size distributions is problematic, since the properties of the projectiles and the targets are not well known. Still, scaling law relationships (and observational data) suggest that projectile size distributions usually produce crater size distributions with similar slope indices (Shoemaker and Wolfe 1982; Shoemaker *et al.* 1990; Rabinowitz 1993; Zahnle *et al.* 1998). Hence, it is probable that the aforementioned crater populations were produced by projectiles with $N(> D) \propto D^{-2.0}$. Since our derived NEO size distribution is $N(> D) \propto D^{-1.8}$, we believe we are probably safe in assuming that the NEO population can be reasonably modeled using a single slope parameter γ. When additional observational data becomes available, we will be in a better position to split our NEO absolute magnitude distribution into cometary, asteroidal, or sub-cometary and sub-asteroidal components.

3.3. The orbital and absolute magnitude distribution of the NEOs

We can now combine the functions from the previous two sections to model the debiased orbital and absolute magnitude distribution of the NEOs, $M(a, e, i, H)$:

$$M\left(a,e,i,H\right) = R_{\rm NEO}\left(a,e,i\right) \times N_{\rm NEO}\left(H\right). \tag{8}$$

Remember that the $\alpha_{\rm IS}$ values are still free parameters at this stage. To determine them, we need to compare $M(a, e, i, H)$ with the known NEOs, which cannot be accomplished until several issues (e.g., observational biases) are addressed.

4. Issues to Consider Prior to Comparing Our NEO Model with Data

4.1. Observational biases

The IAU Minor Planet Center reports that, as of December 20, 2000, 1223 NEO have been discovered with $9.5 < H < 29$ (i.e., 95 Atens, 562 Apollos, and 566 Amors). It is thought that only the NEOs with $H < 14$ can be considered an observationally complete set (e.g., Rabinowitz *et al.* 2000), though some dark and distant NEOs with $H < 14$ may yet be detected in the future. Regardless, the rest of the discovered NEOs, with $H > 14$, have orbital parameters which suffer from observational selection effects. The surveys that are actively searching for NEOs today use a variety of telescopes, detectors, and detection strategies. They are also flux-limited, such that the volume of space each survey investigates varies strongly with H. Without extensive documentation of each NEO discovery and a good understanding of each survey's particular characteristics, any attempt to debias the entire population of observed NEOs is impractical. For this reason, this study uses the discoveries and accidental re-discoveries provided by Spacewatch, whose capabilities and procedures have been well documented over the last ten years (e.g., Rabinowitz 1994).

To debias the Spacewatch NEO population, we apply an analytical method for determining the probability that an object with parameters (a, e, i, H) will be detected by a Spacewatch-like system, one whose limiting magnitude and moving object detection capabilities mimic that of the time-averaged Spacewatch system. (For a more detailed discussion of the procedure, see Jedicke 1996; Jedicke and Metcalfe 1998). The bias per square degree at opposition was calculated as the average bias over a 100 deg^2 region centered at opposition. This bias was then binned in cells of (a, e, i, H) space to obtain a discrete function which we will call $B(a, e, i, H)$.

B has been calculated over the range $0.5 < a < 2.8$ AU, $e < 0.8$, $i < 35°$ and $H < 22$. This region, which we call the constrained target region (hereafter the CTR), is smaller than the extended target region (ETR) described in Sec. 2. High B values correspond to easily detected asteroids, while low B values correspond to difficult-to-detect asteroids. Objects with high B values are bright and/or large objects which move slowly through Spacewatch's search volume (e.g., multi-km main belt asteroids, IMCs, NEOs on low-i orbits with a between 2-3 AU). Conversely, low B values are dim and/or small objects which have such fast angular speeds that they spend little time in Spacewatch's search volume (e.g., sub-km NEOs that rarely approach Earth, high-i asteroids).

Only a small proportion of Spacewatch's detections are NEOs. To separate NEOs from more numerous background asteroids, Spacewatch calculates the angular rate of motion for each detected body and uses this value as a discriminant. At opposition, objects with ecliptic latitude rates between ±0.3 deg/day and ecliptic longitude rates between −0.2 to −0.3 deg/day are usually main belt or IMC asteroids (e.g., Jedicke 1996). Objects with rates of motion outside this zone are often flagged as potential NEOs and can be followed over several observing nights until an orbit solution is obtained. If that solution yields $q < 1.3$ AU, Spacewatch reports an NEO discovery. This method, while useful, eliminates some NEOs; perhaps a third of all of Spacewatch's NEO detections have rates of motion which mimic typical main belt asteroids. Most excluded NEOs have $a > 2$ AU.

It is unclear to us how to properly account for this rate of motion discriminant in our NEO model. As Jedicke (1996) has shown, small differences in the ecliptic longitude rate can lead to an object being classified as a potential NEO or a main belt object. Moreover, this rate discriminant changes as the observer looks for NEOs away from opposition. In typical situations, where 200 objects or more can appear on Spacewatch's monitor after a scan, observer intuition can count as much as probability maps at filtering NEOs out of a background population of main belt objects.

To do the best with the available information, we synthesize these various bias corrections into a simple filter which excludes all objects with ecliptic latitude rates between ±0.3 deg/day and ecliptic longitude rates between −0.2 to −0.3 deg/day. This filter is then incorporated into B; objects with rates of motion in this range are given a zero bias to account for the fact that Spacewatch will not track them. We call this more specific bias $B_{\rm NEO}$. We believe that $B_{\rm NEO}$ is a reasonable compromise for the competing effects described above, but we caution that we may need to cast our "rate of motion" net even further to explain Spacewatch's unique observations. We will return to this important issue in Sec. 5.2.

Using $B_{\rm NEO}$, our predicted distribution for the observed Spacewatch NEOs is:

$$n\left(a,e,i,H\right) = B_{\rm NEO}\left(a,e,i,H\right) \times M\left(a,e,i,H\right) = B_{\rm NEO}\ \left(a,e,i,H\right)\ R_{\rm NEO}\left(a,e,i\right)\ N_{\rm NEO}\left(H\right) \quad (9)$$

$B_{\rm NEO}$ can, in principle, be used to estimate the entire NEO population from the known NEOs without using our numerical integrations; all we have to do is divide the observed population by the bias factor directly. This type of procedure has already been used to estimate the debiased main belt size distribution down to a few km in diameter (Jedicke and Metcalfe 1998). The problem for the NEO orbital distribution, however, is resolution; the limited number of Spacewatch NEOs do not provide enough coverage to normalize a wide-ranging probability distribution without leaving large tracts of (a, e, i, H) space without a single NEO (i.e., our $B_{\rm NEO}$ uses $\sim 30,000$ bins). Until the NEO inventory gains more entries, $B_{\rm NEO}$ cannot be directly used to produce statistically meaningful NEO population estimates. Previous efforts to circumvent this problem can be found in Rabinowitz (1993) and Rabinowitz *et al.* (1994).

Spacewatch has discovered and accidentally re-discovered 166 NEOs with $a \leq 2.8$ AU, $e \leq 0.8$, $i \leq 35°$, and $13 \leq H \leq 22$ (i.e., over the CTR). From these objects, we selected a more specific set based of their distance from opposition at discovery and $P_{\rm rate}$, the probability that an object with a particular rate of motion could be considered an NEO (Jedicke 1996). We found 138 objects detected within 50° of opposition that also had $P_{\rm rate} > 20\%$. Since the (a, e, i) values of these objects were statistically similar to objects found within 20° of opposition, the region where $B_{\rm NEO}$ is most applicable, we used this entire set to constrain our NEO model.

Finally, we point out that our $B_{\rm NEO}$ may not properly account for the population of objects discovered in the JFC region ($2 < T < 3$). Duncan *et al.* (1988) have shown that observed and "integrated" short period comets with $q < 1.5$ AU have argument of perihelion values which, when binned and plotted as a histogram, do not fit a uniform distribution (see their Figure 2). Instead, short period comets have a distribution where the argument of perihelion is maximized near 0° and 180° and is minimized near 90° and 270°. There is roughly a factor of 10 between minimum and maximum bin values on this distribution. This unique shape is probably brought about by the constraints impressed upon the bodies which dynamically evolve into the JFC region and have $T < 3$ and $q < 1.5$ AU. At this time, our debiasing technique assumes the argument of perihelion for all NEOs is uniform. For this reason, the computations' presented in this paper may under- or over-estimate the real population of objects in the JFC region. Future work will be needed to determine the impact of this unusual distribution on our results.

4.2. Degeneracy between the IS regions

An issue which we have not yet discussed but which is important to interpreting the results of our NEO model is *degeneracy*, or the unavoidable problem that some IS regions produce similar $R_{\rm IS}(a, e, i)$ distributions.

Degeneracy usually occurs when IS regions are located so close to one another that they share overlapping orbital pathways. Fig. 8 shows an example of degeneracy between the inner IMC region (solid histogram) and the ν_6 resonance (black line). Except for differences observed near $e = 0.4$-0.5 and $i = 5°$-$10°$, the residence time functions are quite similar (though plotting both $R_{\rm IS}(a, e, i)$ functions as a series of one- dimensional plots may exaggerate the problem). This result suggests that our NEO model may not be able to easily discriminate between these two inner main belt source regions, especially when NEO data are sparse.

EDITOR: PLACE FIGURE 8 HERE.

Recall that our ultimate goal in the paper is to fit our "biased' NEO model $n(a, e, i, H)$ to the NEO data provided by Spacewatch. The shape of $n\,(a, e, i, H)$, therefore, determines the $\alpha_{\rm IS}$ values. If degeneracy is an important factor between two IS regions, our fitting procedure will be unable to construct a unique solution by geometric means. In such a situation, we can expect to generate large formal $\alpha_{\rm IS}$ error bars, possibly because the corresponding error ellipsoid is rotated with respect to our chosen parameter space, or possibly because the error ellipsoid itself has large extrema. Inside the error ellipsoid, each set of $\alpha_{\rm IS}$ values would be equally valid.

To combat degeneracy, we have integrated large sets of test bodies and we have made some effort to distinguish boundaries between adjacent IS regions. The chaotic nature of the inner solar system, however, makes some degeneracy inevitable. For this reason, we use an alternative method to deal with this problem. Observations of main belt asteroids and numerical integration of bodies inside the asteroidal IS regions provide additional constraints which we can be included into our fitting procedure. In particular, we can use the predicted size of the source populations replenishing the IS regions and the flux of material coming from various IS region as additional weighting factors. If computed properly, these new "boundary conditions" will hopefully cause $\alpha_{\rm IS}$ to converge to their true values while also decreasing the size of their associated error bars. Note that these additional boundary conditions must be tuned to just the right level: if they are weighted too heavily, the code will give the correct IS population but will produce a poor match in the NEO region; if they are weighted too lightly, our fitting routine will return a NEO model with large error bars.

In the next two subsections, we describe the formalism needed to produce these model constraints (i.e., the NEO flux from each IS region and the steady state IS populations.)

4.3. Generation rates of NEOs

Using our numerical integration results and our NEO model, we can quantitatively examine the influx rates needed keep the NEO population in steady state as well as the steady state population of each IS region. The parameters needed to generate these values can be used to constrain our NEO model. In this section, we will develop the formalism needed to get these parameters. Our results will be discussed later in Sec. 7.

Up to now, only order–of–magnitude estimates exist on the rates at which main belt asteroids are supplied to the ν_6 and 3:1 resonances via collisions (Farinella *et al.* 1993; Menichella *et al.* 1996; Rabinowitz 1997a,b; Zappalá *et al.* 1999) or semimajor axis mobility caused by the Yarkovsky force (Farinella and Vokrouhlický 1999). Estimates of the number of NEOs supplied by the Mars–crosser population can be found in Migliorini *et al.* (1998), Morbidelli and Nesvorný (1999) and Michel *et al.* (2000b). They are based on statistics of the evolution of *known* asteroids, which constitute a biased sample. Similarly, the rate at which new JFCs are supplied from the Kuiper belt has been estimated in Levison and Duncan (1997) and revised in Levison *et al.* (2000) on the basis of the number of active JFCs and their expected dynamical and physical lifetimes. For the first time, we have the opportunity of computing all these rates with a unique and consistent model.

4.3.1. Flux rate of bodies moving from the IS region to the NEO region

To compute the rates at which new objects are supplied to the NEO population from each IS, we first focus our attention on a simple example. Imagine a system where a *source region* supplies new objects to a *target region*. The bodies spend some time in the target region, until they find their way to the *sink*, where they are destroyed. If arrows represent the influx/outflux of material from each zone, we get:

$$\text{Source Region} \longrightarrow \text{Target Region} \longrightarrow \text{Sink}$$

We define $p(t)$ as the differential probability that a particle spends a time t in the target region. We assume for simplicity that $p(t)$ is effectively 0 for t larger than a given time T. Then, the mean lifetime in the target region is given by:

$$< L_{\rm TR} >= \int_0^\infty tp(t)dt = [tP(t)]_0^T - \int_0^T P(t)dt = T - \int_0^T P(t)dt \ , \tag{10}$$

where $P(t)$ is the integral of $p(t)$ and $P(T) = 1$. We now define I as the steady state influx rate into the target region, namely the number of particles that enter the target region from the source in the time interval dt is Idt. Once the steady state is reached, the number of particles that entered the target region in the time interval $(t_0 - t, t_0 - t + dt)$ and are still resident in the target region at time t_0 is:

$$n(t) = I \int_t^T p(\tau)d\tau \ , \tag{11}$$

independent on t_0. Thus, the steady state number of particles in the target region is:

$$N_{\rm TR} = \int_0^T n(t)dt = I \int_0^T (1 - P(t))dt = I \times [T - \int_0^T P(t)dt] \ . \tag{12}$$

Formulae (10) and (12) prove the relatively well known result in statistical physics that the steady state population in the target region $N_{\rm TR}$, the mean lifetime in the target region $< L_{\rm TR} >$ and the influx rate from the source I are related by the equation:

$$I = \frac{N_{\rm TR}}{< L_{\rm TR} >} \ . \tag{13}$$

Notice that this formula does not involve the *median lifetime* of the bodies, a parameter incorrectly used for this kind of estimates in several recent papers (e.g., Levison *et al.* 1997). It should also be realized that in the above derivation, it is not crucial that the bodies stay solely in the target region until they enter the sink. The bodies can temporarily go back to the source region, or spend some time in a region other than the source and the target regions. As long as we know the steady-state population in the target region and the mean time spent there by the bodies, we can compute the flux from the source for the first time into the target region (*first entry flux*) with formula (13).

Our NEO model is equivalent to this system, with the main difference being that we have five IS regions (ν_6, IMCs, 3:1, OB, JFCs) which are combined into a single NEO residence time probability distribution via weighting factors ($\alpha_{\rm IS}$). Thus, using $\alpha_{\rm IS}$, we can estimate the number of bodies coming from each IS region. In most cases, we define the target region above to be our extended target region (ETR) defined in Sec. 2. The "sink" corresponds to the major and minor sinks defined in Sec. 2.1. Table 3 lists the results of $< L_{\rm ETR} >$ for the five IS region. The formalism for computing the steady-state population of NEOs coming from each IS region will be described in the next section. Our results will be computed in Sec. 7.2.

EDITOR: PLACE TABLE 3 HERE.

4.3.2. Steady–state populations in the intermediate sources

In the previous section, $< L_{\rm TR} >$ and $N_{\rm TR}$ were used to compute the influx rate I from each IS to the NEO region. The route followed by asteroids from the main belt to the sink is:

$$\text{Main belt} \longrightarrow \text{IS} \longrightarrow \text{NEO region} \longrightarrow \text{Sink}$$

If the IS cannot communicate with the sink without passing through the NEO target region (which is effectively true for the ν_6, IMC, 3:1 and OB sources, but not for the Neptune–tangent region of the Kuiper belt where the JFCs come from), the inflow rate of material from the NEO region to the sink must equal the inflow rate from the IS to the NEO region and the inflow rate from the main belt to the IS. In other words, once we calculate the inflow rate anywhere, we have a good estimate of the inflow rate everywhere.

This principle can be used to deduce information about the IS region. Using the mean time spent by bodies in each IS region ($< L_{\rm IS} >$), we can hypothetically compute the steady-state population in each IS by inversion of formula (13). Unfortunately, our simulations cannot be used to compute $< L_{\rm IS} >$ because our test particles were started inside the IS. Information we can extract from the simulations, however, is the initial fractional decay rate of the IS populations. This value is sufficient for our goal of determining the flux rate into the IS regions if we assume that the test body initial conditions described in Sec. 2 are representative of the steady-state orbital distribution of the real IS population. (This condition is probably satisfied for the asteroidal IS regions, where observational data is plentiful, but not for the cometary IS regions). In fact, the simulated situation we used to derive $R_{\rm IS}(a,e,i)$ corresponds to a steady-state in which the IS is suddenly deprived of fresh material. The population of the IS region starts to decay into the sink, passing through the NEO region along the way. Assuming that the particles evolve independently of each other (as opposed to decay due to collisions), the decay flux is given by the equation

$$\frac{dN}{dt} = -\tau_{\rm IS}(t)N \tag{14}$$

where N is the population in the considered IS and $\tau_{\rm IS}(t)$ is its fractional decay rate.

On a sufficiently short time interval from the beginning of the integration, $\tau_{\rm IS}(t)$ can be approximated by a constant value $\tau_{\rm IS}$, so that the population $N(t)$ decays exponentially in time. Note that on a long timescale, the time–dependence of $\tau_{\rm IS}(t)$ cannot be neglected (in general) so that $N(t)$ deviates from an exponential law (Migliorini *et al.* 1997). Our numerical simulations provide the function $N(t)$. $\tau_{\rm IS}$ can be computed by best-fitting the first part of the decay with an exponential law.

Now, in a steady-state, the population in the IS is continuously resupplied by the main belt, so that the outflow rate of bodies into the sink is constant and given by

$$F_{out} = \tau_{\rm IS} N_{\rm IS} \ , \tag{15}$$

where $N_{\rm IS}$ is the steady-state population in the intermediate source and $\tau_{\rm IS}$ is the initial fractional decay rate computed from the simulations. On the other hand, F_{out} must be equal to the inflow rate into the NEO region I computed in the previous section. Thus we can compute $N_{\rm IS}$ from the equation:

$$N_{\rm IS} = \frac{I}{\tau_{\rm IS}} \ . \tag{16}$$

In the case where the particles can go from the IS to the sink without passing through the NEO region (as for the JFCs), we can use two methods. The first is to choose a larger target region (e.g., the entire ECOM region rather than just the JFC region). $\tau_{\rm IS}$ can then be calculated directly using the larger target region. The second method is to evaluate from the simulation the fraction f of the population that enters the NEO region. This sub–population can be used for the computation of the fractional decay rate $\tau_{\rm IS}$. The value $N_{\rm IS}$ obtained through (16) represents the steady-state number of bodies in the sub-population. Hence, the total number of bodies in the IS is simply $N_{\rm IS}/f$. We will employ the first method to examine the JFC/ECOM populations in Sec. 8.

For the computation of $\tau_{\rm IS}$, we consider the function $\ln F(t)$, where $F(t)$ is the fraction of the initial population that is still "active" in the simulation at time t. By "active", we mean that these bodies have not yet entered a sink. For example, in the case of the IMCs, we find that a small fraction of them never pass within a Martian Hill's sphere of Mars in 100 Myr. These bodies are probably protected from Martian encounters because of their non–negligible inclination or because they are in mean motion resonances with Mars, and are therefore considered *false* Mars–crossers. The ratio $F(t)$ is computed with respect to the population of the *true* Mars–crossers. Then, the function $\ln F(t)$ is fitted by the function $y = -\tau_{\rm IS}(t - t_0)$ over the interval $[0, T]$ of t. The coefficient t_0 is introduced to account for the fact that there is some delay between the beginning of the integration and the moment when the particles start to enter the sink, because the IS region and the sink are not adjacent. As discussed above, T should be as small as possible, but if it is too small the computation of $\tau_{\rm IS}$ will be poorly determined. Therefore, we compute the best–fit value of $\tau_{\rm IS}$ as a function of T and look for the range of T values corresponding to a stable value of $\tau_{\rm IS}$. Fig. 9 gives a graphical example of this procedure for the true IMC population. The slope of the fitted line yields $\tau_{\rm IMC} = 0.016$ Myr^{-1}.

EDITOR: PLACE FIGURE 9 HERE.

Table 3 reports $\tau_{\rm IS}$ for all of our primary IS regions. We find that $\sim$ 35-38% of the population initially in the 3:1 and ν_6 resonances go into the sink per Myr, consistent with the median lifetime of 2 Myr reported in Gladman *et al.* (1997). The mortality of IMCs is much lower (1.6% of the population per Myr), which yields a median lifetime of $\sim$ 60 Myr, confirming the value given in Michel *et al.* (2000b). The OB region has a comparable value ($\tau_{\rm OB} = 0.02$ Myr^{-1}). The values for τ for the cometary IS regions will be discussed in Sec. 8.

With $\tau_{\rm IS}$ and $< L_{\rm TR} >$ parameters from the asteroidal IS regions in hand, we now have the information we need to compare our NEO model to NEO data from Spacewatch.

5. Model Fit

5.1. Determination of the parameters of our NEO model

As explained in the previous sections, we have constructed a model, depending on 5 free parameters, that predicts the (a, e, i, H) distribution of NEOs. We now determine the values of the parameters by fitting the model to the data, following the method provided by Lyons (1986).

Let λ_m be the normalized data distribution of 138 NEOs discovered or accidentally re-discovered by Spacewatch in the CTR (i.e., $0.5 \leq a \leq 2.8$ AU; $e \leq 0.8$; $i \leq 35°$; $13 \leq H \leq 22$). We define m as the cell number, which is obtained by binning the data using (0.05 AU $\times 0.02 \times 5° \times 0.5$) cells in (a, e, i, H) space. The resultant λ_m contains 74592 cells. Note that limiting λ_m to 138 NEOs gives most of the λ_m cells zero values. Next, let D_m refer to our normalized biased NEO model $n(a, e, i, H)$. To simultaneously test in four dimensions how well the λ_m and the D_m distributions agree each other, we use a likelihood technique. This technique allows λ_m and D_m to be associated to a number, defined as:

$$\mathcal{L} = \left| \sum_m \lambda_m \log (D_m) \right| . \tag{17}$$

The best fit model is the one that minimizes $\mathcal{L}$. Of course, in Eq. (17) the sum is done over the entries on which the distribution D_m is not zero. If D_m is zero where λ_m is not, the function $\mathcal{L}$ is set to infinity.

5.2. Computing additional constraints for our fit

We also wish to include entries for other bins which can help us avoid the partial degeneracy problems described in Sec. 4.2. As described previously, these bins should act like added weighting factors, allowing $\alpha_{\rm IS}$ to converge to values which are consistent with observational data associated with our IS regions. To make these new boundary conditions, we examine the steady-state population of objects in each IS region. Observational data is hard to come by for three of our IS regions (3:1, ν_6, and JFC). On the other hand, the IMC and OB regions contain enough observational data that it is possible to estimate their total population with reasonable accuracy via extrapolation. For this reason, our new boundary conditions will focus on the IMC and OB regions alone. To this end, we created two additional bins, entries #74593 and #74594 for both λ_m and D_m, and have set them equal to our estimate of the debiased number of $H < 18$ bodies in the IMC and OB regions, respectively. We use $H < 18$ values because they are frequently used to benchmark NEO population estimates.

To compute our new λ_m bins, we approximated the total number of $H < 18$ bodies in the IMC and OB regions using the asteroid database of Ted Bowell (http://asteroid.lowell.edu). Our procedure was as follows:

(i) We computed the cumulative H distribution of the observed population in each region from T. Bowell's catalog.

(ii) Assuming the brightest objects in the $12 < H < 13.5$ range are nearly 100% complete, we extrapolated the power-law slope found among these objects to $H < 15$.

(iii) We computed the ratio between the known objects with $H < 15$ and the projected number of objects with $H < 15$. This value becomes our estimated incompleteness factor (F) for $H < 15$ objects. For the IMCs, $F \sim 80\%$, while for the OBs, $F \sim 50\%$.

(iv) Assuming the slope of the main belt population with $15 < H < 18$ is the same as that of the NEO population over the same range (Jedicke and Metcalfe 1998; Bottke *et al.* 2000a), we estimated the total number of $H < 18$ objects in our population.

Note that Eq. 6 yields $N(H < 18)/N(H < 15) = 11.2$. Thus, the total number of $H < 18$ objects in each region is $N(H < 18) \sim 11.2 \times N_{\rm known}(H < 15)/F$. From Ted Bowell's database, we find that there are 316 and 1367 known $H < 15$ objects in the IMC and OB regions, respectively. This means that $N(H < 18)$ for the IMC and OB populations are ~ 4400 and ~ 30600, respectively. These same values are used for bin entries λ_{74593} and λ_{74594}.

For the D_m function, entries #74593 and #74594 correspond to the steady-state number of $H < 18$ bodies in the IMC and OB regions predicted by our NEO model results (i.e., our choice of $\alpha_{\rm IS}, \tau_{\rm IS}$, and I). Because the corresponding entries in λ_m are the expected number of $H < 18$ bodies rather than the number of *observed* bodies, we do not need to multiply D_{74593} and D_{74594} by any bias function. Thus, with the λ_m and D_m distributions defined consistently with each other, we can solve for D_m using Eq. 16:

$$D_{74593} = N_{\rm IMC}(H < 18) = \frac{\alpha_{\rm IMC} N_{\rm CTR-NEO}(H < 18)}{\tau_{\rm IMC} \langle L_{\rm CTR-IMC} \rangle} \tag{18}$$

and

$$D_{74594} = N_{\rm OB}(H < 18) = \frac{\alpha_{\rm OB} N_{\rm CTR-NEO}(H < 18)}{\tau_{\rm IMC} \langle L_{\rm CTR-OB} \rangle} \tag{19}$$

Note that $N_{\rm CTR-NEO}(H < 18)$ is the number of $H < 18$ NEOs in the CTR, while the average lifetime values $\langle L_{\rm CTR-IMC} \rangle$ and $\langle L_{\rm CTR-OB} \rangle$ are the average lifetimes of bodies in the CTR (rather than the ETR). Accordingly, these values, $< L_{\rm CTR-IMC} >= 2.86$ Myr and $< L_{\rm CTR-IMC} >= 10.5$ Myr, are slightly different than those reported in Table 3. Our $\tau_{\rm IS}$ values are the same as those in Table 3.

We have one more issue to address before we can run our model fit. At this time, our nominal λ_m and D_m functions are defined according to the number of objects discovered by Spacewatch in the target region, while entries #74593 and #74594 are defined as the total number of $H < 18$ objects in the IMC and OB regions. The latter values are much higher than the former values. Thus, if no changes were made to these bin entries, they will overpower any results coming from the NEO model fit. To solve this problem, λ_{74593}, λ_{74594}, D_{74593}, and D_{74594} must all be scaled by a factor $f = 42/(N_{\rm TR-NEO}(H < 18))$, which is the ratio between the total number of $H < 18$ bodies detected by Spacewatch in the target region and the predicted number of NEOs in the same region with the same limiting absolute magnitude. Once f is included, our new bins are in line with the other λ_m, D_m bins.

Finally, the distributions λ_m and D_m must be normalized to unity over all bins, as required by the use of (17). Our $\mathcal{L}$ function is now ready for use.

5.3. Results of our model fit, the quality of fit, and computation of error bars

Using Powell's method (Press *et al.* 1989) to minimize the value of our $\mathcal{L}$ function with respect to our free parameters ($\alpha_{\rm IS}$), we can solve for our best-fit NEO model. Our best-fit parameters are: $\alpha_{\nu_6} = 0.37$, $\alpha_{\rm IMC} = 0.27$, $\alpha_{3:1} = 0.20$, $\alpha_{\rm OB} = 0.10$, and $\alpha_{\rm JFC} = 0.06$. These values (with formal error bars, described below) are reported in Table 3. Hereafter, we denote them by $\alpha_{\rm IS,best}$. Similarly, $D_{m,{\rm best}}$ becomes the distribution D_m obtained with $\alpha_{\rm IS,best}$ and $\mathcal{L}_{\rm best}$ the corresponding value of $\mathcal{L}$.

Note that the best fit is not necessarily a good fit. For a quantitative measure of our fit quality to all bins, including the new λ_m and D_m bins, we used the following procedure. From $D_{m,{\rm best}}$, we randomly generated 2000 distributions ($d_1, \ldots d_{2000}$), each made of 2463 objects (the sum of D_m over all entries, after rescaling of D_{74593}, D_{74594} and before renormalization). Assuming $D_m = D_{m,{\rm best}}$ and $\lambda_m = d_1, \ldots d_{2000}$, we computed 2000 values of $\mathcal{L}$ using (17). These values were then compared to $\mathcal{L}_{\rm best}$. Because the distributions $d_1 \ldots d_{2000}$ have been generated from D_m, this calculation shows what the expected distribution of $\mathcal{L}$ values are if we have a perfect statistical match. Then, the value $\mathcal{L}_{\rm best}$ (obtained with the real data) is compared to this distribution. We found that about 50% of the cases resulted in a $\mathcal{L}$ value which was larger than $\mathcal{L}_{\rm best}$. This means that $D_{m,{\rm best}}$ has a 50% chance of being a statistically perfect fit of the data distribution D_m. We call this value our "quality-of- fit" factor Q. The large value of Q found for this test proves that our model correctly reproduces the repartition of objects among our NEO target region and the IMC and OB regions.

This result does not imply, however, that our model correctly fits the fine orbital-magnitude distribution of the observed NEO population, because bodies in the NEO region represent only a minority of the total D_m distribution (138 bodies over a total of 2463 data). Thus, we decided to run a more severe quality-of-fit test for our NEO model. For this second test, we imposed that $d_i(74593) = \lambda_{74593}$ and $d_i(74594) = \lambda_{74594}$ for all the distributions $d_1, \ldots d_{2000}$, so that only 138 bodies were allowed to be randomly generated from $D_{m,{\rm best}}$ in the NEO target region. In this case, only 0.35% of the cases produced a value of $\mathcal{L}$ which was larger than $\mathcal{L}_{\rm best}$. This low Q value implies that our NEO model is not a statistically good fit to the observed NEO distribution. We stress that our $\mathcal{L}$ function is a rather severe test of our model, since it checks our model simultaneously over 4 dimensions (a, e, i and H).

The surprisingly low Q value obtained by this procedure is in stark contrast to Fig. 10, where we graphically compare the (a, e, i, H) distribution of the 138 Spacewatch NEOs to our best-fit case of $n(a, e, i, H)$ by collapsing our results into four one-dimensional plots. The impressive visual match implies that our IS regions account for the vast majority of known NEOs, enough so that it may not be necessary to invoke additional NEO sources at this time.

EDITOR: PLACE FIGURE 10 HERE.

To resolve this apparent contradiction between Q and Fig. 10, we decided to reexamine several approximations used to generate $n(a,e,i,H)$. After several tests, we determined that our low Q value stemmed from the mismatch between the large number of Amors predicted by our model with ($1.0 < q < 1.3$ AU; $2.0 < a < 2.5$ AU) and the relative paucity of objects discovered in that same region by Spacewatch. Our projected NEOs in this region come predominately from the ν_6 and IMC populations, both which make a significant contribution to our estimated NEO population. Interestingly, we consider this zone somewhat "special" because objects in this region frequently have angular rates of motion which mimic those of main belt asteroids. As described in Sec. 4.1, observers looking for NEOs beyond $a > 2.0$ AU are often unable to filter out NEOs from numerous background objects. Numerical tests suggest the region in question could be greatly afflicted by this effect. Thus, we hypothesized that our poor Q value was a consequence of our relatively simplistic main belt rate cut which was used to generate $B_{\rm NEO}$. In other words, we may need a more sophisticated method to account for the pronounced "hiding in plain sight" effect associated with objects on ($1.0 < q < 1.3$ AU; $2.0 < a < 2.5$ AU) orbits.

To check this hypothesis, we ran two different tests. For our first test, we eliminated all λ_m and D_m bins from the ($1.0 < q < 1.3$ AU; $2.0 < a < 2.5$ AU) region and reran our more severe quality-of-fit test using $D_m = D_{m,\rm best}$. This procedure removed 23 of our 138 Spacewatch objects from our model fit. We found that the modified $n(a,e,i,H)$ function produces a quality-of-fit factor of $Q = 39\%$. This result was quite satisfying to us, since it suggested our previous fit could also be considered reasonable once the "hiding in plain sight" effect was removed. For our second test, we eliminated all λ_m and D_m bins from the ($1.0 < q < 1.3$ AU; $2.0 < a < 2.5$ AU) region and reran Powell's method to minimize the new $\mathcal{L}$ function. In this case, we found $\alpha_{\nu_6} = 0.35$, $\alpha_{\rm IMC} = 0.33$, $\alpha_{3:1} = 0.16$, $\alpha_{\rm OB} = 0.12$, and $\alpha_{\rm JFC} = 0.04$, virtually the same results as $\alpha_{\rm IS,best}$. The quality-of- fit factor was $Q = 32\%$, slightly lower than the previous test. For this reason, and because we would like to use as much NEO data as possible when making our fit, we will use $\alpha_{\rm IS,best}$ for all of the results presented below.

Although $\alpha_{\rm IS,best}$ is not perfect, we believe it provides a satisfactory representation of the observed orbital-magnitude distribution of NEOs, and therefore constitutes an useful tool for future NEO studies. Additional model errors may be due to a combination of factors: (i) the initial conditions chosen for our numerical integrations runs may be inaccurate; (ii) our observational bias functions require further revision; (iii) we may not be in a perfect steady state scenario, (iv) our choice of a single magnitude distribution applicable to all IS regions may be inappropriate, and (v) other approximations used to construct our model may be too simplistic.

To investigate these possibilities, and to test our best-fit NEO model in a different way, we simulated the performance of the Catalina Sky Survey (CSS) and compared our mock NEO detections to those produced by the real CSS from April 1999 through December 1999. Detailed information like the CSS's pointing history, the size of their field-of-view, their limiting magnitude, and their rate-of-motion cuts used to filter NEOs from background asteroids was made available to us by T. Spahr (personal communication, 2000) and was used in our simulation. Though a complete description of our method and results is left for Jedicke *et al.* (2001), we can report that we found a good match between our NEO simulation and the CSS's survey results. The number of Atens, Apollos, and Amors detected by the CSS over this nine-month time period (38 objects in all) was very close to our model predictions. Though these tests cannot tell us whether our best-fit case has correctly weighted the various IS regions, it does help corroborate our predicted orbital and absolute magnitude distribution for the NEOs ($M(a, e, i, H)$). It also gives us increased confidence that $N_{\rm NEO}\,(H)$ was calibrated correctly using the methods described in Sec. 3.2.

The statistical errors associated with the determination of $\alpha_{\rm IS,best}$ were computed using the procedure suggested in Press *et al.* (1989). From $\lambda_{m,\rm best}$, we once again generated many distributions, each made of 2463 objects. The number of these sets was limited to 150 for computational expediency ($d_1, \ldots d_{150}$). For each distribution d_i, we compute the values $\alpha_{{\rm IS},i}$ that allow the best match with our model distribution λ_m. The formal 1σ error bar on $\alpha_{\rm IS,best}$ is then computed as the root mean square dispersion of the $\alpha_{{\rm IS},i}$ values, namely $\sigma_{\alpha_{\rm IS}} = \sqrt{\sum_i (\alpha_{{\rm IS},i} - \alpha_{\rm IS,best})^2/150}$. Hence, $\alpha_{\nu_6} = 0.37 \pm 0.08$, $\alpha_{\rm IMC} = 0.27 \pm 0.03$, $\alpha_{3:1} = 0.20 \pm 0.08$, $\alpha_{\rm OB} = 10.0 \pm 0.01$, and $\alpha_{\rm JFC} = 0.06 \pm 0.04$. (Table 3). Note the error bars for the IMC and OB regions are relatively low due to the added boundary conditions included in our fitting routine. Overall, our NEO model is relatively well constrained, such that we believe it can be effectively used for further studies (e.g., impact probability computations, simulation of survey strategies, etc.).

Similarly, we have also computed the uncertainties of all the quantities that characterize our NEO model (see Table 4) as follows. For a given quantity X, we compute its value X_i for each set of $\alpha_{{\rm IS},i}$ values (i.e., the best–fit parameters found for each distribution of fake NEOs d_i) and define $\sigma_X = \sqrt{\sum_i (X_i - X_{\rm best})^2/150}$, where $X_{\rm best}$ is the value of X in the best–fit model. These uncertainties are also reported in Table 4.

EDITOR: PLACE TABLE 4 HERE.

6. The Debiased NEO Population

6.1. Model predictions

We use the best-fit parameters from Sec. 5 to calculate the debiased orbital and size distributions for the entire NEO region ($M(a, e, i, H)$). First of all, we define the contribution of each primary IS region to the overall NEO population as:

$$\beta_{\rm IS} = \frac{\sum_{a,e,i}^{\alpha_{\rm IS}} R_{\rm IS}(a, e, i)}{\sum_{a,e,i} R_{\rm NEO}(a, e, i)}. \tag{20}$$

This value differs from $\alpha_{\rm IS}$ because the sums are extended over the region ($a < 7.4$ AU, $e < 1.0$, $i < 90°$, and $13 < H < 22$) rather than just the region where the observational biases have been calculated (i.e., the CTR) or the extended target region (ETR). We find that $\beta_{\nu_6} = 0.37 \pm 0.08$, $\beta_{\rm IMC} = 0.25 \pm 0.03$, $\beta_{3:1} = 0.23 \pm 0.09$, $\beta_{\rm OB} = 0.08 \pm 0.01$, and $\beta_{\rm JFC} = 0.06 \pm 0.04$ (Table 3). We can also group the contributions by region by assuming that (i) the inner main belt contribution ($a < 2.5$ AU) is made up of the ν_6, half the 3:1, and the inner–IMC, and (ii) the central main belt ($2.5 < a < 2.8$ AU), is made up of half the 3:1 and the outer–IMC. In this circumstance, we find that $\sim 61\%$ of all $13 < H < 22$ NEOs come from the inner main belt, $\sim 24\%$ come from the central main belt, $\sim 8\%$ come from the outer main belt ($a > 2.8$ AU), and $\sim 6\%$ comes from the Jupiter-family comet region ($2 < T < 3$).

With these values, we can now define $C_{\rm NEO}$ (Eq. 5), the constant needed to normalize $N_{\rm NEO}(H)$ (Eq. 6). The number of $H < 18$ objects with $a < 3.0$ AU is thought to be $\sim 910 \pm 110$ (Bottke *et al.* 2000a). Since the sum of $R_{\rm NEO}(a, e, i)$ divided by the sum of $R_{\rm NEO}(a < 3.0$ AU$, e, i)$ is 1.05, $C_{\rm NEO} = 15.42 \times 1.05 = 17.09$. Thus, we estimate that the number of NEOs with $H < 18$ with $T > 2$ (i.e., $a \lesssim 7.4$ AU) is $\sim 960 \pm 120$. With this value, we use $\beta_{\rm IS}$ to determine the number of $H < 18$ objects coming from each IS region (Table 3).

In this paper, $M(a, e, i, H)$ is graphically represented in two ways. The orbital component of M, what we call $R_{\rm NEO}(a, e, i)$, is shown as a residence time plot in Fig. 11. Next, we show M as a series of 4 one-dimensional plots in a, e, i, and H (Fig. 12). The solid histograms represent the known NEOs with $13 < H < 18$, while the line represents our predicted population over the same H range. We find that slightly less than half of the NEO population ($49 \pm 4\%$) has $a \leq 2$ AU orbits. This portion of the population is longer-lived than the population at $a > 2$ AU because the major sinks are less accessible. The $a < 2$ AU population is slowly resupplied by close encounters from the terrestrial planets moving $a > 2$ AU material onto $a < 2$ AU orbits (e.g., Wetherill 1985). In the process, this material must survive a gauntlet of chaotic resonances located between 1.8-2.0 AU (i.e., the 4:1 and 5:1 mean-motion resonance with Jupiter and the ν_6 and ν_{16} secular resonances).

EDITOR: PLACE FIGURE 11 HERE.

EDITOR: PLACE FIGURE 12 HERE.

Our results suggest that $\sim 44\%$ of the $H < 18$ NEOs have been discovered so far (425 observed / 960 predicted as of December 2000) (Table 4). NEOs with $e \leq 0.4$ or $H < 15.5$ are nearly complete because they are relatively easy targets for NEOs surveys. Objects with high a, e, i and H values are more difficult to detect (Jedicke *et al.* 2001, in preparation). Finding the rest of the $H < 18$ NEOs, however, will be easier than finding the rest of the $D > 1$ km NEOs. Observations show that NEO albedos generally get darker with increasing heliocentric distance (e.g., Rabinowitz *et al.* 1998), such that a typical $H = 18$ body at 4 AU is larger than the typical one at 1 AU. Until the albedos distribution of the NEO population is understood, the number of km-sized NEOs cannot be accurately determined. This important task will need to be addressed in the future.

We find that objects with a given H on Amor, Apollo, and Aten orbits make up 32±1%, 62±1%, and 6±1% of the $H < 22$ NEO population, respectively (Table 4). Figs. 13-16 show the predicted and observed Amor, Apollo, and Aten populations with $H < 18$ as a series of one-dimensional plots in a, e and i, while Table 4 contains various useful quantities from these regions. Some comments on these populations are warranted:

Amors. There are 310 ± 46 bodies with $H < 18$ in the Amor population; nearly 66% of them discovered so far (Fig. 13). This discovery fraction is much higher than the Apollos or Atens, probably because these objects spend all of their time outside of Earth's orbit. Note that we have a slight mismatch between our predictions and the observations for $a \sim 1.9$ AU, $0.2 < e < 0.4$, and $i \sim 30°$. We believe the imprecision in this case stems from our decision to exclude the Hungaria population from our NEO model. Orbital integration results suggest that the Hungarias contribute a small but dynamically distinct component to the overall NEO population (e.g., Michel *et al.* 2000b). Otherwise, most of the Amors which have escaped detection so far have orbits which keep them in the far reaches of the NEO population. According to our five-source best-fit case, the inner main belt produces $\sim$ 53% of all Amors, $\sim$ 24% come from the central main belt, $\sim$ 14% come from the outer main belt, and $\sim$ 9% come from the JFC region.

EDITOR: PLACE FIGURE 13 HERE.

Apollos. We estimate there are 590 ± 80 bodies with $H < 18$ in this population; only 33% have been discovered so far (Fig. 14). This discovery fraction is smaller than that for the Atens, probably because Apollos move very fast as they approach and move interior to the Earth's orbit. The rest of the time, these objects inhabit regions far from the Earth, where they are faint and slow-moving. Most undiscovered Apollos with $a \sim$ 1-2 AU have large e values and/or i values. It is likely that inner solar system resonances like the ν_{13}, ν_{14}, and ν_{16} secular resonances are responsible for some of these extreme inclination values. The inner main belt produces $\sim$ 64% of all Apollos, $\sim$ 24% come from the central main belt, $\sim$ 6% comes from the outer main belt, and $\sim$ 6% come from the JFC region.

EDITOR: PLACE FIGURE 14 HERE.

Atens. The number of $H < 18$ Atens predicted by our model is 58 ± 12, with 45% discovered so far (Fig. 15). Note that Atens, by definition, can never be more than 1 AU from the Earth at opposition, such that they may be somewhat easier targets for many NEO surveys than the

Apollos. Some slight mismatches can be seen on the e, i plots, but we attribute this more to small number statistics rather than model error. For example, a population of 60 fake NEOs derived directly from our probability distribution for the Aten region will often produce similar mismatches. The model eccentricity distribution has an odd shape, with a peak near 0.8. This may be produced by the interplay between the Kozai resonance and secular resonances, which helps protect objects in this region by pumping them up to high inclination values (Michel and Thomas 1996; Michel 1997; 1998; Michel *et al.* 2000a). This result can also be seen in the shape of the inclination distribution. The inner main belt produces $\sim$ 79% of all Atens, while the rest come from the central main belt.

EDITOR: PLACE FIGURE 15 HERE.

IEOs. Finally, we comment on a putative population of objects interior to the Earth orbit (i.e., with $Q < 0.983$). They are referred to by Michel *et al.* (2000a) as the IEO population, while many in the observational community refer to them as "Apoheles", an Hawaiian word for "orbit" (B. McMillian, personal communication, 2001). We assume these objects come from the NEO population and not from the Vulcanoids, putative belt of bodies which reside inside Mercury's orbit. Recent work suggests that the Vulcanoid population, if it ever existed, has been decimated by collisional disruption and Yarkovsky drag, such that it is unlikely to be an important present-day source of material (Stern and Durda 2000; Vokrouhlický *et al.* 2000) Fig. 16 represents the predicted orbital distribution of the IEO objects. The ratio of the IEO population to that of the NEO population is about 2%; 20 ± 4 $H < 18$ objects are estimated to exist in this region. None have been observed so far. We do not consider the paucity of IEO discoveries surprising, since there are few targets and the observing circumstances are demanding (Tedesco *et al.* 2001). The ultimate cause of the spikiness seen in the e plot is unclear to us; we believe it may be caused by several factors: resonances, the IEO's close association with Venus, and/or small number statistics in our integrations. Like the Atens, the inner main belt produces about 75% of all IEOs, with the rest coming from the central main belt.

EDITOR: PLACE FIGURE 16 HERE.

MOID values. Using our model, we can also estimate the MOID (minimum orbital intersection distance) values between our NEO population and the Earth. MOID is defined as the closest possible approach distance between the osculating orbits of two objects, provided there are no protective resonances in action. MOID values are often used to gauge the likelihood that an object will evolve onto a collision trajectory with Earth. To compute these values, we created a population of fake NEOs based on $M(a, e, i, H)$. We found that 21% of the fake NEOs had a MOID < 0.05 AU, 1% had a MOID smaller than the Moon's distance from Earth, and 0.025% had a MOID smaller than Earth's radii. Assuming there are 960 NEOs with $H < 18$ and $T > 2$, we estimate that 0.24 such objects should have MOIDs smaller than Earth's radius today. On the other hand, assuming there are 24,500 NEOs with $H < 22$ and $T > 2$ (Eq. 5), we estimate that 6 such objects should have MOIDs smaller than Earth's radius. This result does not necessarily imply a collision with Earth is imminent, though, since both Earth and the small NEO still need to rendezvous at the same location. Further implications of this study will be discussed in Jedicke *et al.* (2001).

6.2. Comparison with previous work

Our estimate of the number of NEOs with $H < 18$ and $T > 2$, $\sim 960 \pm 120$, appears to be comparable to many previous estimates of the NEO population (e.g., Shoemaker *et al.* 1983; Shoemaker *et al.* 1990; Morrison 1992; Rabinowitz *et al.* 1994; Rabinowitz *et al.* 2000; Stuart 2000, D'Abramo *et al.* 2001, among others). Direct comparisons between our value and previous values are problematic, though, because these studies typically do not state where in (a, e, i) space their computations are considered valid. To determine this range, surveys need to model their NEO detection performance, accounting for factors such as observational biases and the limiting magnitude of their telescope. We suspect that the inability to precisely account for (a, e, i) regions with zero detections may partially explain why estimates of the NEO population have modestly fluctuated over the past three decades. Thus, we believe that many previous NEO population estimates are probably consistent with one another, with the differences caused by peculiar sampling over an (a, e, i) range which (i) varies from estimate to estimate and (ii) whose limits are poorly understood. Another possible reason the NEO numbers have fluctuated over time is that several groups have computed their NEO population limit in terms of $D > 1$ km rather than $H < 18$. Converting between D and H is problematic, since it requires one to covert H to D for many different albedos and phase functions, and predict the debiased ratio of bright, S-type NEOs vs. dark, C-type NEOs, which has not been computed since 1990 (Luu and Jewitt 1989; Shoemaker *et al.* 1990). Since $N_{\rm NEO}(H)$ can be modeled as a power-law function, slight differences in the conversion process can result in significant changes to the total number estimate.

A literature search indicates that Rabinowitz (1993) and Rabinowitz *et al.* (1994) were the only groups to publish debiased probability distributions for the (a, e, i) distributions of km-sized NEOs prior to Bottke *et al.* (2000a). Both these works were based on the NEO debiasing procedure described in Rabinowitz (1993) (see also Bowell and Muinonen 1994). Bias functions, computed separately in (a, e) space and in i space from fabricated NEO orbits, were used to correct the observed orbits of "large" NEOs discovered by Spacewatch and other NEO surveys (e.g., $H < 18$ photographic observations with the Palomar 18" Schmidt telescope; Helin and Dunbar 1991). In contrast, our orbital distribution was calibrated using the population of objects with $13 < H < 22$ found by Spacewatch alone. Rabinowitz divided the function we call $R_{\rm NEO}(a, e, i)$ into two independent probability distributions called $P(a, e)$ and $P(i)$. This separation was made after Rabinowitz examined the observed distribution of a vs. e for different ranges of i and saw no obvious correlation in the Palomar photographic data (Rabinowitz, personal communication, 2000). Peculiar sampling of the NEO population by different NEO surveys produced some blank bins in Rabinowitz's $P(a, e)$ function, and there is a sparceness of data with $a > 3.0$ AU. Despite these problems, Rabinowitz's work can be graphically compared to our study.

Fig. 17 shows Rabinowitz's $P(a, e)$ and $P(i)$ functions and our $R_{\mathrm{NEO}}(a, e, i)$ function as a series of one-dimensional histograms in (a, e, i) space. The solid histograms represent the data from Rabinowitz *et al.* (1994), while the line represents our predicted NEO population. Each histogram has been normalized over the limits so that the sum of all values is 1.0. The bin spacings were set to $\delta a = 0.2$ AU, $\delta e = 0.1$, and $\delta i = 5°$.

EDITOR: PLACE FIGURE 17 HERE.

Rabinowitz *et al.* (1994) predicts a more "flat" inclination distribution, while we predict a gradual fall-off with increasing i. This mismatch is probably caused by our ability to "sample" high inclination NEOs beyond 2 AU using numerical integration runs. Note that limited $a > 3$ AU data was available to Rabinowitz *et al.* when they made their computations. It is also worth pointing out that resonant action pumps up NEOs with $a < 2$ AU to high inclinations (Fig. 10); this region may not have been well sampled by the NEO surveys used by Rabinowitz at the time of his study. Regardless, the reasonable match between our work and that of Rabinowitz gives us added confidence that both debiased distributions do a good job of mapping out the debiased population of NEOs.

7. NEO Flux Rates and the Steady State Populations in the Intermediate Sources

7.1. Resupplying the asteroidal component of the NEO population

With our completed NEO model, we can now generate the influx rates and the steady-state population estimates for our IS regions using the equations described in Sec. 4.3. The mechanisms capable of supplying new bodies from the asteroid belt to the IS regions are collisions (e.g., Farinella *et al.* 1993), chaotic diffusion (Morbidelli and Nesvorný 1999; Carruba *et al.* 2000), and the Yarkovsky–driven semimajor axis mobility (e.g., Farinella and Vokrouhlický 1999; Bottke *et al.* 2001; 2002). Observational evidence and physical modeling suggest that one of these mechanisms may be more important than the other two. The JFCs are a more complicated case, since they are simply a subset of the ECOM region which contains many sinks. Their values will be discussed in Sec. 8.

The influx rates for the IS regions (I) obtained using Eq. (13) can be found in Table 3. They should be considered the rates at which new NEOs are generated from each IS (expressed in terms of the number of $H < 18$ objects per Myr). For the IS regions originating in the main belt, whose objects effectively cannot reach the sink without passing through the NEO target region, the rates reported in Table 3 are also the replenishment rates from the asteroid belt in a steady–state scenario. Overall, we predict that the flux of $H < 18$ asteroids needed to keep the NEA population in steady state is 790 ± 200 Myr^{-1}. The flux rate is highest for the OB region, which loses 570 ± 120 $H < 18$ asteroids Myr^{-1}. Note that the high OB flux rate compensates for the short lifetimes of OB objects once they reach the NEO region. The flux rate for the inner and central main belt IS regions is lower, with 220 ± 80 $H < 18$ asteroids Myr^{-1} needed to maintain steady state.

From Table 3, we find that the sum of the rates for the 3:1 and ν_6 resonances is 160 ± 70 bodies with $H < 18$ per Myr. With a model of the collisional evolution of the asteroid belt, using ejection velocities derived from asteroid family studies, Menichella *et al.* (1996) estimated that 160 bodies larger than 1 km in diameter are injected into these resonances per Myr. Similar results have been obtained by Zappalá *et al.* (1999). Assuming that $H = 18$ asteroids are ~ 1 km in diameter (Eq. 7), their collisional estimates are comparable to our estimates. We caution, however, that this match may be fortuitous; recent results suggest that the inferred velocity distributions of main belt families may be too high (Nesvorný *et al.* 2001; Bottke *et al.* 2001).

Using Eqs. 6 and 7, we estimate that the main belt mass flux lost via $13 < H < 22$ objects is $\sim 3 \times 10^{16}$ kg Myr^{-1}. This value is the mass equivalent of a $D \approx 30$ km body being lost every Myr. It is useful to combine this flux value with the mass flux of $H < 13$ NEOs. At the moment, we know of 3 such NEOs: (1036) Ganymed, with $H = 9.45$, (433) Eros, with $H = 11.16$, and (4954) Eric, with $H = 12.6$. Their loss rate can be approximated by multiplying their total number (3) by the ratio of the flux of $H < 18$ bodies (790) over the number of $H < 18$ NEOs (960). Thus, roughly 2 $H < 13$ NEOs are lost every Myr. Assuming those lost bodies have masses equivalent to (1036) Ganymed and (433) Eros, we find that an additional $\sim 4 \times 10^{16}$ kg are lost every Myr from the main belt. Thus, the total mass flux lost from the main belt, provided that most of the mass is in the $H < 22$ bodies, is $\sim 7 \times 10^{16}$ kg Myr^{-1}. Assuming this flux has been constant for 3.0 Gyr, we estimate that the main belt has lost $\sim 2 \times 10^{20}$ kg over that time. This value corresponds to 5% of the total mass of the current main belt (i.e., assuming that the main belt's mass is 5% the mass of the Moon). Thus, our NEO flux rate does not appear to have depleted the main belt of much of its mass over this time.

The absolute magnitude distribution of NEAs provided by our model, with a cumulative size distribution of type $N(> D) \propto D^{-1.75}$, suggests that collisional injection probably does not play a dominant role in resupplying the resonant population with new bodies. If it did, we would expect the NEAs, populated by fragments from catastrophic break–ups, to have a steep size distribution just like that observed in asteroid families (i.e., $N(> D) = D^{-\delta}$ with $\delta > 3$) (Tanga *et al.* 1999; Campo Bagatin *et al.* 2000). Recall that the mean lifetime in the NEO region is only a few Myr, too short for collisions to significantly change the size distribution for fresh debris back to such a shallow slope (i.e., $H = 22$ NEA, with a diameter of about 170 m, has a collisional lifetime > 100 My; Bottke *et al.* 1994a,b). Moreover, it is unclear how collisional injection can explain the relative abundance of multi-kilometer objects in the NEO population. According to standard collision models, only the largest (and most infrequent) catastrophic disruption events are capable of throwing multi-kilometer objects into an IS region (Menichella *et al.* 1996; Zappalá *et al.* 1999).

Interestingly, our estimate of the NEO size distribution, which is in general agreement with the independent work of Rabinowitz *et al.* (2000) (see Sec. 6.2), shows some similarities to the main belt size distribution. At present, the main belt size distribution is only known for $D > 3$ km asteroids (Jedicke and Metcalfe 1998), but its shape over this same range is similar to that observed in our NEO distribution. In addition, though the shape of the main belt's size distribution is unknown in the sub-km range, estimates provided by the numerical simulations of Durda *et al.* (1998) suggest the main belt's size distribution is shallower than a Dohnanyi-type distribution ($N(> D) \propto D^{-2.5}$) for $0.2 < D < 5$ km asteroids (Fig. 18). If true, one way to explain the size distribution of the NEA population is to assume it randomly samples asteroid population throughout the main belt.

EDITOR: PLACE FIGURE 18 HERE.

To explain the apparent shallow slope index seen among sub-km asteroids, we favor a scenario where main belt resonances are resupplied by the Yarkovsky effect, a thermal drag force which causes bodies to drift in semimajor axis as a function of size, spin, and surface properties (Farinella *et al.* 1998; Farinella and Vokrouhlický 1999; Bottke *et al.* 2000b). Yarkovsky drift rates for km-sized bodies are slow enough ($\sim \pm 10^{-4}$ AU Myr^{-1}) that fresh collisional debris would have a chance to collisionally evolve back to a more shallow slope. This mechanism would also sample the main belt more-or-less evenly, explaining the consistency between the main belt size distribution, the NEO size distribution, and the crater size distribution on the terrestrial planets (e.g., Bottke *et al.* 2002).

The long-term evolution of small asteroids in the main belt via Yarkovsky drag is analogous to that of meteorites, whose cosmic ray exposure ages are in general an order of magnitude longer than the mean resonant transport times to the Earth (Morbidelli and Gladman 1998). The Yarkovsky effect could explain these apparent paradoxes, because the bodies spend most of their lifetime in the main belt before drifting into a transportation resonance (Farinella *et al.* 1998; Bottke *et al.* 2000b; Vokrouhlický and Farinella 2000; Bottke *et al.* 2001). We point out that the age of NEA (433) Eros, as deduced from crater counting on NEAR images (Veverka *et al.* 2000), is much longer than the typical dynamical lifetime of NEOs with $a < 2$ AU (i.e., billions of years old compared to tens of millions of years).

Using the asteroid number density in the vicinity of the 3:1 resonance published in Jedicke and Metcalfe (1998), D. Vokrouhlický (personal communication, 2000) has recently performed a back-of-the-envelope computation which suggests that ~ 65 bodies with $H < 18$ should fall into the resonance every Myr due to the Yarkovsky effect. The errors on this measurement are unknown. From our Table 3 results, we estimate the influx into the 3:1 resonance is 100 ± 50.

Thus, the estimated asteroid flux from the Yarkovsky effect is well within our error bars. We hope to address this matter more thoroughly in the near future.

Concerning the IMC population, Table 3 indicates that about 65 ± 15 bodies with $H < 18$ should become NEOs every Myr. These Mars-crossers are gradually replaced by main belt objects having their eccentricities slowly increased by a multitude of weak mean–motion resonances. Chaotic diffusion appears to be the dominant mechanism for sustaining the IMC population, with the Yarkovsky effect and collisions continuously refilling the weak transporting resonances. If we focus on just the inner-IMC region, the we can decrease our flux rate by a factor of ~ 2, such that the flux of $H < 18$ objects coming from the 2.1-2.5 AU range is 33 ± 8. Comparing this value to previous work, we find that Migliorini *et al.* (1998) estimated an escape rate of 5 bodies Myr^{-1} larger than 5 km, equivalent to 85 bodies larger than 1 km (roughly $H < 18$) according to our estimated size distribution (Eqs. 7 and 6). Michel *et al.* (2000b), using more extensive integrations than Migliorini *et al.* (1998), dropped this estimate to 32 km-sized objects Myr^{-1}. This value was also obtained by Morbidelli and Nesvorný (1999) estimated that $\sim$ 30 km–sized bodies become Mars–crossers from inner-IMC region. Since Eq. (7) suggests that a $H < 18$ object converts to the $D = 1$ km body, we believe our flux rate for the inner-IMC region is in good agreement with previous work.

Finally, we report one caveat about the results presented in this section. Our analysis assumes that the material flux entering the IS regions from the main belt can be well-represented by the same size distribution. It is possible, though, that the proportion of main belt material entering each IS region (i.e., α_{IS}) is size-dependant, particularly if the Yarkovsky effect is the dominant means for delivering main belt material to the IS regions. Bottke *et al.* (2000b) showed that meter-size objects have such fast da/dt rates that they frequently "jump" over the tiny resonances supplying the IMC region to enter the powerful 3:1 or ν_6 resonances. Similar behavior is seen among km-sized bodies, though their evolutionary tracks are more complex (Bottke *et al.* 2001a, b). On the other hand, multi-km NEAs like (433) Eros would hardly be affected by the Yarkovsky effect, such that their most likely source would be the IMC region. Therefore, it is possible that the IMC source may be more important for supplying multi- km NEAs than described here, while the 3:1 and ν_6 resonances may be more important for $D \sim 100$ m bodies. Our method of using weighting factors to measure the relative importance of each IS regions is simply the best we can do with the available Spacewatch data. In terms of our model results, the α_{IS} values we find may be more characteristic of km and sub-km NEAs than multi-km NEAs, since two-thirds of the Spacewatch NEAs have $18 < H < 22$.

7.2. The steady state number of objects in the asteroidal intermediate sources

Using τ_{IS} and I from Table 3, we can use Eq. (16) to determine N_{IS} values for the asteroidal IS regions. Our results are shown in the last column of Table 3. They suggest that a few hundred bodies with $H < 18$ should be in the ν_6 and 3:1 resonances at any given time. Because these resonances are ~ 0.05 and ~ 0.025 AU wide, respectively, the steady-state resonant populations have a linear density of $\sim 320 \pm 100$ and $\sim 1100 \pm 520$ bodies per 0.1 AU. To compare, Jedicke and Metcalfe (1998) estimate the asteroid belt has a linear density of 28,500 bodies with $H < 18$ per 0.1 AU in the vicinity of the ν_6 resonance and 46,500 bodies per 0.1 AU on each side of the 3:1 resonance. Thus the resonances, although not completely void of objects, are definitely associated with deep gaps in the asteroid distribution.

The steady state population of the *true* IMCs with $H < 18$ is 4000 ± 940 in our model, about 4 times the size of the NEO population. This value is a good match to the best-guess size of the IMC population found from observational data alone (Sec. 5). This large IMC population must be accounted for when attempting to estimate the present-day impact flux on Mars. We estimate the steady state OB population (i.e., objects in zones OB1-OB5, as defined in Table 2) is comprised of 28000 ± 6000 $H < 18$ objects, much larger than any other asteroidal IS. We intend to examine the region more closely in the near future.

8. Understanding the Ecliptic Comet Populations

8.1. New Estimates of the Jupiter-Family Comet and Ecliptic Comet Populations

The population of ecliptic comets (ECOMs) has recently been estimated by Levison and Duncan (1997), Duncan and Levison (1997), and Levison *et al.* (2000). By comparing the orbital paths of artificial JFCs generated by numerical integration (see Sec. 2.6) to known JFCs with $q < 2.0$ AU, they deduced that (i) active comets fade from sight and become extinct some 12,000 years (on average) after reaching the JFC region for the first time and (ii) extinct comets make up $\sim 78\%$ of the total ECOM population. These results were used to calibrate the integration runs, such that Levison and Duncan predicted that the total number of ecliptic comets with total absolute magnitude $H_{\mathrm{T}} < 9$ was 1.2×10^7. (Note: H_{T} is essentially an absolute magnitude for comets which incorporates the coma and tail, but the calibration of this value is vastly different than that for asteroids; Zahnle *et al.* 1998). Duncan and Levison (1997) increased this value to 1.3×10^7. Approximately 90% of these objects reside beyond Neptune today.

Levison *et al.* (2000) defined a scaling factor S to convert the population of ECOMs with $H_{\mathrm{T}} < 9$ to those with $D > 1$ km. Obtaining this value, however, is problematic for several reasons: (i) Converting between H_{T} and comet diameter is not well understood; published estimates of the nucleus size of $H_{\mathrm{T}} = 9$ comets range from $D = 0.8$ km (Bailey *et al.* 1994) to $D = 2$ km (Weissman 1990). (ii) The shape of the size distribution for these comets is unknown. (iii) The ratio of extinct comets to all comets is unknown; Levison and Duncan (1997) suggest that values between 67% and 88% provide reasonable fits to data. Calculating S using several different methods, Levison *et al.* (2000) determined that $S = 5$ was a reasonable compromise value considering the unknowns involved. The error in S was thought to be a factor of 5 or more. Using this value, they estimated that the number of km- sized ECOMs was 6.5×10^7. Since the ratio of the total residence time of JFCs with $q < 1.3$ AU (i.e., none are found beyond 7.4 AU) over the total residence time of all ECOMs is 1.0×10^{-5}, their results suggest there are 650 km-sized NECs in the JFC region.

Using the integration results from Levison *et al.* (2000) and our calibrated results for the JFC region, we can independently check this outcome. From Table 3, we find that $\sim 6\%$ of the 960 NEOs with $H < 18$ reside on JFC orbits. Since this value does not consider active JFCs, we predict there are 61 ± 50 extinct comets with $H < 18$ in the JFC-NEO region. If we assume that an extinct comet with $H = 18$ has an albedo of 0.04 like those measured from comet nuclei (Jewitt 1991), we get a diameter of 1.7 km (Bowell *et al.* 1989). Since our NEO size distribution has the form $N(> D) \propto D^{-1.75}$, the number of km-sized extinct comets in the ECOM region is $(1\,\mathrm{km}/1.7\,\mathrm{km})^{-1.75} \times 61 \sim 150$. Finally, by dividing the extinct comet population by the percentage of extinct comets in the ECOM population (78%; Levison and Duncan 1997), we conclude that the total number of km-sized NEOs in the JFC region is 200 ± 160, a factor of ~ 3 smaller than the value predicted by Levison *et al.* (2000).

Typical Earth-crossing JFCs are ~ 3 times less likely to strike the Earth than a typical Earth-crossing asteroid (e.g., Shoemaker *et al.* 1994). Nevertheless, this population may be large enough to constitute an important fraction of the total impact hazard to the Earth. These issues will be discussed further in a future paper.

Taking a ratio of the residence times, we estimate that the total number of km-sized ECOMs is $\sim 2.2 \pm 1.8 \times 10^7$, once again about 3 times smaller than the value quoted in Levison *et al.* (2000). To get the scale factor S for converting $H_{\mathrm{T}} < 9$ comets to a population having km-sized nuclei, we divide this value by 1.3×10^7, leaving $S = 1.7 \pm 1.4$. This assumes, of course, that 100% of the JFCs fade rather than self-destruct. If two- thirds of the JFC population self-destructed, our value for S would be the same as that estimated by Levison *et al.* (2000). The importance of comet splitting events to the JFC population is unknown at this time.

By calculating I and τ for the ECOM population and assuming the Kuiper belt was the sole source of ECOMs, Levison and Duncan (1997) determined the approximate size of the Kuiper belt population within 50 AU. These values were updated in Levison *et al.* (2000). Using our new calibration, we update their numbers once more here. The mean dynamical lifetime of an ecliptic comet is $< L_{\mathrm{ECOM}} >= 190$ Myr (Levison *et al.* 2000). Using $N_{\mathrm{ECOM}} = 1.3 \times 10^7$ bodies with $H_{\mathrm{T}} < 9$, we get a flux rate of comets into the ECOM region of $I = 0.068\ \mathrm{Myr}^{-1}$. The fractional decay rate of particles that leave the Kuiper belt per year is approximately $\tau_{\mathrm{ECOM}} \approx 4 \times 10^{-11}$ (Duncan *et al.* 1995). Hence, the number of objects in the Kuiper belt within 50 AU is $N_{\mathrm{KB}} = I/\tau_{\mathrm{ECOM}} = 1.7 \times 10^9$ with $H_{\mathrm{T}} < 9$. Multiplying this value by $S = 1.7 \pm 1.4$, we estimate there are $2.8 \pm 2.3 \times 10^9$ km-sized objects in the Kuiper belt population. To get the number of $H < 18$ objects, we scale this value by $(1\,\mathrm{km}/1.7\,\mathrm{km})^{-1.75} = 2.5$, yielding $1.1 \pm 0.9 \times 10^9$ $H < 18$ objects.

In a follow-up paper to Levison and Duncan (1997), Duncan and Levison (1997) reported that their Kuiper belt integrations also produced a disk of scattered objects beyond the orbit of

Neptune. They claimed that this disk could conceivably be the ultimate source of the steady-state JFC population. If true, the lower limit on the size of the scattered disk population would be $\sim 6 \times 10^8$ comets with $H_{\rm T} < 9$. Updated values reported in Levison *et al.* (2000) would increase this population to $\sim 7 \times 10^8$. Using our calibration factor S, this would correspond to $\sim 1.2 \pm 0.9 \times 10^9$ km-sized and $\sim 4.6 \pm 3.8 \times 10^8$ $H < 18$ objects.

8.2. The dynamical identification of extinct comets in the NEO population

As we described in the Introduction, discriminating NECs from NEAs, both in a dynamical and spectroscopical sense, has long been an outstanding problem (e.g., Weissman *et al.* 1989; Shoemaker *et al.* 1994). Using our 5-source NEO model, we can begin to attack this problem from a dynamical sense. Every $R_{\rm NEO}(a,e,i)$ bin in our model is constructed from a series of five IS probability values ($P_{\rm IS}$) which must add up to 1.0. Thus, we can use the (a,e,i) orbit of an NEO to predict the probability that it was derived from one of our five IS regions (i.e., ν_6, IMCs, 3:1, OB, and JFCs). Because our method cannot yet make Encke- type objects (see Sec. 2.6), however, we are careful to restrict ourselves to particular problems of interest for this paper.

Ideally, extinct comets should have orbits consistent with filled $R_{\rm JFC}(a,e,i)$ bins. They should also show few signs of cometary outgassing. Taking the list of asteroids from the December 2000 database of Ted Bowell (http://asteroid.lowell.edu), we find 46 NEOs with a $P_{\rm JFC} > 10\%$ chance of coming from the ECOM population (Table 5). Nearly all of these bodies have $2 < T < 3$. Fig. 19 shows a plot of the (a,e) positions of the 46 objects listed in Table 5. The objects with the highest $P_{\rm JFC}$ values, in descending order, are: (3552) Don Quixote ($P_{\rm JFC} = 1.0$); 1997 SE5 ($P_{\rm JFC} = 1.0$), 1982 YA ($P_{\rm JFC} = 0.97$), 1984 QY1 ($P_{\rm JFC} = 0.96$), 2000 PG3 ($P_{\rm JFC} = 0.93$), and 2000 EB107 ($P_{\rm JFC} = 0.90$). Each of these objects has a $P > 90\%$ chance of being an extinct comet in our model.

EDITOR: PLACE TABLE 5 HERE.

EDITOR: PLACE FIGURE 19 HERE.

Several extinct comet candidates have been examined spectroscopically (Luu 1993; Hicks *et al.* 1998; Rabinowitz 1998; Rabinowitz and Hicks 1998; Hicks *et al.* 2000a,b). In general, results from these studies show that extinct comet candidates have featureless spectra with flat to modest red slopes spanning the dynamic range between C to D-type asteroids. These features are consistent with the spectral diversity of cometary nuclei (Luu 1993) and of Trojan bodies (Jewitt and Luu 1990).

In broader terms, NEO spectra appear to follow an orbit dependant trend, such that bright, S-type spectra (which includes high albedo classes Q-, V-, and E-types) dominate among NEOs with $a < 2.3$ AU and dark, C, D-type spectra (which includes low albedo classes like F-, T-, and G-types) dominate among NEOs with $a > 2.3$ AU (Rabinowitz 1998). These observations are consistent with our results from the 5-source NEO model. We find that NEOs with $a < 2.3$ AU mostly come from the inner main belt, which is dominated by S-type material (e.g., Gradie *et al.* 1989). On the other hand, NEOs with $a > 2.3$ AU mostly come from the central/outer main belt and the JFC region, where bodies with C, D-type asteroid spectra are prevalent. Determining the ratio of S-type and C-type asteroids in various parts of the NEO population can be done, but it will require careful work, particularly because the observed S-to-C ratio among NEOs is heavily biased (Luu and Jewitt 1989). Previous estimates suggest the debiased S-to-C ratio for NEOs with a given H is close to 2:1 (Luu and Jewitt 1989; Shoemaker *et al.* 1990), though these works are over 10 years old now. We hope to quantitatively investigate this further using our model in the near future.

Finally, we briefly discuss a few objects which have been suspected of being extinct comets: (2201) Oljato, (3200) Phaethon, and (4015) Wilson-Harrington (Bowell *et al.* 1992; Chamberlin *et al.* 1996; Dumas *et al.* 1998). Our model results indicate that both (2201) Oljato ($a = 2.17$ AU, $e = 0.71$, $i = 2.5°$) and (3200) Phaethon ($a = 1.27$ AU, $e = 0.89$, $i = 22.1°$) have a $P = 0\%$ chance of coming from the JFC or OB region, a $P \sim 20\%$ chance of coming from the central main belt, and a $P \sim 80\%$ chance of coming from the inner main belt. Thus, one could infer that these objects are probably asteroids. Observational work provides some support for this hypothesis; (3200) Phaethon has been classified as an F-type asteroid (e.g., McFadden *et al.* 1989), while (2201) Oljato has been designated as an S- or possible even an E-type asteroid (McFadden *et al.* 1993) We note that a reservoir of F-type objects is located adjacent to the 3:1 resonance in the Polana asteroid family (Doressoundiram *et al.* 1998). Thus, a plausible wellspring for (3200) Phaethon would be the main belt. On the other hand, a limitation of our NEO model is that we cannot yet make Encke-type objects, such that the *actual* probability of these two objects coming from the JFC region may be much higher than zero. For this reason, it is useful to examine the results of our OB integrations, which included perturbations from the terrestrial planets (Fig. 6) As pointed out in Sec. 2.6, OB objects reaching $T < 3$ orbits may have dynamical paths similar to JFCs integrated with the Jovian and terrestrial planets included. We find that (2201) Oljato and (3200) Phaethon have orbits which are near filled residence time bins produced by $R_{\rm OB}(a, e, i)$. Thus, we cannot rule out the possibility that these objects are extinct comets gravitationally decoupled from Jupiter. More positively, (4015) Wilson-Harrington ($a = 2.64$ AU, $e = 0.62$, $i = 2.78°$) has a $P \sim 4\%$ chance of coming from the JFC region and a 65% chance of coming from the OB region. Given the limited information we have on the dark and volatile-rich bodies which dominate both populations, we will have to defer the question of (4015) Wilson- Harrington's provenance for now. More observation work and higher resolution integration data will be needed to conclusively determine the nature of these unusual objects.

9. Summary of Results

We briefly summarize the key results from this paper. For reference, the sections which discuss each point are listed.

- Using numerical integration, we have modeled the NEO orbital and absolute magnitude size distributions for $13 < H < 22$ objects using five intermediate source (IS) regions: the ν_6 resonance, the intermediate source Mars-crossers (IMC), the 3:1 resonance, the outer main belt (OB), and the Transneptunian disk (which provides active and inactive Jupiter-family comets). Our model does not include the nearly-isotropic population comets (NIC), which nominally has a Tisserand parameter with respect to Jupiter of $T < 2$. The outermost boundary of our NEO model has been set to 7.4 AU. Beyond this limit, the contribution of NICs may be predominant. We believe NICs produce a significant number of NEOs, but we are unable to determine their contribution at this time. The paucity of NIC discoveries with $a < 7.4$ AU, however, makes us suspect they are only minor contributors to the overall NEO population with $a < 7.4$ AU. Objects from potential asteroidal source regions such as the Hungaria/Phocaea asteroid regions do not produce enough long-lived NEOs to make a significant contribution to the overall NEO population (Sec. 2.).

- The comet integrations used in this paper do not include planetary perturbations from the terrestrial planets. For this reason, we cannot precisely determine how many extinct comets reach Encke-type orbits ($T > 3$, $a < a_J$). Insights derived from our OB integrations suggest the total number of extinct comets with $a < 2.5$ AU is unlikely to overwhelm the NEO contribution from the main belt (Sec. 2.6).

- Our NEO model was calibrated by fitting it to a biased population of 138 NEOs discovered or accidentally rediscovered by Spacewatch (Sec. 5). We estimate there are $\sim 960 \pm 120$ NEOs with $T > 2$ and $H < 18$. The fractional contributions from our 5 intermediate source (IS) regions derived from our best-fit case for $H < 22$ NEOs are: $\beta_{\nu_6} = 0.37 \pm 0.08$, $\beta_{\rm IMC} = 0.25 \pm 0.03$, $\beta_{3:1} = 0.23 \pm 0.09$, $\beta_{\rm OB} = 0.08 \pm 0.01$, and $\beta_{\rm JFC} = 0.06 \pm 0.04$ (Table 3). These results suggest that $\sim 61\%$ of all $H < 22$ NEOs come from the inner main belt, $\sim 24\%$ come from the central main belt, $\sim 8\%$ come from the outer main belt, and $\sim 6\%$ come from the JFC region. (Sec. 6).

- Based on our estimates, over 44% of the $H < 18$ objects have been discovered so far (as of December 2000). NEOs having $e \leq 0.4$ or $H < 15.5$ are nearly complete. Many of the undiscovered $H < 18$ NEOs reside on highly eccentric or inclined orbits (Sec. 6) .

- The cumulative power-law size-frequency distribution of our debiased NEO population has a slope index of -1.75 (i.e., $N(> D) \propto D^{-1.75}$). This result is similar to the estimated slope indices of the youthful crater populations found on the terrestrial planets and Galilean satellites (Sec. 3.2). This shallow slope suggests that the material reaching the NEO population is collisionally-evolved rather than being fresh ejecta. This result implies that the primary dynamical mechanism delivering NEOs to transportation resonances in the main belt is the Yarkovsky effect and not collisional injection (Sec. 7.1).

- Using our NEO model, we find that Amors, Apollos, and Atens make up 32±1%, 62±1%, and 6±1% of the $H < 22$ NEO population, respectively. The population of objects inside Earth's orbit (IEOs) are equivalent to 2% the size of the NEO population. Asteroids with $H < 22$ from the inner main belt ($2.1 < a < 2.48$ AU), produce $\sim 53\%$, $\sim 64\%$, $\sim 79\%$, and $\sim 75\%$ of the Amor, Apollo, Aten, and IEO populations, respectively. Additional NEO population details can be found in Table 4 (Sec. 6).

- The replenishment rate from the main belt needed to keep the $H < 18$ NEA population in steady-state is 790 ± 200 objects per Myr (Table 2). 72% of these objects come from the outer main belt, where chaotic diffusion of objects is strong. Results suggest that the Yarkovsky effect may be the primary transportation mechanism moving material into these IS regions. By assuming our estimated NEO flux have been constant for the last 3 Gyr, we calculate that the main belt has lost $\sim 5\%$ of its mass over the last 3 Gyr (Sec. 7.1).

- Based on our best-fit NEO model, the steady-state population of $H < 18$ asteroids in the ν_6 resonance, IMCs, and 3:1 resonance is 160 ± 53, 4000 ± 940, and 270 ± 130, respectively. This result implies that the IMC population is ~ 4 times the size of the NEO population. Accordingly, the IMCs provide a large share of the impactors striking Mars. (Sec. 7.2)

- We estimate that there are 60 ± 51 extinct comets with $H < 18$ in the JFC-NEO region. This value corresponds to 200 ± 160 km-sized comets in the JFC region, with 78% of them being extinct comets. These results are a factor of 3 lower than previous estimates provided in Levison *et al.* (2000), as are our estimates of the number of km-sized comets residing in the ecliptic, Kuiper belt, and scattered disk comet populations. We estimate that the multiplicative factor needed to convert $H_T < 9$ comets into km-sized nuclei is $S = 1.7 \pm 1.4$. (Sec. 8.1). Note that these results assume that 100% of the JFCs fade rather than disintegrate.

- Based on our 5-source NEO model, we identified 46 NEOs with a $P > 10\%$ chance of coming from the JFC region (Table 5), making them likely candidates to be extinct comets. Most of these objects have $2 < T < 3$ orbits. Because our comet integrations cannot yet make Encke-type objects, our probability factors may be systematically too low and/or may be missing some objects (Sec. 8.2).

- It is unclear whether (2201) Oljato, (3200) Phaethon, and (4015) Wilson- Harrington are asteroids or extinct comets. Our NEO model results indicate the first two are asteroids, but our comet integrations do not yet include perturbations from the terrestrial planets. Insights derived from our OB integrations suggest these objects could possibly be extinct comets, though more work is needed to substantiate this. (4015) Wilson-Harrington, on the other hand, has a 5% chance of coming from the JFC region and a 65% change of combing from the OB region (Sec. 8.2).

Acknowledgements

We thank Joe Burns, Luke Dones, Brett Gladman, Alan Harris, Tom Loredo, Brian Marsden, Bob McMillian, David Nesvorný, Dave Rabinowitz, Tim Spahr, J. Scott Stuart, Paul Weissman, George Wetherill, and David Vokrouhlický for valuable discussions and input to this study. We also thank referees Giovanni Valsecchi and Rick Binzel for their careful and constructive reviews. We are indebted to the late Paolo Farinella and Gene Shoemaker, whose influential papers on the NEO and active/extinct comet populations inspired much of the work completed here. Part of this research was conducted using the resources of the Cornell Theory Center (CTC), which receives funding from Cornell University, New York State, federal agencies, and corporate partners. In addition, we gratefully acknowledge the computational resources provided to us for this project by the University of Texas, the University of Arizona, the Osservatorio Astronomico di Torino, and the Observatoire de la Côte d'Azur. Finally, we thank Chris Pelkie and the CTC for their help in making visualizations used to support this work. Observations by Spacewatch and research by Robert Jedicke are supported by grants from NASA (NAG5-7854 and NAG5-6611), AFOSR (F49620-98-1-0006 and F49620-00-1-0126), The David and Lucile Packard Foundation, The Steven and Michele Kirsch Foundation, John and Ilene Nitardy, and other contributors. Research funds for William Bottke were provided by NASA Grants NAGW-310 and NAG5-9082. Alessandro Morbidelli's work was subsidized by ESA Contract 14018/2000/F/TB. Travel support was provided by grants from NATO and NSF/CNRS.

REFERENCES

Bailey, M. E. 1994. Formation of the outer solar system bodies: Comets and planetesimals. IAU Symp. 160: Asteroids, Comets, Meteors 1993, 160, 443

Binzel, R. P., S. J. Bus, T. H. Burbine, and J. M. Sunshine. 1996. Spectral properties of near-earth asteroids: Evidence for sources of ordinary chondrite meteorites. Science 273, 946-948

Bottke, W. F., M. C. Nolan, R. Greenberg and R. A. Kolvoord. 1994a. Velocity distributions among colliding asteroids. Icarus 107, 255-268

Bottke, W. F., M. C. Nolan, R. Greenberg, and R. A. Kolvoord 1994b. Collisional lifetimes and impact statistics of near-Earth asteroids. In *Hazards Due to Comets and Asteroids* (T. Gehrels, M. S. Matthews, Eds.), pp. 337–357. Univ. of Arizona Press, Tucson.

Bottke, W. F., R. Jedicke, A. Morbidelli, J.-M. Petit and B. Gladman. 2000a. Understanding the distribution of near-Earth asteroids. Science 288, 2190-2194

Bottke, W. F., D. P. Rubincam and J. A. Burns. 2000b. Dynamical evolution of main belt meteoroids: Numerical simulations incorporating planetary perturbations and Yarkovsky thermal forces. Icarus 145, 301-331

Bottke, W. F., D. Vokrouhlický, M. Brož, D. Nesvorný, and A. Morbidelli. 2001. Dynamical spreading of asteroid families via the Yarkovsky effect: The Koronis family and beyond. Science, in press.

Bottke, W. F., D. Vokrouhlický, D. Rubincam, and M. Brož. 2002. Dynamical evolution of asteroids and meteoroids using the Yarkovsky effect. In *Asteroids III* (W. F. Bottke, A. Cellino, P. Paolicchi, and R. Binzel, Eds.) Univ. of Arizona Press, Tucson, in press.

Bowell, E., R. M. West, H. -. Heyer, J. Quebatte, L. E. Cunningham, S. J. Bus, A. W. Harris, R. L. Millis and B. G. Marsden 1992. (4015) 1979 VA = Comet Wilson-Harrington (1949 III). IAU Circ.5585, 1

Bowell, E., B. Hapke, D. Domingue, K. Lumme, J. Peltoniemi and A. W. Harris 1989. Application of photometric models to asteroids. In *Asteroids II* (R. P. Binzel, T. Gehrels, and M. S. Matthews, Eds.), pp. 524–556. Univ. of Arizona Press, Tucson.

Bowell, E., and K. Muinonen 1994. Earth-crossing asteroids and comets: Groundbased search strategies. In *Hazards Due to Comets and Asteroids* (T. Gehrels, M. S. Matthews, Eds.), pp. 417–462. Univ. of Arizona Press, Tucson.

Campo Bagatin, A., V. J. Martinez and S. Paredes. 2000. Multinomial fits to the observed main belt asteroid distribution. AAS/Division of Planetary Sciences Meeting 32, 0813

Carusi, A., L. Kresak, E. Perozzi, and G. B. Valsecchi 1987. High-order librations of Halley-type comets. Astron. Astrophys. 187, 899

Carruba, V., J. A. Burns, W. Bottke and A. Morbidelli 2000. Asteroid mobility due to encounters with Ceres, Vesta, Pallas: Monte Carlo codes versus direct numerical integrations. AAS/Division of Planetary Sciences Meeting 32, 1406

Chamberlin, A. B., L. McFadden, R. Schulz, D. G. Schleicher and S. J. Bus 1996. 4015 Wilson-Harrington, 2201 Oljato, and 3200 Phaethon: Search for CN emission. Icarus 119, 173-181

Cruikshank, D. P., D. J. Tholen, J. F. Bell, W. K. Hartmann, and R. H. Brown 1991. Three basaltic earth-approaching asteroids and the source of the basaltic meteorites. Icarus 89, 1-13

Culler, T. S., T. A. Becker, R. A. Muller, and P. R. Renne. 2000. Lunar impact history from $^{40}Ar/^{39}Ar$ dating of glass spherules. Science 287, 1785-1788.

D'Abramo, G., A. W. Harris (JPL), A. Boattini, A. W. Harris (DLR), and G. B. Valsecchi. 2001. A simple probabilistic model to estimate the population of Near Earth Asteroids. Icarus, in press.

Dohnanyi, J. W. 1969. Collisional models of asteroids and their debris. J. Geophys. Res. 74, 2531-2554

Dones, L., B. Gladman, H. J. Melosh, W. B. Tonks, H. F. Levison and M. Duncan 1999. Dynamical lifetimes and final fates of small bodies: Orbit integrations vs. Öpik calculations. Icarus 142, 509-524

Doressoundiram, A., A. Cellino, M. di Martino, F. Migliorini and V. Zappalà 1998. The puzzling case of the Nysa-Polana family finally solved? AAS/Division of Planetary Sciences Meeting 30, 0505

Dumas, C., T. Owen and M. A. Barucci 1998. Near-infrared spectroscopy of low-albedo surfaces of the solar system: Search for the spectral signature of dark material. Icarus 133, 221-232

Duncan, M., T. Quinn and S. Tremaine 1987. The formation and extent of the solar system comet cloud. Astron. J. 94, 1330-1338

Duncan, M., Quinn, T., & Tremaine, S. 1988. The origin of short-period comets. ApJ, 328, L69-L73

Duncan, M. J., H. F. Levison and S. M. Budd 1995. The dynamical structure of the Kuiper Belt. Astron. J. 110, 3073

Duncan, M. J. and H. F. Levison 1997. A scattered comet disk and the origin of Jupiter family comets. Science 276, 1670-1672

Durda, D. D., R. Greenberg and R. Jedicke 1998. Collisional models and scaling laws: A new interpretation of the shape of the main-belt asteroid size distribution. Icarus 135, 431-440

Farinella, P., R. Gonczi, C. Froeschlé and C. Froeschlé 1993. The injection of asteroid fragments into resonances. Icarus 101, 174-187

Farinella, P., C. Froeschlé, C. Froeschlé, R. Gonczi, G. Hahn, A. Morbidelli and G. B. Valsecchi 1994. Asteroids falling onto the Sun. Nature 371, 315

Farinella, P., D. Vokrouhlicky and W. K. Hartmann 1998. Meteorite delivery via Yarkovsky orbital drift. Icarus 132, 378-387

Farinella, P. and D. Vokrouhlicky 1999. Semimajor axis mobility of asteroidal fragments. Science 283, 1507-1510

Froeschlé, C. and A. Morbidelli 1994. The secular resonances in the solar system. IAU Symp. 160: Asteroids, Comets, Meteors 1993, 160, 189

Gladman, B. J., F. Migliorini, A. Morbidelli, V. Zappalà, P. Michel, A. Cellino, C. Froeschlé, H. F. Levison, M. Bailey and M. Duncan 1997. Dynamical lifetimes of objects injected into asteroid belt resonances. Science 277, 197-201

Gladman, B., P. Michel and C. Froeschlé 2000. The near-Earth object population. Icarus 146, 176-189

Gradie, J. C., C. R. Chapman and E. F. Tedesco 1989. Distribution of taxonomic classes and the compositional structure of the asteroid belt. In *Asteroids II* (R. P. Binzel, T. Gehrels, and M. S. Matthews, Eds.), pp. 316-335. Univ. of Arizona Press, Tucson.

Grieve, R. A. F., and E. M. Shoemaker 1994. The record of past impacts on Earth. In *Hazards Due to Comets and Asteroids* (T. Gehrels, M. S. Matthews, Eds.), pp. 417–462. Univ. of Arizona Press, Tucson.

Gustafson, B. A. S. 1989. Geminid meteoroids traced to cometary activity on Phaethon. Astron. Astrophys. 225, 533-540

Harris, A. W. 2000. The population of near-Earth asteroids. AAS/Division of Dynamical Astronomy Meeting 32, 0604

Hicks, M. D., U. Fink and W. M. Grundy 1998. The unusual spectra of 15 near-Earth asteroids and extinct comet candidates. Icarus 133, 69-78

Hicks, M. D., B. J. Buratti, R. L. Newburn and D. L. Rabinowitz 2000a. Physical Observations of 1996 PW and 1997 SE5: Extinct comets or D-type asteroids? Icarus 143, 354-359

Hicks, M. D., B. J. Buratti and D. L. Rabinowitz 2000b. Preliminary results of the Palomar spectral survey: Near-Earth asteroids, Centaurs, and extinct comet candidates. AAS/Division of Planetary Sciences Meeting 32, 0704

Hörz, F. 2000. Time-variable cratering rates? Science 288, 2095a.

Jedicke, R. 1996. Detection of near-Earth asteroids based upon their rates of motion. Astron. J. 111, 970

Jedicke, R. and T. S. Metcalfe 1998. The orbital and absolute magnitude distributions of main belt asteroids. Icarus 131, 245-260

Jedicke, R., A. Morbidelli, J.-M. Petit, T. Spahr, and W. F. Bottke. 2001. Earth and space-based NEO survey simulations: Prospects for achieving the Spaceguard goal. Icarus, in preparation.

Jewitt, D. 1991. Cometary photometry. In *Comets in the Post-Halley Era. Vol. 1* (R. L. Newburn, M. Neugebauer, and J. Rahe, Eds.) pp. 19-65. Kluwer Academic Publishers, Dordrecht, The Netherlands.

Jewitt, D. C. and J. X. Luu 1990. CCD spectra of asteroids. II - The Trojans as spectral analogs of cometary nuclei. Astron. J. 100, 933-944

Keller, H. U., W. A. Delamere, H. J. Reitsema, W. F. Huebner and H. U. Schmidt 1987. Comet P/Halley's nucleus and its activity. Astron. Astrophys. 187, 807-823

Kresak, L. 1979. Dynamical interrelations among comets and asteroids. In *Asteroids* (T. Gehrels, Eds.), pp. 289-309. Univ. of Arizona Press, Tucson.

Levison, H. F. 1996. Comet taxonomy. ASP Conf. Ser. 107: Completing the Inventory of the Solar System 173-191

Levison, H. F. and M. J. Duncan 1997. From the Kuiper belt to Jupiter-family comets: The spatial distribution of ecliptic comets. Icarus 127, 13-32

Levison, H. F. and M. J. Duncan 1994. The long-term dynamical behavior of short-period comets. Icarus 108, 18-36

Levison, H., E. M. Shoemaker, and C. S. Shoemaker 1997. The dispersal of the Trojan asteroid swarm. Nature 385, 42-44

Levison, H. F., M. J. Duncan, K. Zahnle, M. Holman and L. Dones 2000. Planetary impact rates from ecliptic comets. Icarus 143, 415-420

Levison, H. F., L. Dones, and M. J. Duncan 2001. The origin of Halley-type comets: Probing the inner Oort cloud. Astron. J. 121, 2253-2267

Luu, J. X. 1993. Spectral diversity among the nuclei of comets. Icarus 104, 138-148

Luu, J. and D. Jewitt 1989. On the relative numbers of C types and S types among near-earth asteroids. Astron. J. 98, 1905-1911

Lyons, L. 1986. Statistics for Nuclear and Particle Physicists. Cambridge: University Press, 1986

McFadden, L., D. J. Tholen, and G. J. Veeder 1989. Physical properties of Aten, Apollo and Amor asteroids. In *Asteroids II* (R. P. Binzel, T. Gehrels, and M. S. Matthews, Eds.), pp. 442-467. Univ. of Arizona Press, Tucson.

McFadden, L. A., A. L. Cochran, E. S. Barker, D. P. Cruikshank and W. K. Hartmann 1993. The enigmatic object 2201 Oljato - Is it an asteroid or an evolved comet?. J. Geophys. Res. 98, 3031-3041

Menichella, M., P. Paolicchi and P. Farinella 1996. The main belt as a source of near-Earth asteroids. Earth Moon and Planets 72, 133-149

Michel, P. 1997. Effects of linear secular resonances in the region of semimajor axes smaller than 2 AU. Icarus 129, 348-366

Michel, P. 1998. Dynamical behaviour of Near-Earth asteroids in the terrestrial planet region : the role of secular resonances. Planet. Space Sci. 46, 905-910

Michel, P. and F. Thomas 1996. The Kozai resonance for near-Earth asteroids with semimajor axes smaller than 2AU. Astron. Astrophys. 307, 310-318

Michel, P., V. Zappalà, A. Cellino and P. Tanga 2000a. Estimated abundance of Atens and asteroids evolving on orbits between Earth and Sun. Icarus 143, 421-424

Michel, P., F. Migliorini, A. Morbidelli and V. Zappalà 2000b. The population of Mars-crossers: Classification and dynamical evolution. Icarus 145, 332-347

Migliorini, F., A. Morbidelli, V. Zappalà, B. J. Gladman, M. E. Bailey and A. Cellino 1997. Vesta fragments from ν_6 and 3:1 resonances: Implications for V-type NEAs and HED meteorites. Meteoritics and Planetary Science 32, 903-916

Migliorini, F., P. Michel, A. Morbidelli, D. Nesvorný and V. Zappalá 1998. Origin of Earth-crossing asteroids: a quantitative simulation. Science 281, 2022-2024

Moons, M. 1997. Review of the dynamics in the Kirkwood gaps. Celestial Mechanics and Dynamical Astronomy 65, 175-204

Morbidelli, A., R. Gonczi, C. Froeschlé and P. Farinella 1994. Delivery of meteorites through the ν_6 secular resonance. Astron. Astrophys 282, 955-979

Morbidelli, A. and M. Moons 1995. Numerical evidence on the chaotic nature of the 3/1 mean motion commensurability. Icarus 115, 60-65

Morbidelli, A. and B. Gladman 1998. Orbital and temporal distributions of meteorites originating in the asteroid belt. Meteoritics and Planetary Science 33, 999-1016

Morbidelli, A. and D. Nesvorny 1999. Numerous weak resonances drive asteroids toward terrestrial planets orbits. Icarus 139, 295-308

Morrison, D. 1992. The Spaceguard Survey: Report of the NASA International Near-Earth-Object Detection Workshop. NASA, Washington, D.C.

Nesvorný, D. and A. Morbidelli 1998. An analytic model of three-body mean Motion resonances. Celestial Mechanics and Dynamical Astronomy 71, 243-271

Nesvorný, D. and A. Morbidelli 1999. The long-term evolution of the main asteroidal belt and the origin of large Mars-and Earth-crossers. IAU Colloq. 173: Evolution and Source Regions of Asteroids and Comets, 321

Nesvorný, D. A. Morbidelli, D. Vokrouhlický, W. F. Bottke, and M. Brož. 2001. The Flora family: A case of the dynamically dispersed collisional swarm? Icarus, in press.

Passey, Q. R. and E. M. Shoemaker 1982. Craters and basins on Ganymede and Callisto - Morphological indicators of crustal evolution. In *Satellites of Jupiter* (D. Morrison, Eds.), pp. 379-434. Univ. of Arizona Press, Tucson.

Press, W. H., B. P. Flannery, S. A. Teukolsky and W. T. Vetterling 1989. Numerical recipes in Fortran. The art of scientific computing. Cambridge: University Press, 1989

Rabe, E. 1971. Trojans and comets of the Jupiter group. IAU Colloq. 12: Physical Studies of Minor Planets (T. Gerhels, Ed.) NASA SP-267, 407.

Rabinowitz, D. L. 1993. The size distribution of the earth-approaching asteroids. Astrophys. J. 407, 412-427

Rabinowitz, D. L. 1994. The size and shape of the near-Earth asteroid belt. Icarus 111, 364-377

Rabinowitz, D. L. 1997a. Are main-belt asteroids a sufficient source for the Earth-approaching asteroids?. Part I. Predicted vs. observed orbital distributions. Icarus 127, 33-54

Rabinowitz, D. L. 1997b. Are main-belt asteroids a sufficient source for the Earth-approaching asteroids? Part II. Predicted vs. observed size distributions. Icarus 130, 287-295

Rabinowitz, D. L. 1998. Size and orbit dependent trends in the reflectance colors of Earth-approaching asteroids. Icarus 134, 342-346

Rabinowitz, D. L. and M. D. Hicks 1998. The Table Mountain photometric survey of near-Earth asteroids. AAS/Division of Planetary Sciences Meeting 30, 1608

Rabinowitz, D., E. Bowell, E. M. Shoemaker, and K. Muinonen 1994. The population of Earth-crossing asteroids. In *Hazards Due to Comets and Asteroids* (T. Gehrels, M. S. Matthews, Eds.), pp. 285–312. Univ. of Arizona Press, Tucson.

Rabinowitz, D. L. E. Helin, K. Lawrence, and S. Pravdo. 2000. A reduced estimate of the number of kilometre-sized near-Earth asteroids. Nature 403, 165-166

Schaber, G. G., R. G. Strom, H. J. Moore, L. A. Soderblom, R. L. Kirk, D. J. Chadwick, D. D. Dawson, L. R. Gaddis, J. M. Boyce and J. Russell 1992. Geology and distribution of impact craters on Venus - What are they telling us?. J. Geophys. Res. 97, 113257

Shoemaker, E. M. 1983. Asteroid and comet bombardment of the Earth. Annual Review of Earth and Planetary Sciences 11, 461-494

Shoemaker, E. M. and R. F. Wolfe 1982. Cratering time scales for the Galilean satellites. In *Satellites of Jupiter* (D. Morrison, Eds.), pp. 277-339. Univ. of Arizona Press, Tucson.

Shoemaker, E. M., R. F. Wolfe, and C. S. Shoemaker. 1990. Asteroid and comet flux in the neighborhood of Earth. In *Global Catastrophes in Earth history* (V. L. Sharpton and P. D. Ward, eds.), Geol. Soc. Amer. Spec. Paper 247, 335-342.

Shoemaker, E. M., P. R. Weissman, and C. S. Shoemaker 1994. The flux of periodic comets near Earth. In *Hazards Due to Comets and Asteroids* (T. Gehrels, M. S. Matthews, Eds.), pp. 313–335. Univ. of Arizona Press, Tucson.

Stern, S. A. and D. D. Durda 2000. Collisional evolution in the Vulcanoid region: Implications for present-day population constraints. Icarus 143, 360-370

Strom, R. G., S. K. Croft and N. G. Barlow 1992. The Martian impact cratering record. In *Mars* (H. H. Kieffer, B. M. Jakosky, C. W. Snyder, M. S. Matthews, Eds.), pp. 383-423. Univ. of Arizona Press, Tucson.

Stuart, J. S. 2000. The near-Earth asteroid population from LINEAR project data. AAS/Division of Planetary Sciences Meeting 32, 1603

Tanga, P., A. Cellino, P. Michel, V. Zappalà, P. Paolicchi and A. Dell'Oro 1999. On the size distribution of asteroid families: The Role of Geometry. Icarus 141, 65-78

Tedesco, E. F., K. Muinonen and S. D. Price 2000. Space-based infrared near-Earth asteroid survey simulation. Planet. Space Sci. 48, 801-816

Tholen, D. J. and M. A. Barucci 1989. Asteroid taxonomy. In *Asteroids II* (R. P. Binzel, T. Gehrels, and M. S. Matthews, Eds.), pp. 298-315. Univ. of Arizona Press, Tucson.

Ward, W. R. 1992. Long-term orbital and spin dynamics of Mars. In *Mars* (H. H. Kieffer, B. M. Jakosky, C. W. Snyder, M. S. Matthews, Eds.), pp. 298-320. Univ. of Arizona Press, Tucson.

Weissman, P. R. 1980. Physical loss of long-period comets. Astron. Astrophys. 85, 191-196

Weissman, P. R. 1996. The Oort Cloud. ASP Conf. Ser. 107: Completing the Inventory of the Solar System 265-288

Weissman, P. R. 1990. The Oort cloud. Nature 344, 825-830

Weissman, P. R., M. F. A'Hearn, H. Rickman and L. A. McFadden 1989. Evolution of comets into asteroids. In *Asteroids II* (R. P. Binzel, T. Gehrels, and M. S. Matthews, Eds.), pp. 442–467. Univ. of Arizona Press, Tucson.

Weissman, P. R. and H. F. Levison 1997. Origin and evolution of the unusual object 1996 PW: Asteroids from the Oort cloud?. Ap. J. Lett. 488, L133

Wetherill, G. W. 1976. Where do the meteorites come from - A re-evaluation of the earth-crossing Apollo objects as sources of chondritic meteorites. Geochim. Cosmochim. Acta 40, 1297-1317

Wetherill, G. W. 1979. Steady state populations of Apollo-Amor objects. Icarus 37, 96-112

Wetherill, G. W. 1985. Asteroidal source of ordinary chondrites. 1984. Meteoritics 20, 1-22

Wetherill, G. W. 1987. Dynamical relations between asteroids, meteorites and Apollo-Amor objects. Royal Society of London Philosophical Transactions Series 323, 323-337

Wetherill, G. W. 1988. Where do the Apollo objects come from?. Icarus 76, 1-18

Wetherill, G. W. and J. G. Williams 1979. Origin of differentiated meteorites. Origin and Distribution of the Elements. 19-91

Wiegert, P. and S. Tremaine 1999. The evolution of long-period comets. Icarus 137, 84-121

Wilhelms, D. E. 1993. To a rocky moon - A geologist's history of lunar exploration. University of Arizona Press.

Wisdom, J. 1983. Chaotic behavior and the origin of the 3/1 Kirkwood gap. Icarus 56, 51-74

Wisdom, J. and M. Holman 1991. Symplectic maps for the n-body problem. Astron. J. 102, 1528-1538

Valsecchi, G. B. 1999. From Jupiter-family comets to objects in Encke-like orbit. IAU Colloq. 173: Evolution and Source Regions of asteroids and Comets. 353

Veverka, J., M. Robinson, P. Thomas, S. Murchie, J. F. Bell III, N. Izenberg, C. Chapman, A. Harch, M. Bell, B. Carcich, A. Cheng, B. Clark, D. Domingue, D. Dunham, R. Farquhar, M. J. Gaffey, E. Hawkins, J. Joseph, R. Kirk, H. Li, P. Lucey, M. Malin, P. Martin, L. McFadden, W. J. Merline, J. K. Miller, W. M. Owen Jr., C. Peterson, L. Prockter, J. Warren, D. Wellnitz, B. G. Williams, D. K. Yeomans. 2000. NEAR at Eros: Imaging and spectral results. Science 289, 2088-2097

Vokrouhlický, D. and P. Farinella 2000. Efficient delivery of meteorites to the Earth from a wide range of asteroid parent bodies. Nature 407, 606-608

Vokrouhlický, D., P. Farinella, and W. F. Bottke 2000. The depletion of the putative vulcanoid population via the Yarkovsky effect. Icarus 148, 147-152

Zahnle, K., L. Dones and H. F. Levison 1998. Cratering rates on the Galilean satellites. Icarus 136, 202-222

Zappalà, V., A. Cellino, P. Michel and P. Tanga 1999. Looking for parent bodies of km-sized NEAs. AAS/Division of Planetary Sciences Meeting 31, 0105

Table Captions

Table 1. Glossary of acronyms and important variables.

Table 2. Integration of 5 sets of outer main belt asteroids (OB1-OB5). All asteroids have $i < 15°$ and were tracked for 100 Myr. Those entering $q < 1.3$ AU orbits were followed until they entered a sink. The mean time spent in the NEO region by each particle is given by $< L_{\rm NEO} >$.

Table 3. Properties of the NEO intermediate sources. $< L_{\rm ETR} >$ is the mean lifetime spent in the extended target region ($q < 1.3$ AU; $a < 4.2$ AU; $e < 1.0$; $i < 90°$; and $13 < H < 22$) by particles coming from each source. $\tau_{\rm IS}$ lists the "initial" mortality rate of the particles from each source, in terms of the fraction of population dying per Myr. $\alpha_{\rm IS}$ shows the fraction of the steady-state NEO population in the "constrained target region" ($q < 1.3$ AU; $a < 4.2$ AU; $e < 0.8$; $i < 35°$; and $13 < H < 22$) sustained from each intermediate source, while $\beta_{\rm IS}$ shows the contributions over the extended target region. This latter value, multiplied by the estimated number of $H < 18$ NEOs yields $N_{\rm NEO}$. I is the first-entry rate into the NEO region, in terms of number of bodies with $H < 18$ per Myr, computed from Eq. (13). $N_{\rm IS}$ is the expected steady-state number of $H < 18$ bodies from each IS source computed from Eq. (16).

Table 4. Statistics of steady-state NEO and IEO ($Q < 0.983$ AU) populations. The percentages refer to predicted values for $H < 18$ objects.

Table 5. Extinct comet candidates. Using our 4-source NEO model, we compute P, the probability that an NEO with a given (a, e, i) orbit is derived from the Jupiter-family comet (JFC) intermediate source region. We list the NEOs which have $P_{\rm JFC} > 0.1$. We suspect some of these objects are extinct comets. T is the Tisserand parameter calculated from Eq. (1).

Figure Captions

Fig. 1. An (a, e) representation of 138 $H < 22$ NEOs discovered (or accidentally re-discovered) by Spacewatch. NEOs have perihelia $q \leq 1.3$AU and aphelia $Q \geq 0.983$ AU. Apollos ($a \geq 1.0$ AU; $q \leq 1.0167$ AU) and Atens ($a < 1.0$ AU; $Q \geq 0.983$ AU) are on Earth-crossing orbits. These objects are plotted as circles and triangles, respectively. Amors (1.0167 AU $< q \leq 1.3$ AU) are on nearly-Earth-crossing orbits. These objects are plotted as stars. IEOs ($Q < 0.983$ AU) are inside Earth's orbit. None have been found so far. The Jupiter-family comet (JFC) region is defined using two lines of constant Tisserand parameter $2 < T < 3$ (Eq. 1). The shaded region shows where $2 < T < 3$ for $i = 0°$. The nearly-isotropic comet (NIC) region is defined as having $T < 2$. We caution that T is a function of (a, e, i), such that projections like this onto the $i = 0°$ can be misleading. For example, $T < 2$ moves to $a \gtrsim 2.6$ AU as i approaches 90°. The $Q = 4.61$ AU line represents the (a, e) parameters needed to cross Jupiter's Hill sphere. The $q < 1.66$ AU line defines the present-day boundary between objects on Mars-crossing orbits and those in the main belt. Various mean-motion resonances are shown as dashed lines; the width of each resonance is not represented. The $i = 0°$ position of the ν_6 secular resonance is shown as a dashed line (Sec. 2.3). The solid line bracketing the inner and outer IMC region indicates where known asteroids with $q < 1.82$ AU were integrated for at least 100 Myr. The regions designated OB1-OB5 are the outer main belt regions where known asteroids were integrated for at least 100 Myr (Sec. 2.5).

Fig. 2. A representation of the probability distribution of residence time ($R_{3:1}(a, e, i)$) for test bodies evolving out of the 3:1 mean-motion resonance with Jupiter. The sum of the (a, e, i) bins with $q < 1.3$ AU, 0.5 AU $< a < 4.2$ AU; $e < 0.8$, and $i < 35°$ has been normalized to 1.0. To display as much of the (a, e, i) distribution as possible in two dimensions, the i bins were summed before plotting $R_{3:1}(a, e)$, while the e bins were summed before plotting $R_{3:1}(a, i)$. The color scale depicts the expected density of NEOs in a scenario of steady-state replenishment from the 3:1 resonance. Red colors indicate where NEOs are statistically most likely to spend their time. Bins whose centers have perihelia $q > 1.3$ AU are not used and are colored white. The gold curved lines divide the NEO region into Amor, Apollo, and Aten components. The curves in the upper right show where $2 < T < 3$ for $i = 0°$ (See Fig. 1). The maximum level on the color bar scale was chosen to show off interesting features in the distribution.

Fig. 3. A representation of the probability distribution of residence times for test bodies evolving out of the ν_6 secular resonance ($R_{\nu_6}(a, e, i)$). See Fig. 2 for additional plot details and Sec. 2.3 for more information on this intermediate source.

Fig. 4. A representation of the probability distribution of residence time for test bodies evolving out of the intermediate-source Mars-crosser (IMC) population ($R_{\rm IMC}(a, e, i)$). See Fig. 2 for additional plot details and Sec. 2.4.1 for more information on this intermediate source.

Fig. 5. Orbital distribution of the known Mars-crossing asteroids on $1.3 < q < 1.66$ AU orbits.

The osculating values (a, i) are shown, as are the boundaries of various Mars-crossing populations (i.e., IMC, HU, MB2, and EV).

Fig. 6. A representation of the probability distribution of residence time for test bodies evolving out of the outer main belt ($R_{\rm OB}(a,e,i)$). The source region is shown in Fig. 1. See Fig. 2 for additional plot details and Sec. 2.5 for more information on this intermediate source.

Fig. 7. A representation of the probability distribution of residence time for test bodies evolving out of Transneptunian region (see text) and onto orbits with $q < 1.3$ AU and $a < 7.4$ AU ($R_{\rm JFC}(a,e,i)$). These so-called ecliptic comets frequently reach the Jupiter-family comet (JFC) region, defined by $2 < T < 3$. Planetary perturbations from the terrestrial planets were not included in this set of integrations. See Fig. 2 for additional plot details and Sec. 2.6 for more information on this intermediate source.

Fig. 8. The probability distributions $R_{\rm inner-IMC}(a,e,i)$ (solid histogram) and $R_{\nu_6}(a,e,i)$ shown as a series of one-dimensional histograms. Each distribution has been normalized so that its sum over the plotted (a,e,i) limits is 1.0. Other than minor differences near $e = 0.4$-0.5 and $i = 5°$-$10°$, the residence time functions are comparable. This degeneracy implies that our NEO model may not be able to easily discriminate between these two inner main belt IS regions.

Fig. 9. The exponential decay of the integrated IMC population (described in Sec. 2.4.1) into the sinks. The particles must pass through the NEO region to reach a major sink (e.g., ejection from the inner solar system; striking the Sun). The slope of the line fit to the decay curve yields the fractional decay rate $\tau_{\rm active-IMC} = 0.016$ Myr^{-1}.

Fig. 10. A comparison between the 138 Spacewatch NEOs (shaded histogram) and $n(a,e,i,H)$ (dark solid line), our best-fit of the observed NEO probability distribution assuming $\alpha_{\nu_6}, \alpha_{\rm IMC}, \alpha_{3:1}, \alpha_{\rm OB}, \alpha_{\rm JFC} = 0.37, 0.27, 0.20, 0.10, 0.06$, respectively. The parameters are linked to the constrained target region (i.e., $q < 1.3$ AU, 0.5 AU $< a <$ 4.2 AU, $e < 0.8$, $i < 35°$, and $13 < H < 22$), where the observational biases were calculated. Note that $n(a,e,i,H)$ has been collapsed into one dimension for this comparison.

Fig. 11. A representation of the probability distribution of residence time for the debiased NEO population ($R_{\rm NEO}(a,e,i)$). See Fig. 2 for additional plot details and Sec. 6 for more information on this plot.

Fig. 12. The debiased orbital and size distribution of the NEOs for $H < 18$. The predicted NEO distribution (dark solid line) is normalized to 960 NEOs. It is compared with the 426 known NEOs (as of December 2000) from all surveys (shaded histogram). NEO observational completeness is $\sim 44\%$. Most discovered objects have low e and i.

Fig. 13. The debiased orbital distribution of the $H < 18$ Amor objects (solid line), compared to the known Amors (shaded histogram). We believe the mismatch at $a \sim 1.7$-1.9 AU and at $i \sim 25°$-$30°$ is caused by our exclusion of the Hungaria asteroid region in our NEO model.

Fig. 14. The debiased orbital distribution of the $H < 18$ Apollo objects (solid line) compared to the known Apollos (shaded histogram).

Fig. 15. The debiased orbital distribution of the $H < 18$ Aten objects (solid line) compared to the known Atens (shaded histogram).

Fig. 16. The debiased orbital distribution of the $H < 18$ IEOs (solid line) compared to the known IEOs (shaded histogram).

Fig. 17. A graphical comparison between the debiased NEO population produced by Rabinowitz *et al.* (1994) (solid histogram) and $R_{\rm NEO}(a, e, i)$ (solid line). The histogram has been normalized over the limits so that the sum of all values is 1.0.

Fig. 18. The size distribution of the main belt population computed by Durda *et al.* (1998), based on their collisional evolution model. The solid points are the debiased population of main belt asteroids computed by Jedicke and Metcalfe (1998). The upper curve is the initial "assumed" main belt population. The population of main belt asteroids with diameter $D > 30$ km is also shown. Note that this model does not yet include the Yarkovsky effect.

Fig. 19. The orbital distribution of extinct comet candidates on NEO orbits described in Table 5. The q lines represent the boundaries of the Amor/Apollo region. The remaining lines show where $2 < T < 3$ for $i = 0°$.

Table 1. Glossary

Acronym/Variable	Definition
NEO	Near-Earth object ($q \leq 1.3$ AU and $Q \geq 0.983$ AU)
NEA	Near-Earth asteroid
NEC	Near-Earth comet
Amor	NEO with 1.0167 AU $< q \leq 1.3$ AU
Apollo	NEO with $a \geq 1.0$ AU and $q \leq 1.0167$ AU
Aten	NEO with $a < 1.0$ AU and $q \leq 1.0167$ AU
IEO	Object residing inside Earth's orbit ($Q < 0.983$ AU)
Apohele	Alternate name of IEO
IS	Intermediate source
IMC	Intermediate source Mars-crossing asteroid
HU	Mars-crossing asteroid derived from Hungaria population
PH	Mars-crossing asteroid derived from Phocaeas population
MB2	Mars-crossing asteroid with $a > 2.5$ AU and high i
OB	Asteroid coming from outer main belt
ECOM	Ecliptic comet
JFC	Jupiter-family comet
NIC	Nearly isotropic population comets
LPC	Long period comet
HTC	Halley-type comet
a	Semimajor axis
e	Eccentricity
i	Inclination
H	Absolute magnitude
q	Perihelion distance
Q	Aphelion distance
T	Tisserand parameter
$R(a,e,i)$	Residence time probability distribution
$N(H)$	Absolute magnitude distribution
γ	Exponent of absolute magnitude distribution
CTR	Constrained target region ($a \leq 2.8$ AU, $e \leq 0.8$, $i \leq 35°$, and $13 \leq H \leq 22$)
ETR	Extended target region ($a \leq 4.2$ AU, $e \leq 1.0$, $i \leq 90°$, and $13 \leq H \leq 22$)
$M(a,e,i,H)$	Model NEO distribution
$B(a,e,i,H)$	Observational biases
$n(a,e,i,H)$	Model of observed (and biased) NEO distribution
α	Weighting function for IS contribution to NEOs in CTR
β	Weighting function for IS contribution to NEOs ($a < 7.4$ AU)
I	Steady state influx rate of objects into some region
L	Mean lifetime of objects in some region
τ	Fractional decay rate of some population
λ_m	Normalized data distribution of Spacewatch objects in CTR
D_m	Normalized (and biased) NEO model $n(a,e,i,H)$
m	Cell number
Q	Quality factor telling us goodness-of-fit
$\mathcal{L}$	Log-likelihood value

Table 2. Integration of the Outer Main Belt Asteroids

Set	a range (AU)	q range (AU)	Initial No. of Asteroids	No. reaching $q < 1.3$ AU	$< L_{\rm NEO} >$ (Myr)
OB1	2.83-2.95	1.66-2.40	449	73	0.19
OB2	2.83-2.95	2.40-2.60	359	6	0.19
OB3	2.95-3.03	1.66-2.40	285	100	0.11
OB4	2.95-3.03	2.40-2.60	303	35	0.11
OB5	3.03-3.50	1.66-2.40	568	149	0.13

Table 3. Properties of the NEO Intermediate Sources

	ν_6	IMCs	3:1	OB	JFCs	ECOMs
$< L_{\rm ETR} >$ (Myr^{-1})	6.54	3.75	2.16	0.14	–	45
$\tau_{\rm IS}$ (Myr^{-1})	0.35	0.016	0.38	0.020	–	4×10^{-5}
$\alpha_{\rm IS}$	0.37 ± 0.08	0.27 ± 0.03	0.20 ± 0.08	0.10 ± 0.01	0.06 ± 0.04	–
$\beta_{\rm IS}$	0.37 ± 0.08	0.25 ± 0.03	0.23 ± 0.08	0.08 ± 0.01	0.06 ± 0.04	–
$N_{\rm NEO}$ ($H < 18$)	360 ± 120	240 ± 60	220 ± 110	79 ± 17	61 ± 50	–
I (Bodies My^{-1})	55 ± 18	65 ± 15	100 ± 50	570 ± 120	–	0.29
$N_{\rm IS}$ ($H < 18$)	160 ± 53	4000 ± 940	270 ± 130	28000 ± 6000	–	1.3×10^{10}

Table 4. Statistics of Steady State NEO and IEO Populations

	NEO	Amor	Apollo	Aten	IEO
Predicted pop. size w.r.t. NEO pop. (%)	100	32 ± 1	62 ± 1	6 ± 1	2 ± 0
No. of predicted NEOs with $H < 18$	960 ± 120	310 ± 46	590 ± 80	58 ± 12	20 ± 4
No. of known NEOs with $H < 18$	425	204	195	26	0
Obs. Completeness for $H < 18$ NEOs (%)	44	66	33	45	0
$a < 2.0$ AU (%)	49 ± 4	27 ± 3	55 ± 4	100	100
$e < 0.4$ (%)	15 ± 1	25 ± 3	9 ± 1	27 ± 0	48 ± 1
$e < 0.6$ (%)	52 ± 2	87 ± 4	34 ± 2	52 ± 1	73 ± 1
$i < 10°$ (%)	26 ± 1	41 ± 2	20 ± 1	5 ± 0	9 ± 0
$i < 20°$ (%)	55 ± 2	74 ± 1	48 ± 2	19 ± 0	25 ± 0
$i < 30°$ (%)	72 ± 1	87 ± 1	67 ± 1	42 ± 0	49 ± 0

Table 5. Extinct JFC Candidates with $q < 1.3$ AU

	a (AU)	e	$i(^\circ)$	H	q (AU)	T	P
(3552) Don Quixote	4.232	0.714	30.816	13.0	1.211	2.314	1.000
(5324) Lyapunov	2.959	0.615	19.495	15.2	1.140	2.880	0.190
(5370) Taranis	3.342	0.632	19.027	15.7	1.229	2.731	0.205
(6178) 1986 DA	2.811	0.586	4.307	15.1	1.165	3.039	0.152
(14827) 1986 JK	2.800	0.680	2.139	18.3	0.896	2.933	0.534
(16064) 1999 RH27	2.885	0.577	4.396	16.9	1.221	3.017	0.152
1982 YA	3.657	0.700	35.270	16.1	1.096	2.400	0.971
1983 LC	2.686	0.716	1.528	18.2	0.763	2.940	0.349
1984 QY1	2.939	0.914	17.732	14.2	0.254	2.353	0.961
1985 WA	2.831	0.607	9.803	18.4	1.113	2.993	0.287
1991 XB	2.942	0.590	16.305	18.1	1.207	2.934	0.139
1992 UB	3.070	0.582	15.945	16.1	1.283	2.896	0.412
1994 AB1	2.850	0.590	4.523	16.3	1.168	3.017	0.152
1994 LW	3.167	0.619	22.999	16.8	1.206	2.770	0.709
1995 DV1	2.802	0.650	3.512	23.0	0.982	2.971	0.218
1995 QN3	3.304	0.644	14.793	17.1	1.176	2.753	0.280
1995 SA15	2.753	0.739	0.971	14.3	0.719	2.871	0.599
1997 EN23	3.261	0.634	6.966	22.8	1.192	2.811	0.157
1997 QK1	2.794	0.642	2.886	20.0	1.001	2.985	0.109
1997 SE5	3.727	0.667	2.609	14.9	1.243	2.657	1.000
1997 UZ10	2.868	0.618	12.763	23.0	1.096	2.953	0.148
1997 VM4	2.622	0.812	14.137	18.2	0.493	2.788	0.290
1997 YM3	3.242	0.673	4.014	16.9	1.060	2.769	0.155
1998 FR11	2.797	0.711	6.597	16.5	0.809	2.885	0.653
1998 GL10	3.183	0.668	8.673	18.2	1.057	2.786	0.677
1998 HN3	3.132	0.614	9.215	18.5	1.209	2.870	0.543
1998 KO3	2.622	0.773	54.642	19.8	0.595	2.506	0.354
1998 MX5	2.918	0.611	9.707	18.1	1.134	2.951	0.578
1998 SH2	2.710	0.722	2.484	20.8	0.754	2.918	0.599
1998 ST4	2.820	0.597	9.292	16.6	1.136	3.011	0.114
1998 SY14	2.850	0.665	3.517	20.6	0.955	2.929	0.534
1998 SE35	3.005	0.594	14.817	19.0	1.219	2.913	0.401
1998 US18	2.623	0.680	9.661	20.7	0.839	3.010	0.195
1998 VD31	2.652	0.803	10.234	19.4	0.522	2.800	0.290
1999 AF4	2.828	0.618	12.571	18.2	1.080	2.972	0.148
1999 DB2	2.999	0.620	11.608	19.1	1.139	2.901	0.424
1999 GT6	2.830	0.578	4.277	17.0	1.195	3.039	0.152
1999 HA2	2.789	0.700	15.085	17.6	0.837	2.875	0.163
1999 LT1	2.976	0.658	42.608	17.4	1.019	2.587	0.738
1999 LD30	2.901	0.606	8.729	20.5	1.144	2.968	0.578
1999 RU2	2.807	0.560	5.449	20.2	1.236	3.065	0.114
1999 RD32	2.630	0.777	6.681	16.3	0.586	2.867	0.534
1999 SE10	3.210	0.621	6.897	20.0	1.217	2.843	0.157
1999 VQ11	2.810	0.595	7.940	17.5	1.137	3.021	0.114
1999 VX15	3.010	0.599	12.337	18.9	1.206	2.918	0.401
2000 DN1	2.884	0.669	7.769	19.7	0.954	2.900	0.645
2000 EB107	3.032	0.585	25.283	17.2	1.260	2.836	0.904
2000 GV127	2.823	0.622	17.936	19.0	1.067	2.940	0.120
2000 GC147	2.735	0.601	2.278	20.3	1.092	3.060	0.109
2000 HD74	2.922	0.594	49.373	18.2	1.186	2.566	0.138
2000 KE41	3.000	0.865	50.450	17.2	0.404	2.219	0.842
2000 LF6	2.911	0.611	14.826	19.7	1.131	2.932	0.424

Table 5—Continued

	a (AU)	e	$i(^\circ)$	H	q (AU)	T	P
2000 PG3	2.825	0.859	20.454	15.8	0.399	2.549	0.929
2000 PF5	3.237	0.642	6.156	20.0	1.159	2.810	0.157
2000 QS7	2.701	0.665	3.202	19.8	0.905	3.001	0.373
2000 QN130	2.902	0.573	2.564	17.3	1.240	3.016	0.156

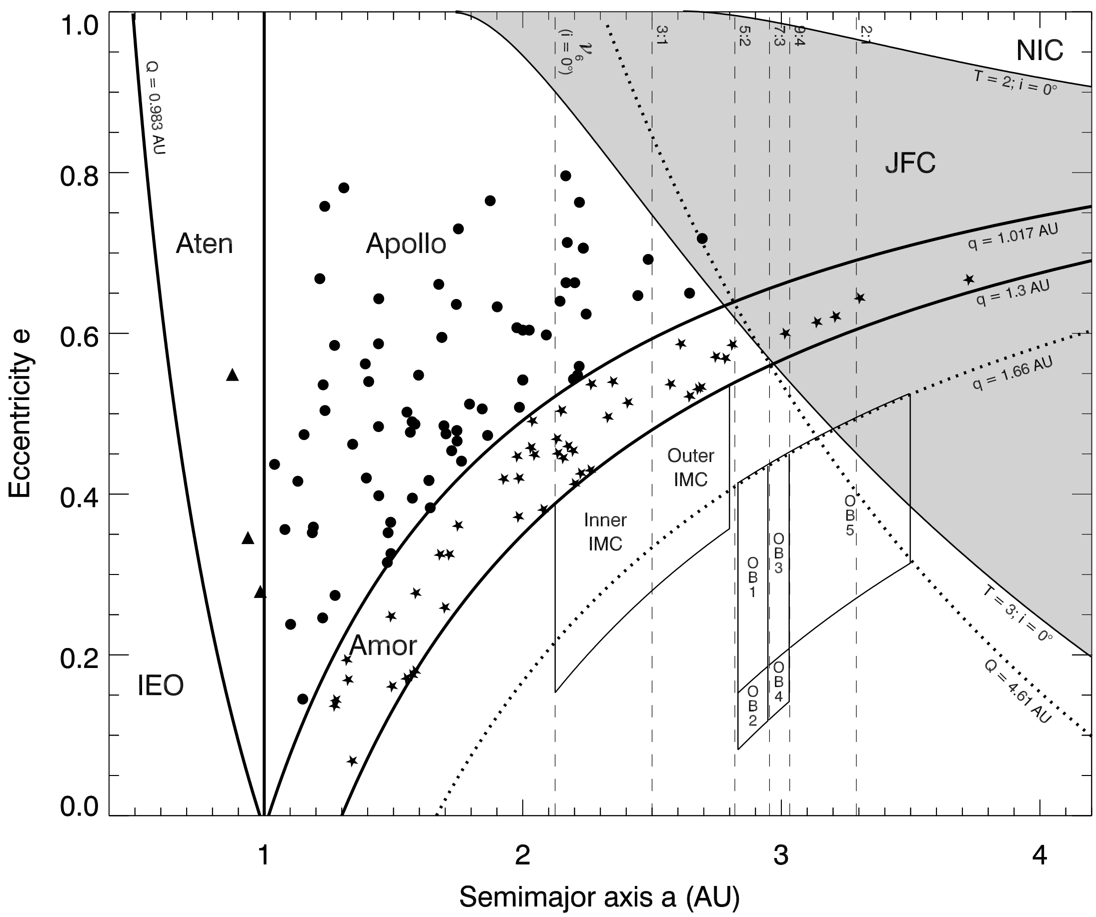

Fig. 1.— NEO figure

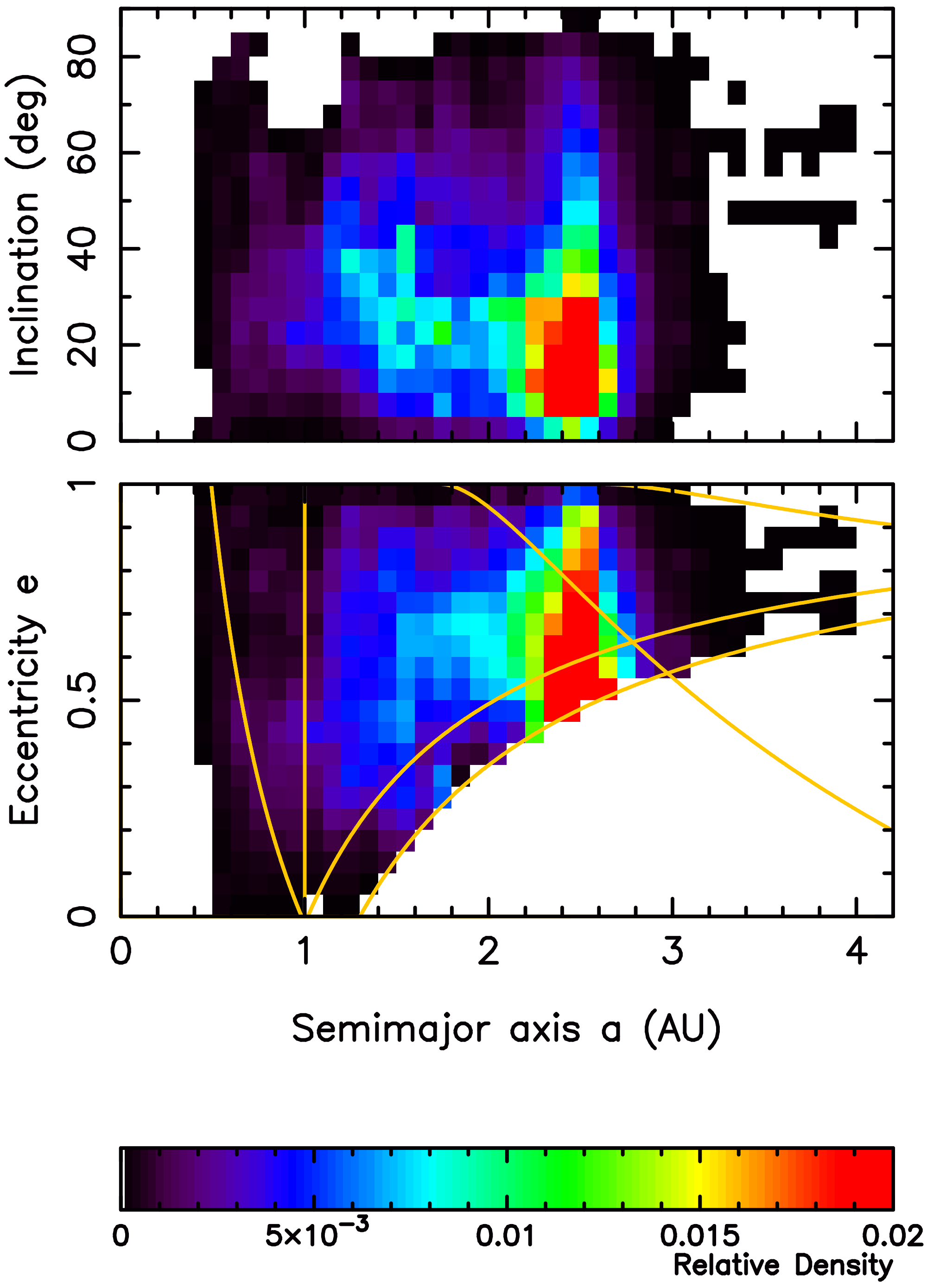

Fig. 2.— 3:1 resonance

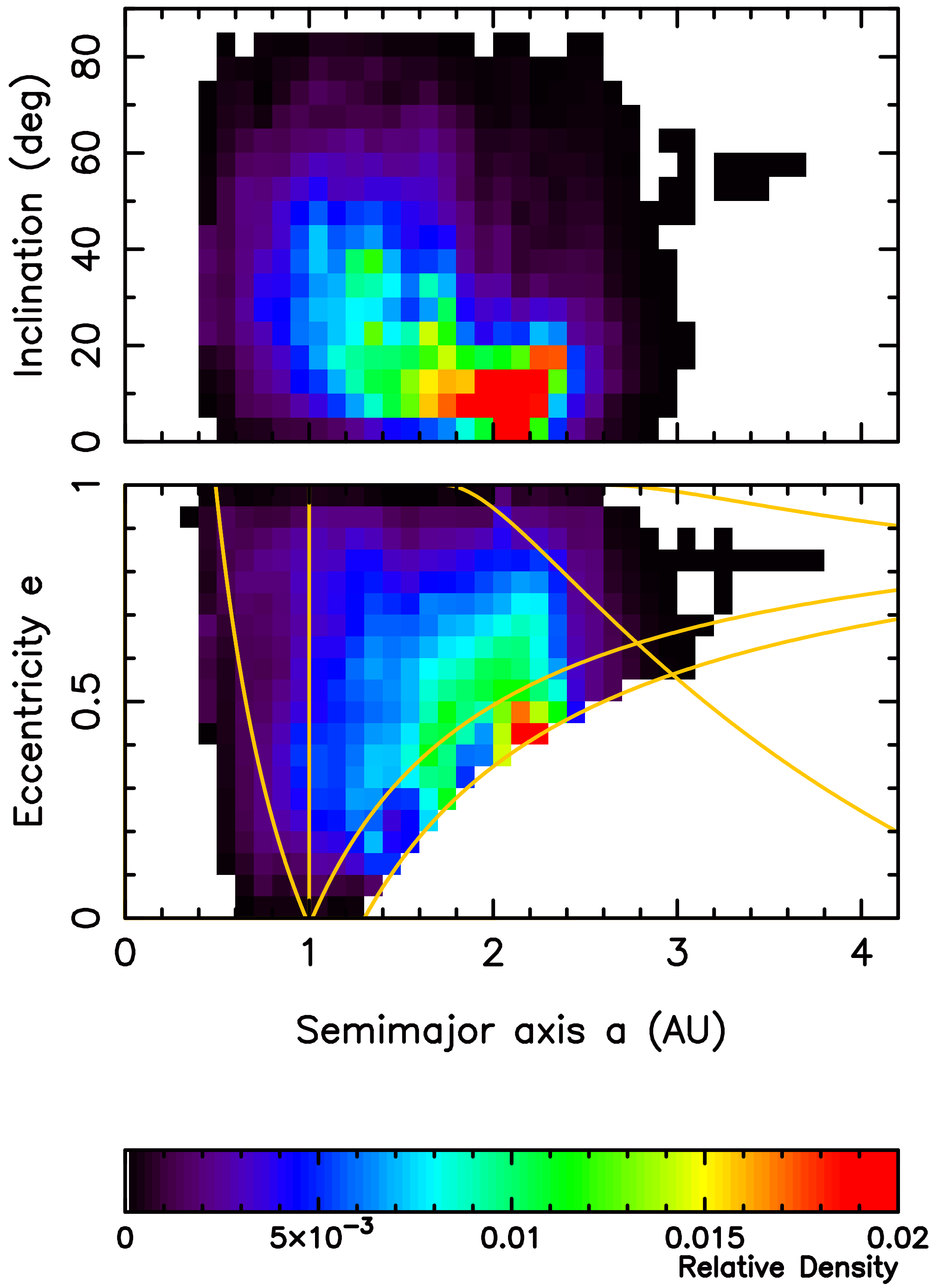

Fig. 3.— ν_6 resonance

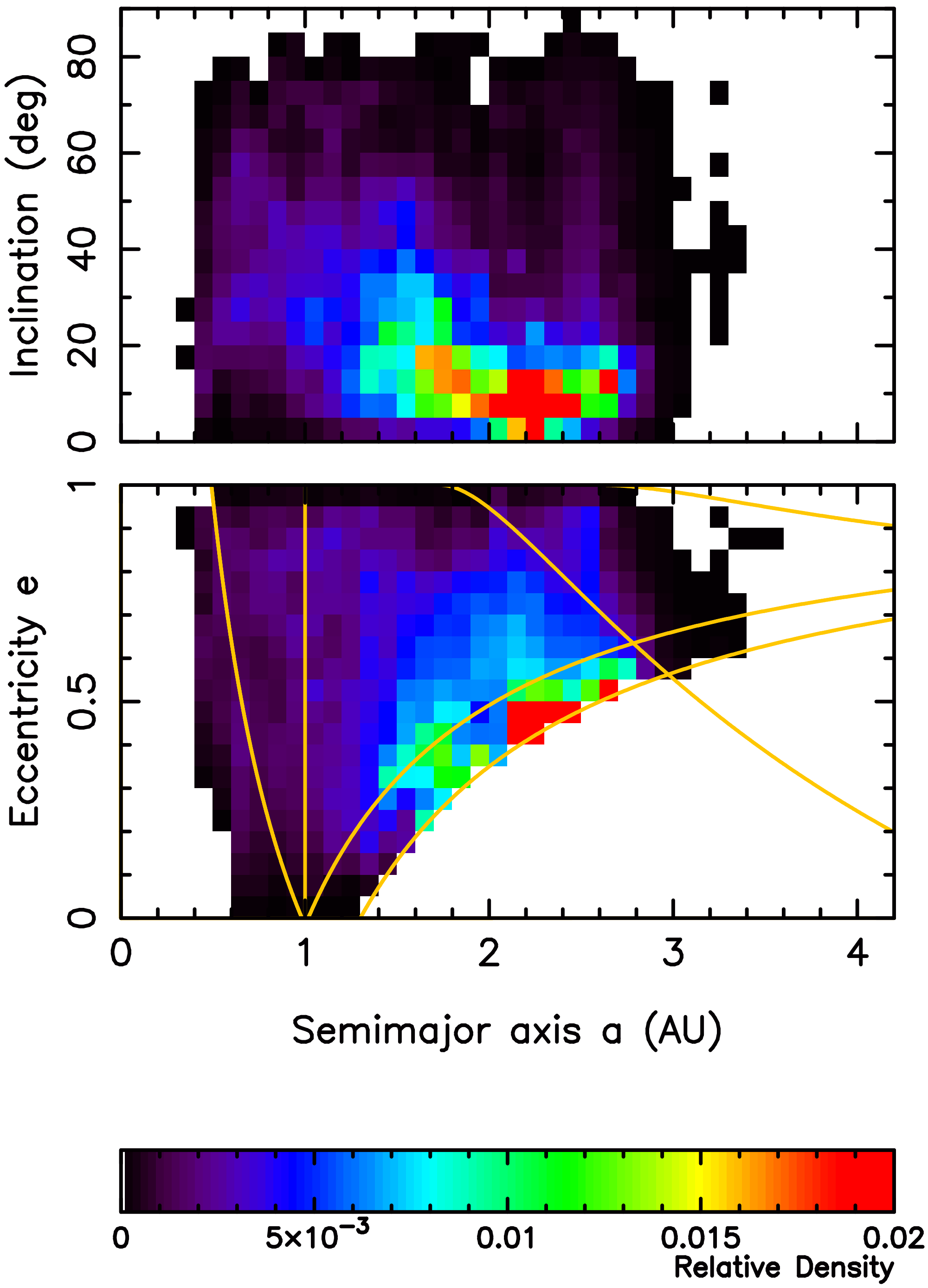

Fig. 4.— IMC region

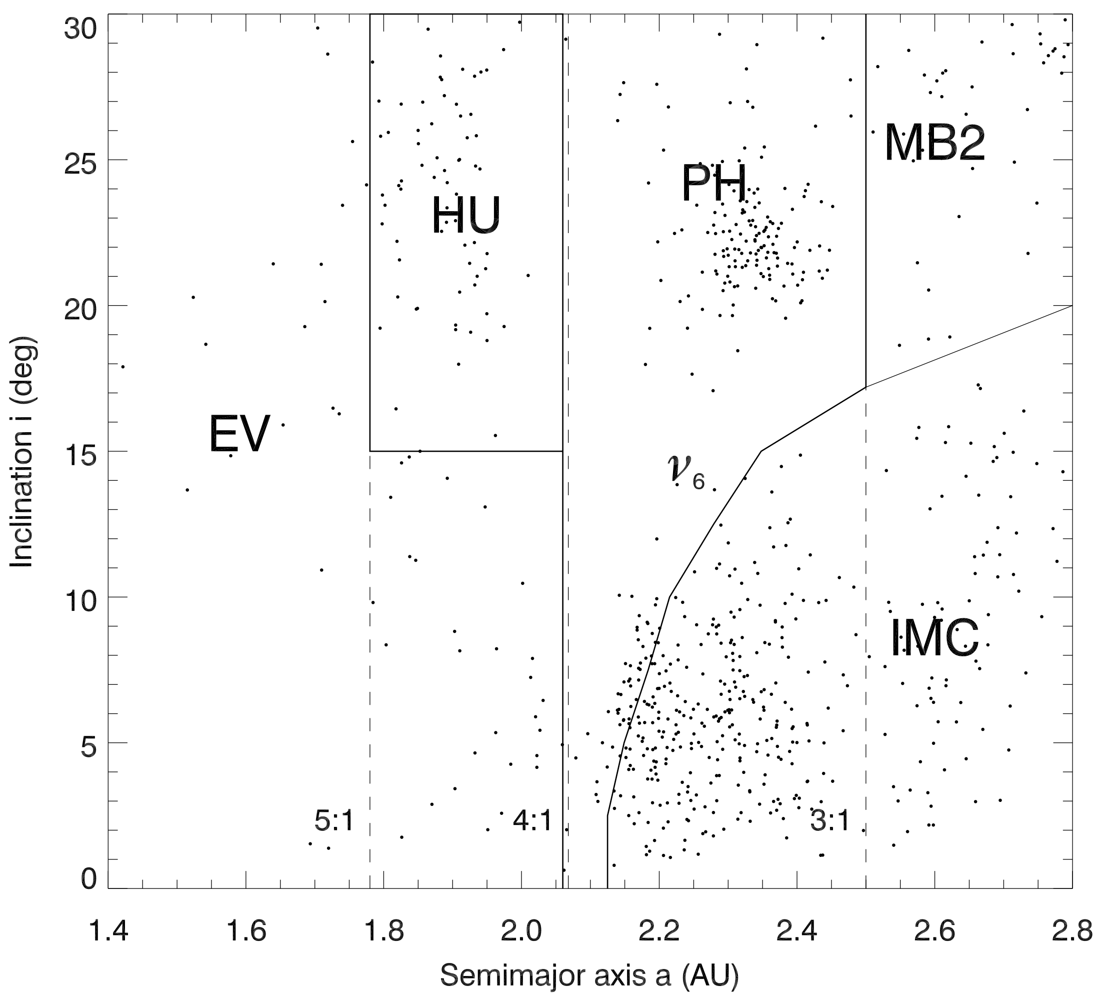

Fig. 5.— Mars-crossing asteroids

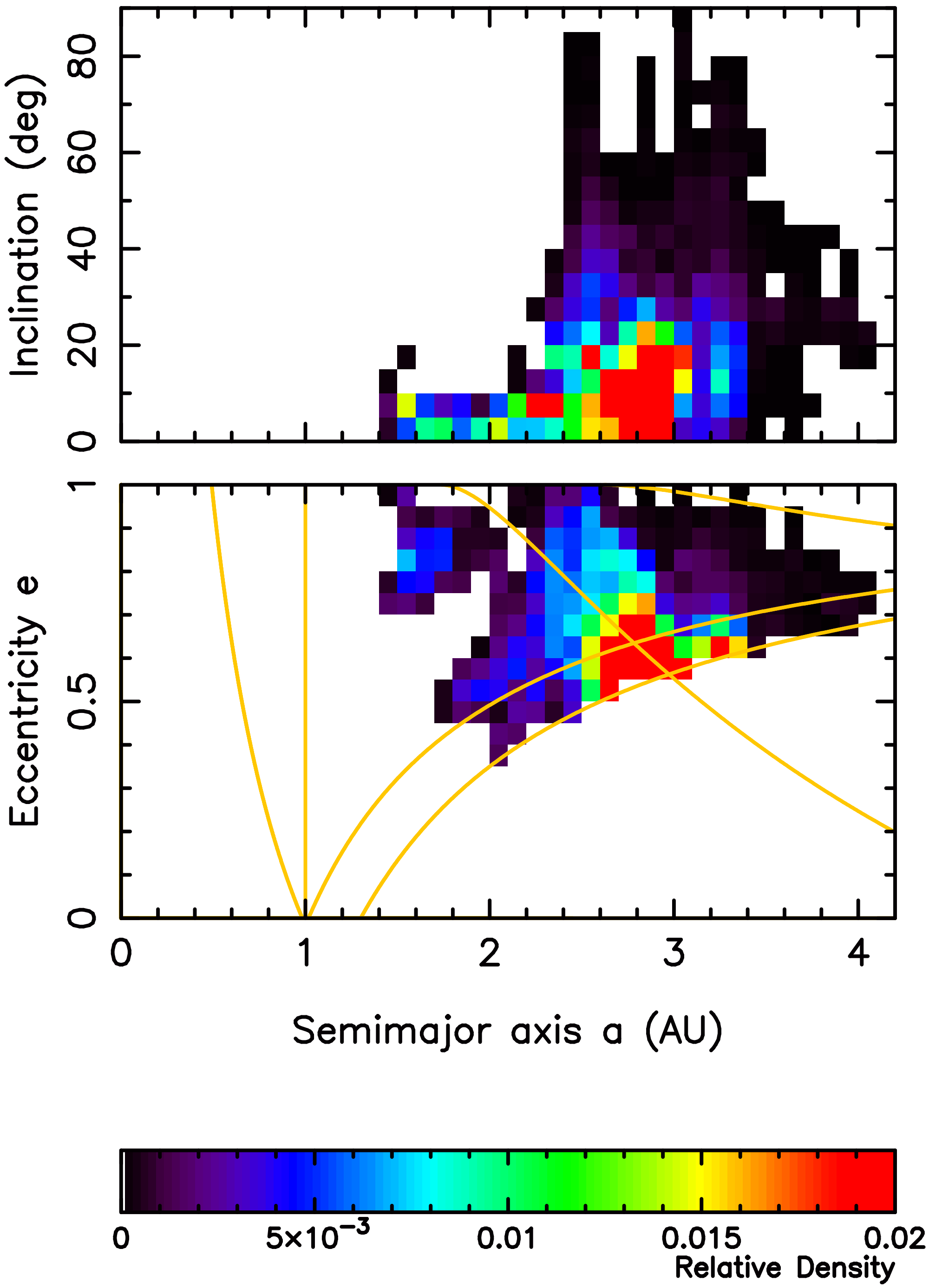

Fig. 6.— Outer main belt (OB)

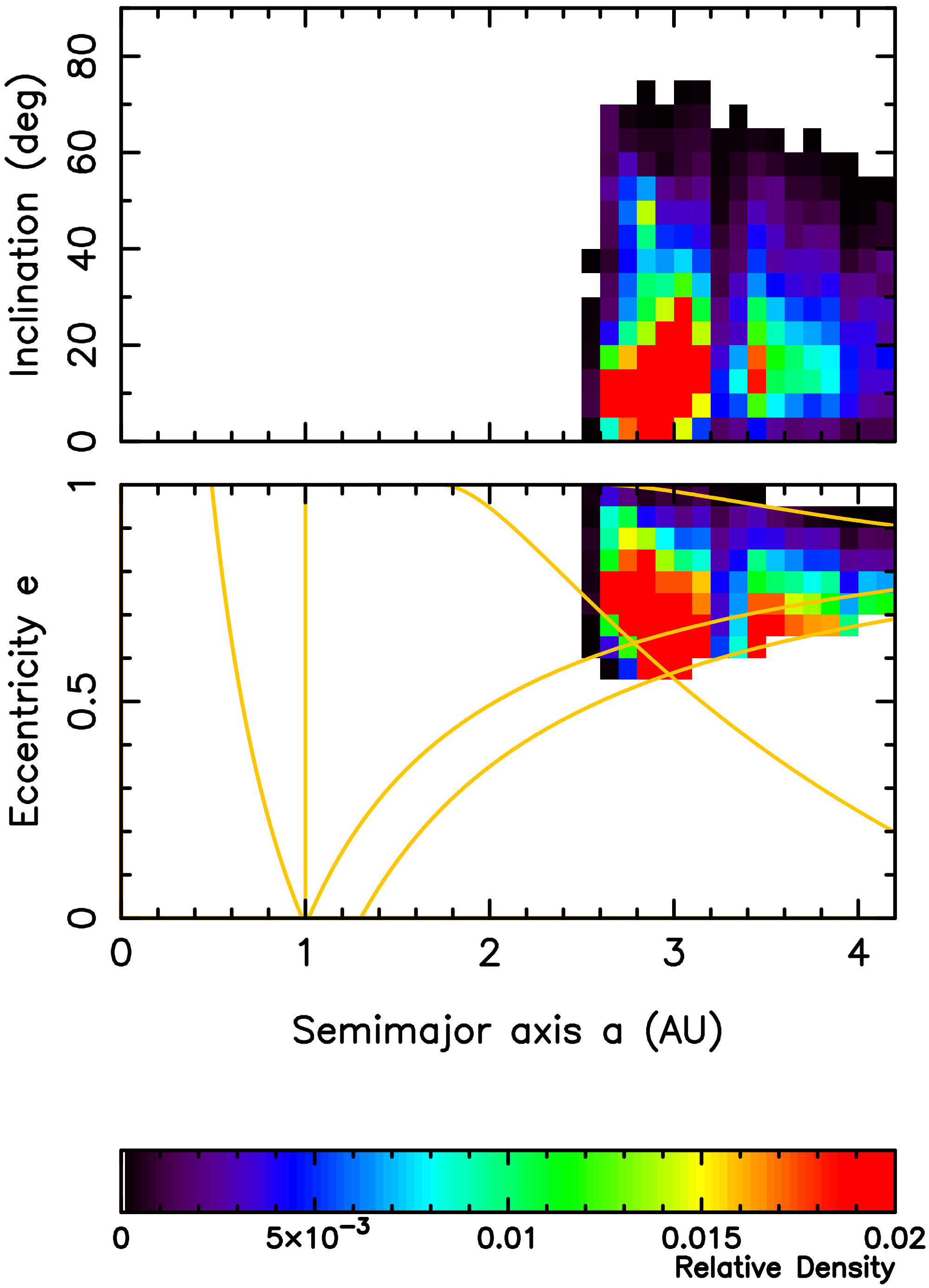

Fig. 7.— Jupiter-Family comets (JFCs)

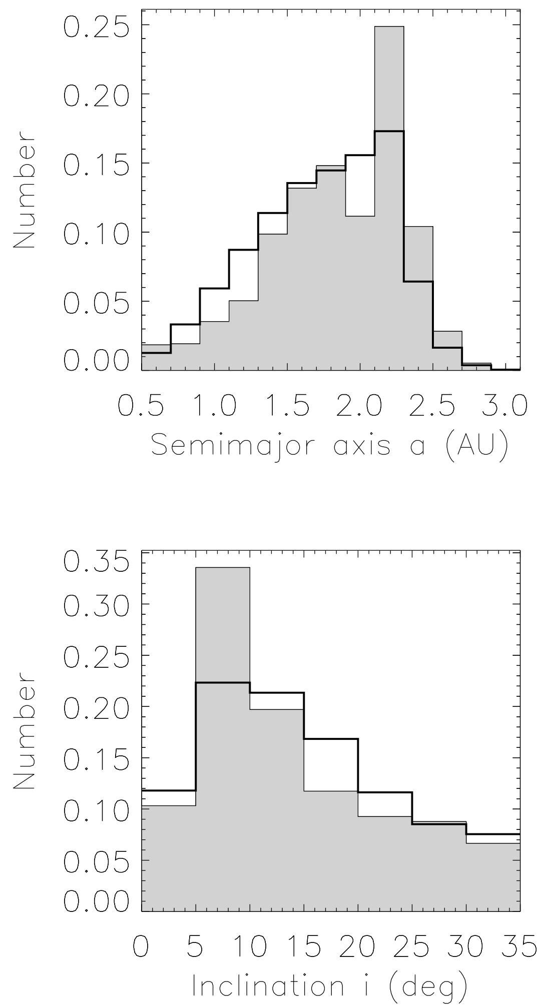

Fig. 8.— Degeneracy between inner-IMC and ν_6

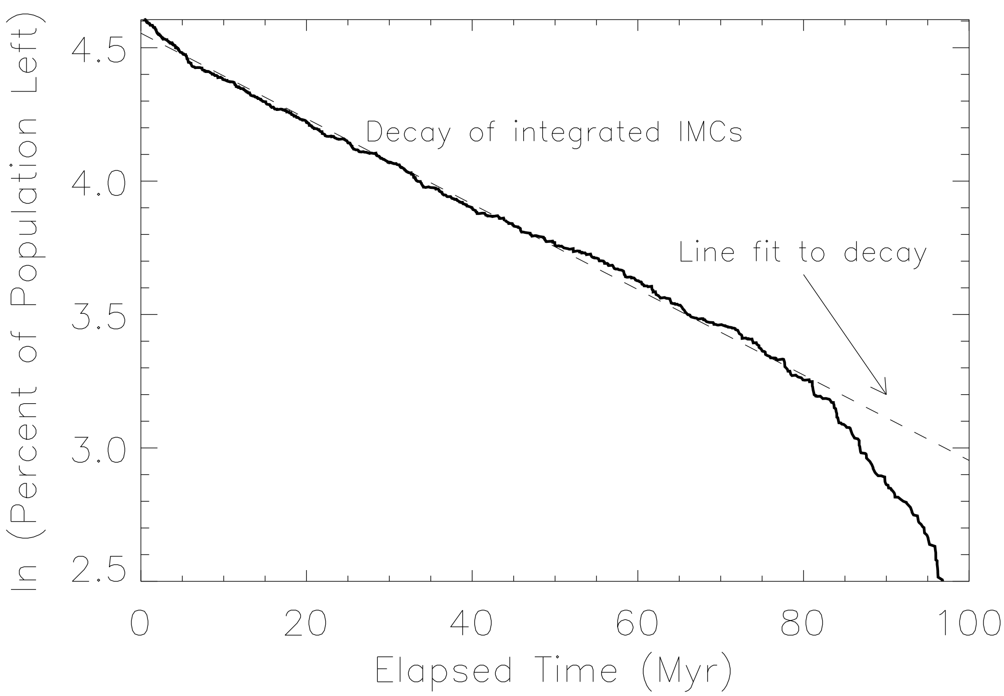

Fig. 9.— Decay of IMC population

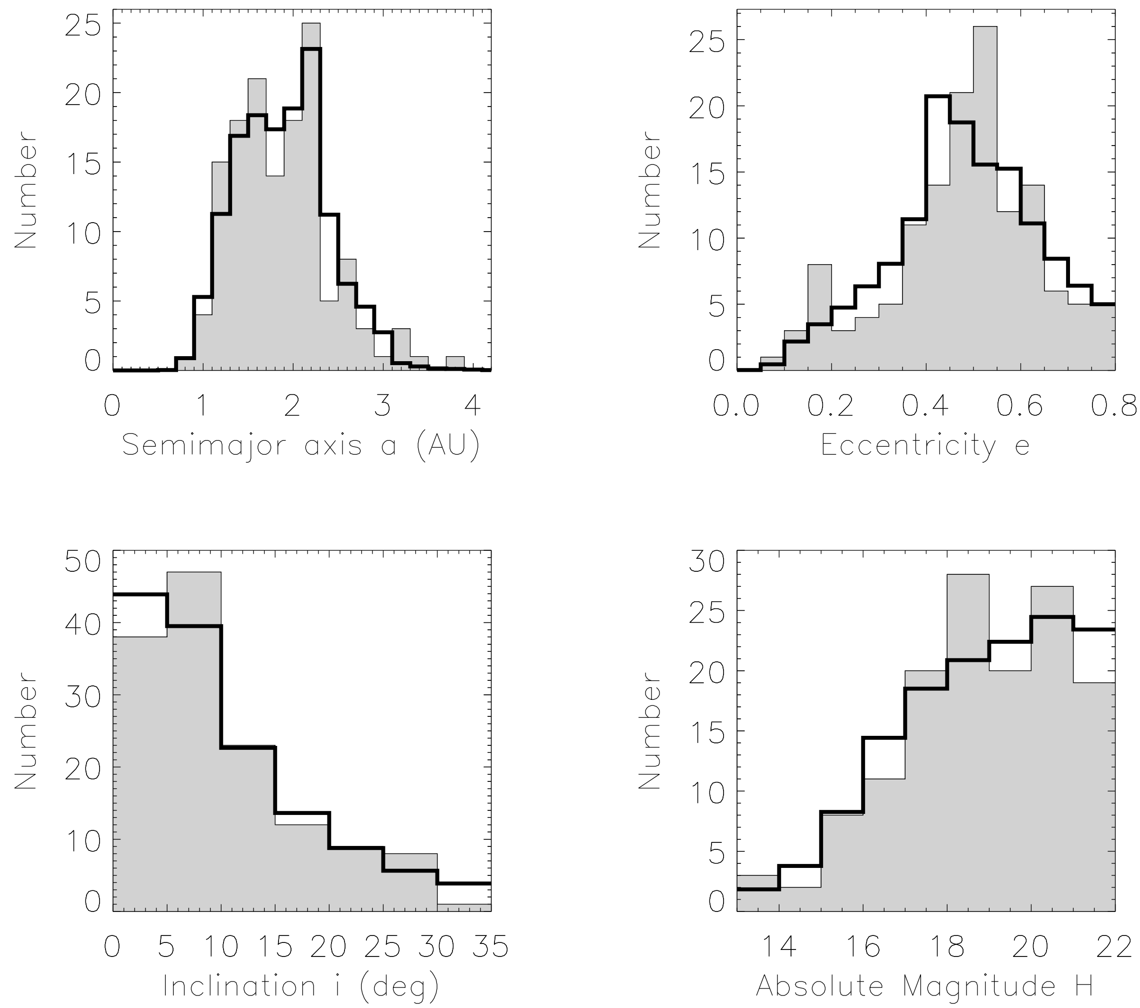

Fig. 10.— Fit between NEO model and Spacewatch data

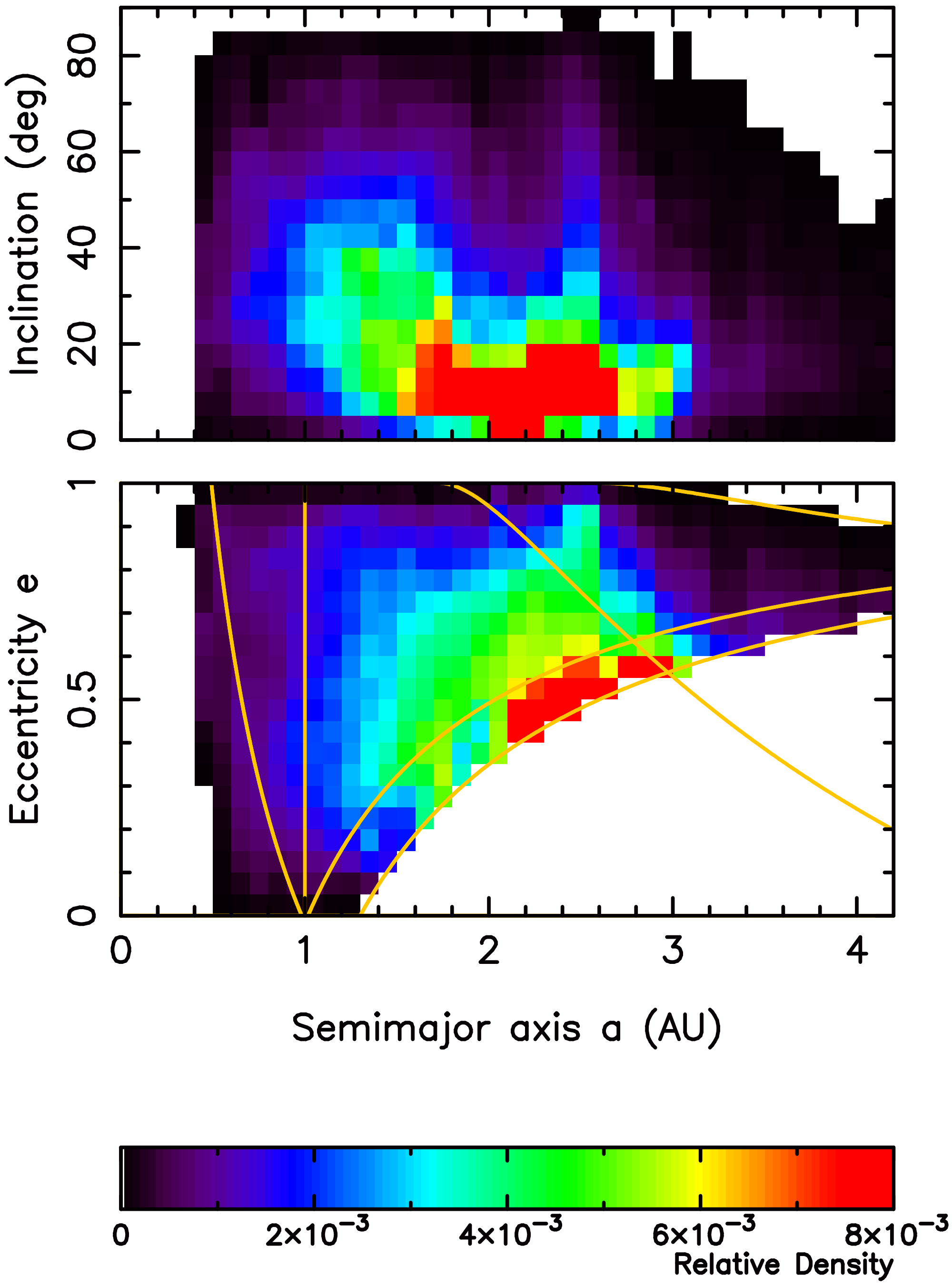
Inclination (deg)
0
20
40
60
80
Eccentricity e
0
0.5
1
0
1
2
3
4
Semimajor axis a (AU)
0
2×10^{-3}
4×10^{-3}
6×10^{-3}
8×10^{-3}
Relative Density

Fig. 11.— NEOs

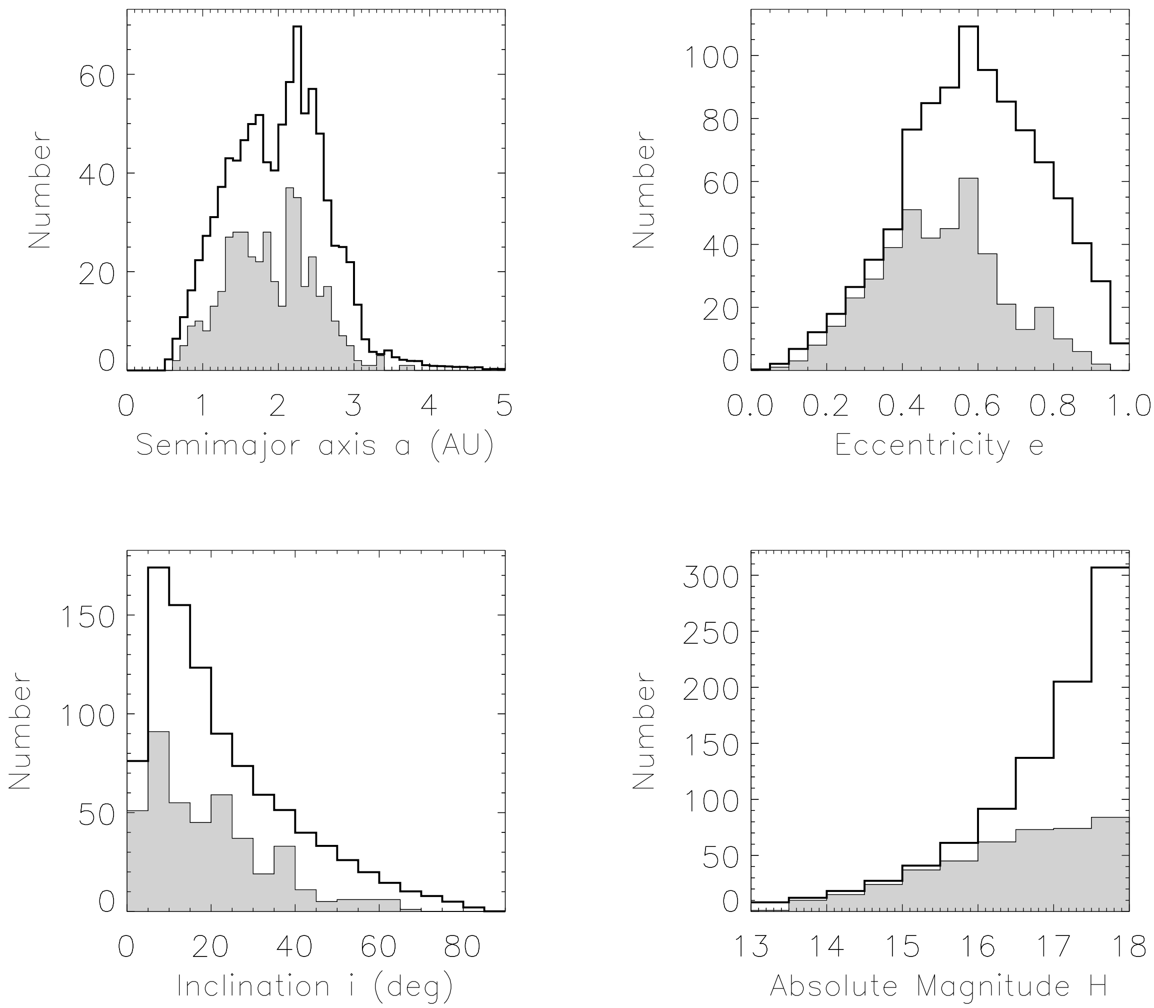

Fig. 12.— Predicted and observed NEOs

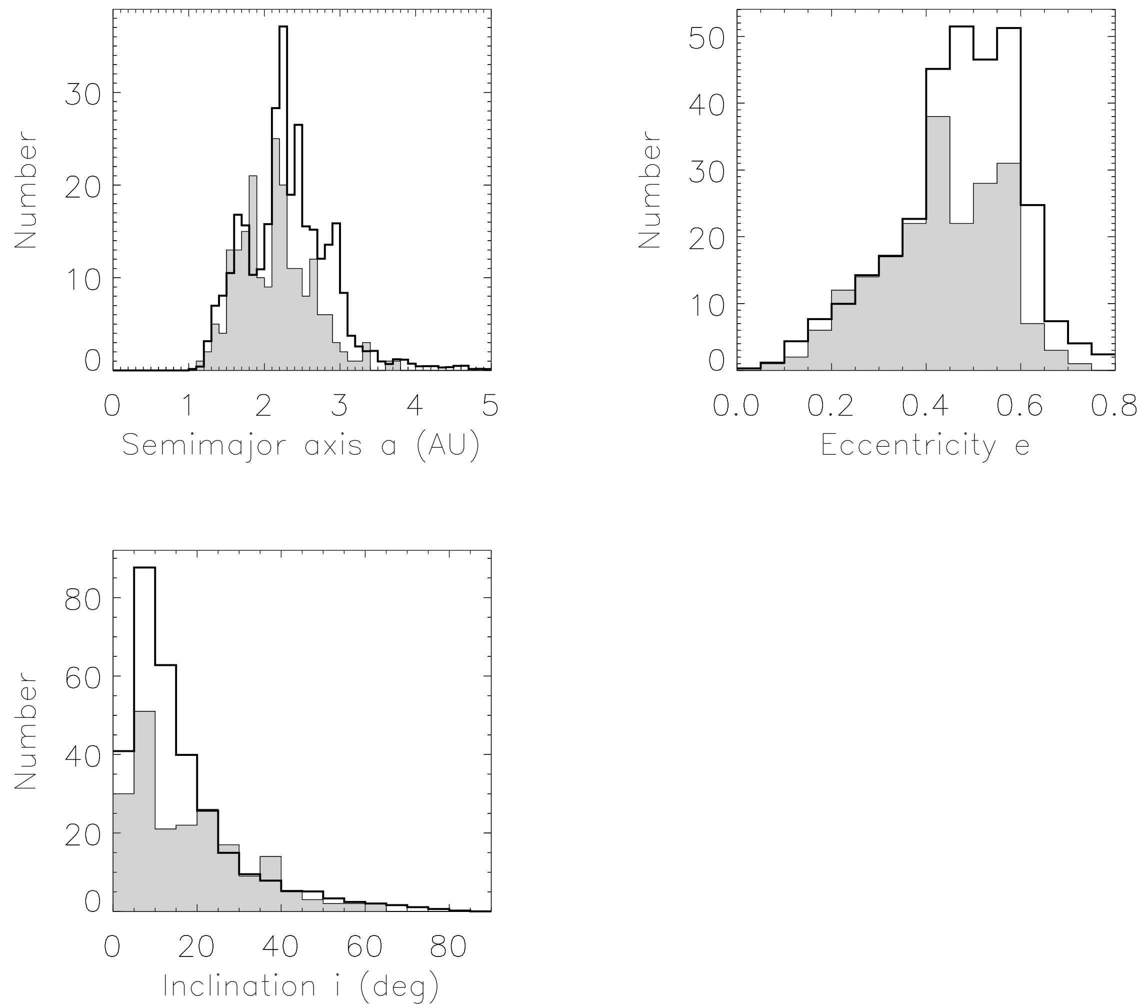
Number
Semimajor axis a (AU)
Number
Eccentricity e
Number
Inclination i (deg)

Fig. 13.— Amors.

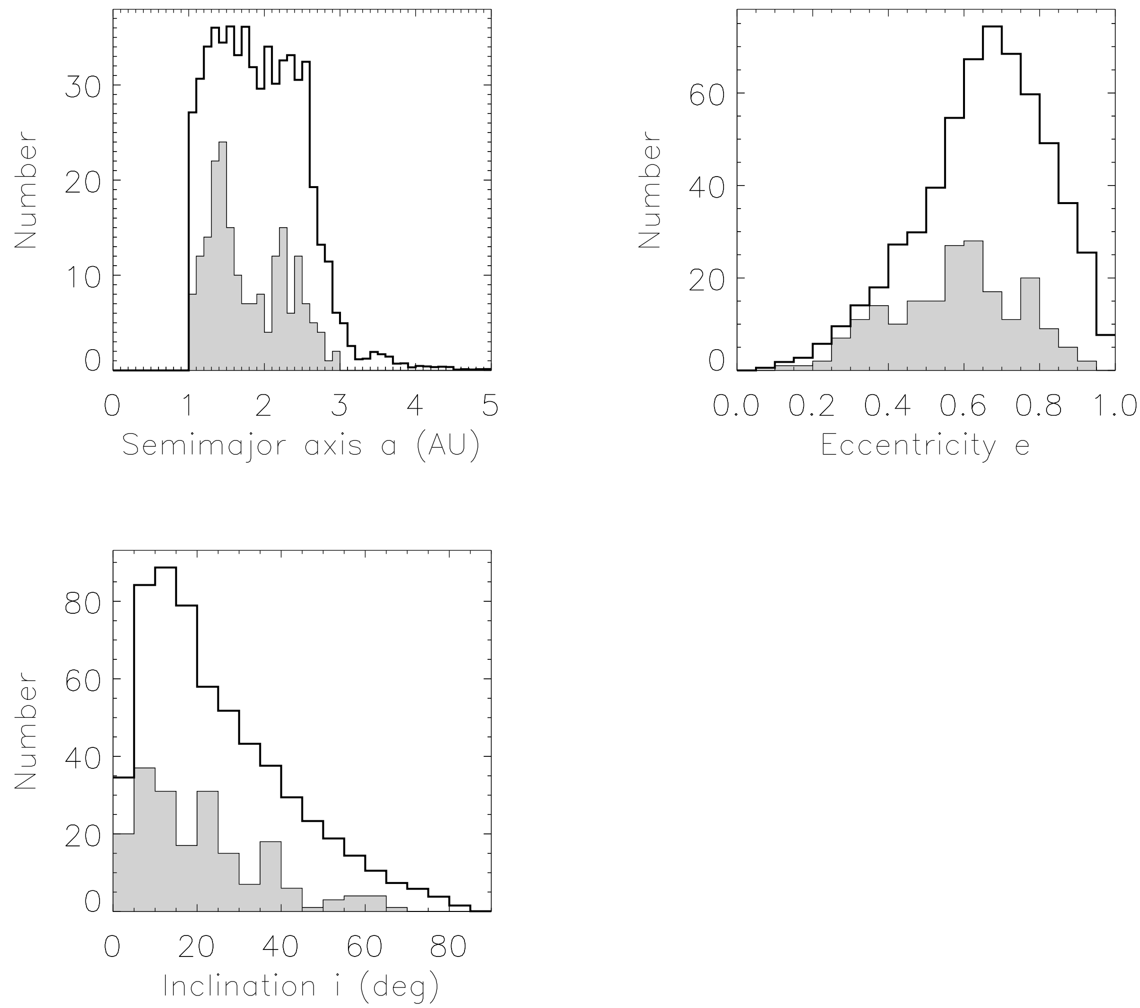

Fig. 14.— Apollos.

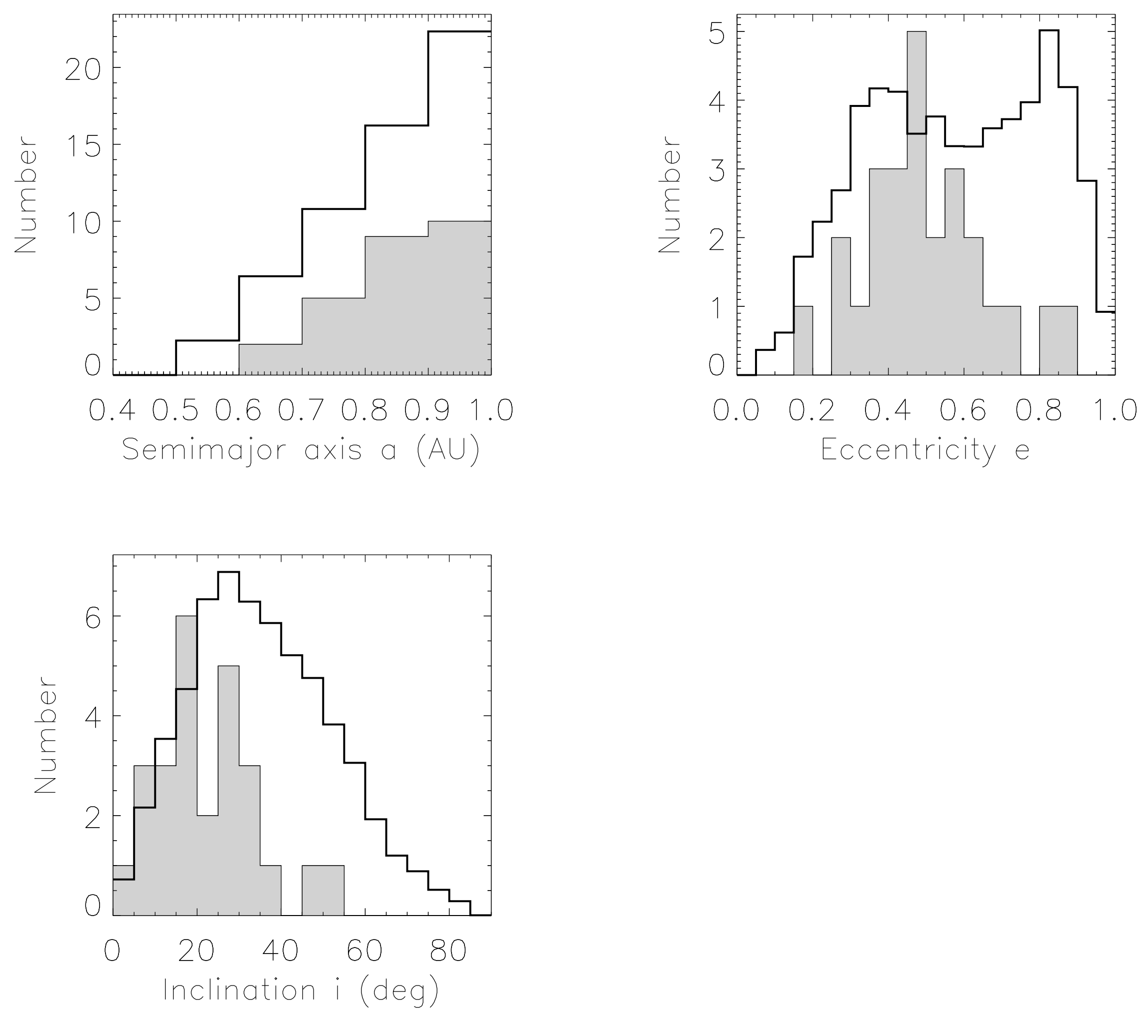
Number
Semimajor axis a (AU)
Number
Eccentricity e
Number
Inclination i (deg)

Fig. 15.— Atens.

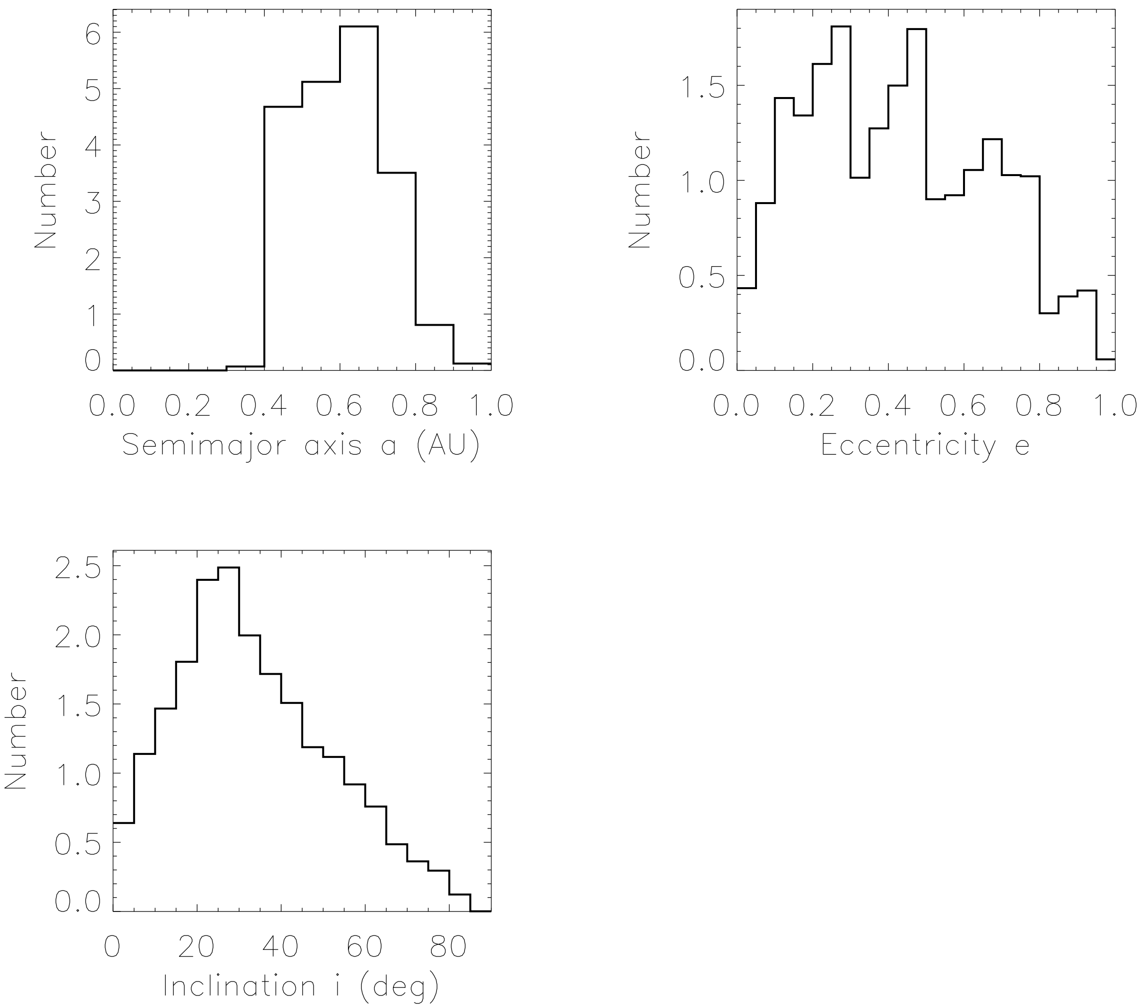
Number
Semimajor axis a (AU)
Number
Eccentricity e
Number
Inclination i (deg)
0.0
0.2
0.4
0.6
0.8
1.0
0
1
2
3
4
5
6
0.5
1.0
1.5
2.0
2.5
20
40
60
80

Fig. 16.— IEOs.

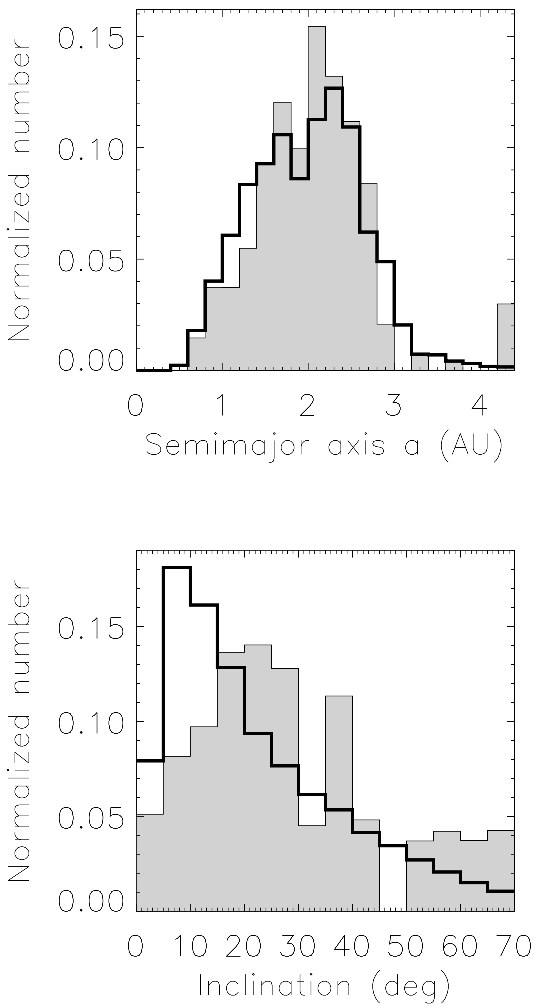

Fig. 17.— Comparison with Rabinowitz estimates

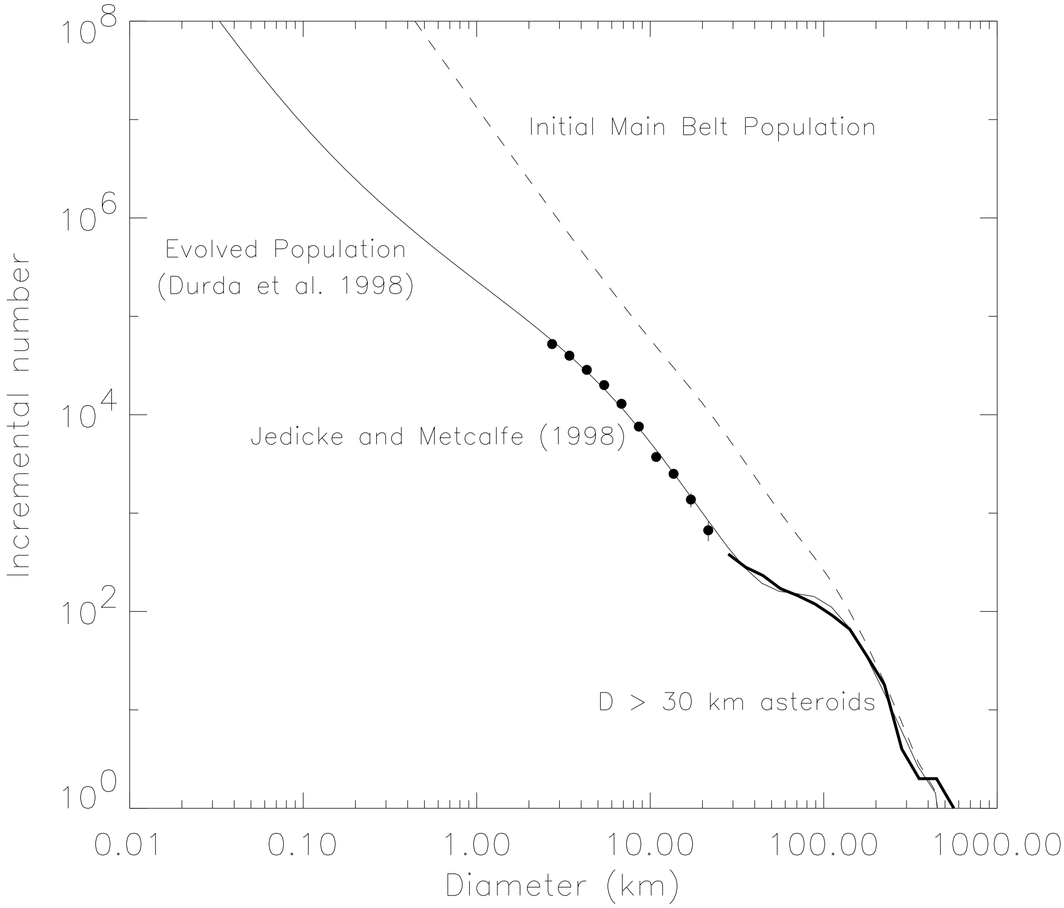

Fig. 18.— Size distribution of main belt

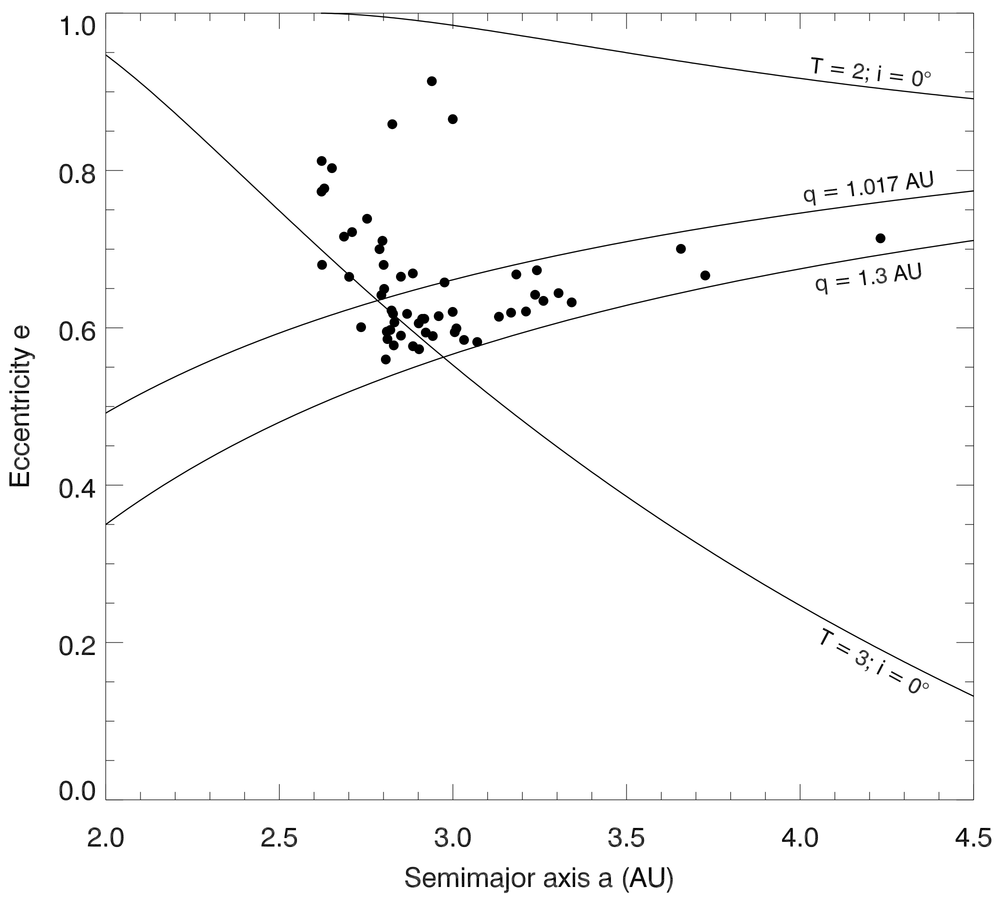

Fig. 19.— Extinct comet candidates.